Metals and Ceramics Division

Heavy Vehicle Propulsion Materials Program
Quarterly Progress Report for
January through March 2002

D. R. Johnson
Technical Project Manager

Prepared for
U.S. Department of Energy
Assistant Secretary for Energy Efficiency and Renewable Energy
Office of FreedomCAR and Vehicle Technologies Program
EE 07 01 00 0

Prepared by the
OAK RIDGE NATIONAL LABORATORY
Oak Ridge, Tennessee 37831-6066
Managed by
UT-Battelle, LLC
for the Department of Energy
Under contract DE-AC05-00OR22725

CONTENTS

Cost Effective High Performance Materials and Processing

Development of Low Cost Austenitic Stainless Diesel Engine Components with Enhanced High-Temperature Reliability (ORNL and Caterpillar, Inc.)

Cost-Effective Smart Materials for Diesel Engine Applications (ORNL)

Low-Cost Manufacturing Processes for Ceramic and Cermet Diesel Engine Components (SIU-C)

Low Cost High Toughness Ceramics (ORNL)

Synthesis of TiC and Nickel Aluminide Powders (University of Colorado)

Advanced Manufacturing Technology

Intermetallic-Bonded Cermets (ORNL)

Cylindrical Wire Electrical Discharge Machining (EDM) and Temperature Measurement (North Carolina State University)

Testing and Characterization

NDE/C Technology for Heavy Duty Diesel Engines: Fuel Delivery and Insulating Materials (Argonne National Laboratory)

NDE Development for Ceramic Valves for Diesel Engines (Argonne National Laboratory)

Processing and Characterization of Structural and Functional Materials for Heavy Vehicle Applications (North Carolina A&T State University)

Life Prediction of Diesel Engine Components (ORNL)

Durability of Diesel Engine Component Materials (ORNL)

Materials and Testing Standards

Implementing Agreement for a Programme of Research and Development on Advanced Materials for Transportation Applications (ORNL)

Standards for Reliability Testing of Heavy Vehicle Propulsion Materials (NIST)

Mechanical Property Testing and Standards Development (NIST)

Development Of Low-Cost Austenitic Stainless Diesel Engine Components With Enhanced High-Temperature Reliability

P.J. Maziasz and R.W. Swindeman
Oak Ridge National Laboratory
and
M.E. Frary
Caterpillar, Inc.

Objective/Scope

The objective of this work is to evaluate cast austenitic stainless steels as high-performance alternatives to SiMo ductile cast iron, which is currently the standard material used in most diesel engines for exhaust manifold and turbocharger housing components. The new material must be able to withstand prolonged exposure at temperatures of 750°C or above, as well as to survive the severe thermal cycling from near room temperature to such high-temperatures without developing cracks. This project has tested commercially available cast alloys, as well as developed new, modified cast alloys with significantly enhanced performance. The ultimate project goal is to provide high-performance, reliable materials that are also cost-effective for such applications. This advanced diesel engine work is part of a broader CRADA (Cooperative Research and Development Agreement) project (ORNL99-0533) that began July 21,1999 and was scheduled to end July 22, 2001, but has been extended for 12 more months. Any more detailed information on this project must be requested directly from Caterpillar, Inc.

Technical Highlights, 2nd Quarter, FY2002

Background

Advanced large diesel engine require higher fuel efficiency as well as reduced exhaust emissions, without sacrificing durability and reliability. Therefore, exhaust manifold and turbocharger-housing materials must withstand temperatures ranging from 70 to 750°C or higher in a normal duty cycle that includes prolonged, steady high-temperature exposure as well as more rapid and severe thermal cycling. New technology to reduce emissions and heavier duty cycles will push temperatures in these critical components even higher. Current exhaust components are made from SiMo ductile cast iron, and higher engine temperatures would push such materials beyond their current strength and corrosion limits. Therefore, the goals of this project were to generate new data on alternate higher performance materials like cast austenitic stainless steels to enable materials selection and component lifing. There is limited industrial experience on cast austenitic stainless steels like CN12, especially for diesel engine applications, and little high-temperature mechanical properties data available, particularly creep and fatigue. The main purpose of this project is to produce data comparing cast CN12 and SiMo cast iron for such diesel exhaust component applications. Another component of this project was a parallel alloy development effort to further optimize the cost-effective performance of such cast austenitic stainless steels.

Approach

Commercial cast CN12 austenitic stainless steel (Fe-25Cr-13Ni-1.8Nb, C, N, S) was chosen as the baseline alloy for evaluation relative to SiMo ductile cast iron. Materials were evaluated in the as-cast condition as well as after appropriate thermal aging at temperatures up to 850°C. Tensile and isothermal cyclic fatigue properties were evaluated selectively from room temperature up to 900°C, together with some high-temperature creep-rupture and oxidation/corrosion testing. Microstructure analysis was performed on some of the specimens to better understand mechanisms associated with the properties changes. In a parallel effort, new alloying element modifications were made to CN12 and studied to further enhance the high-temperature performance.

Technical Progress

Previously, the commercial cast iron and baseline CN12 materials were obtained, all mechanical properties specimens machined, and all tensile and creep testing of unaged and aged specimens has been done. High-cycle isothermal fatigue testing at 700°C and 850°C at ORNL has been completed, and thermal fatigue testing over this temperature range was completed at Caterpillar on one of the new modified CN12 alloys last quarter. Microstructural analyses of selected specimens of as-cast or as-cast and aged materials have been completed to better understand the properties behavior and to establish the effects of aging on the baseline CN12 material. CN12 has a clear tensile strength advantage and an overwhelming creep-strength advantage over SiMo cast iron above 550-600°C. The isothermal fatigue data at room temperature and at 700°C also shows an enormous fatigue life advantage of CN12 over the SiMo cast iron as well.

To date, eight smaller heats (15 lbs each) of modified CN12 austenitic stainless steels have been produced at ORNL and have been evaluated. Initial screening of as-cast or cast and aged material with tensile testing, and of as-cast material with creep-rupture testing at 850°C indicates that significant improvements have been achieved in high-temperature strength and aging resistance. The improvement of the best modified CN-12 alloys is five to ten times better relative to the standard commercial CN-12 alloy for creep-rupture testing at 850°C and 110 MPa.

In addition to the modified CN12 austenitic stainless steels, similar efforts were made to modify a less costly and more castable CF8C (Fe-19Cr-12Ni-Nb, C) austenitic stainless steel that has previously been considered as a candidate for diesel exhaust applications (but dismissed for lack of high-temperature strength), and which also finds use in some gas-turbine exhaust components at 650°C or below. Three smaller heats of modified CF8C were made at ORNL (one baseline unmodified alloy and two modified alloys) and screened using tensile tests and creep-rupture testing at 850°C. The dramatic improvement in creep resistance of the best modified CF8C steel at 850°C relative to commercial material was shown last quarter. Both modified CF8C steels are several orders of magnitude better than the standard commercial CF8C steel. One modified CF8C steel ruptured after almost 13,000 h last quarter, while the other modified CF8C steel still has not ruptured after almost 20,000 h of creep testing. Additional creep test of standard, commercial CN12 steel began previously for comparison with the best modified CF8C steel at the same creep conditions and that test has lasted for almost 10,000 h. These remaining creep tests of the modified CF8C and standard CN12 steels probably will continue next quarter.

Communications/Visits/Travel

Team communications between ORNL and Caterpillar occur in detail at least several times a week. This quarter, the current CRADA was extended another 6 months, and the statement of work for a new CRADA was finalized. The new CRADA is focused on commercial scale-up of the best modified CF8C and CN12 steels to obtain more mechanical properties data on these new steels, including fatigue and thermal fatigue data. Production and evaluation of prototype components with the new alloys will also be included in this new CRADA project.

An invention disclosure and patent application on cast austenitic stainless alloys with improved performance were completed by Caterpillar and filed with the U.S. Patent Office in December 2000. It is entitled "Heat and Corrosion Resistant Cast Stainless Steels With Improved High Temperature Strength and Ductility," by P.J. Maziasz (ORNL), T. McGreevy (U. of Bradley/CAT), M.J. Pollard (CAT), C.W. Siebenaler (CAT), and R.W. Swindeman (ORNL).

Status of Milestones

Formal milestones were imbedded in the CRADA and are not part of the HVPM Program FWP. However, all milestones have achieved on or significantly ahead of schedule.

Publications

There have been several detailed internal reports on this project at Caterpillar Technical Center.

Several highlights for this project have been produced for the DOE HVPM program, and a highlight entitled "Cast Stainless Steels are Stronger at Higher Temperatures," was published in the ASM-International magazine Advanced Materials and Processes, volume 160, no.1, January, 2002, p. 13.

Cost-Effective Smart Materials for Diesel Engine Applications

J. O. Kiggans, Jr., F. C. Montgomery, T. N. Tiegs,
and L. C. Maxey
Oak Ridge National Laboratory

Objective / Scope

There are two objectives for this project. The first is to evaluate the cost-effectiveness and maturity of various "Smart Materials Technologies," which are under consideration for diesel engine applications, such as fuel injection systems. The second is to develop "Smart Materials" to be incorporated into working actuators and sensors.

Task 1 - Multilayer Electroded Laminates

The purpose of this study is to find satisfactory methods for the preparation of PZT laminates with internal electrodes from tape cast materials. This task is in progress with no new results to share in this report.

Task 2 – Compositional Alteration of PZT-4

A major task of this project is to develop cost-effective PZT compositions and processing methods that will give PZT powders that will sinter to high density at a temperature below 960°C. This goal is driven by the need to lower the cost of multilayer PZT actuators by reducing the cost of the interlayer electrodes. Commercial hard PZT powders require sintering at temperatures exceeding 1200°C and, thus, multilayer devices must use costly Pd/Ag electrodes.

In earlier progress reports we have provided data that supports our contention that small additions of bismuth oxide compounds can lower the PZT sintering temperature sufficiently that Ag or Ag/Pd alloy (70/30) can be used as internal electrodes. In the last quarterly report we reported that ball milled PZT-840 powder containing a sintering aid consisting of 2 wt % Bi_2O_3 with an acceptor ion oxide resulted in a powder that sintered to greater than 93% of the theoretical density after 3 h at 945°C. Furthermore, the sintered PZT had piezoelectric properties which were as good as the properties of commercial PZT sintered at ~1275°C and, because of the acceptor ion, the electromechanical Q was significantly higher than that of either the undoped powder or commercially sintered PZT-840.

It is well known that finer particle size powders can often be sintered at lower temperatures and more rapidly than coarser powders. In the previous study the sintering aids were mixed into the commercial PZT-840 powder by a low energy ball milling process. Attrition milling is quicker and is more efficient at achieving fine particle size than ball milling.[1] Thus, in order to obtain a powder with a finer particle size, a batch of PZT-840 was prepared using attrition milling for comminution.

Experimental

Preparation of Ball Milled Powder

Commercial PZT-840 powder (American Piezo Ceramics, Inc.) was mixed with 2.0 wt % Bi_2O_3 (Alfa Products, 99.8%) and additive A using standard ceramic powder techniques. Two wt % of a 1:1 (wt:wt) mixture of Polyvinylpyrrolidone (Aldrich Chemical, average molecular weight ~ 10,000) and Carbowax 8000 was added as a binder to aid in compact formation. The mixture was homogenized by ball milling in ethyl alcohol (200 proof Aaper) for 24 h with 10 mm spherical ZrO_2 using a media to PZT weight ratio of 12:1.

Preparation of Attrition Milled Powder

Two samples of attrition milled powder were prepared. The first was commercial PZT-840 without any ORNL sintering aids. The second batch included the ORNL sintering aids. Both were prepared in the same way except that the first batch was only milled for 6 h.

The procedure used for the second sample is described herein. Into a polybottle was placed ethanol (92g), Polyvinylpyrrolidone (3 g) Carbowax 8000 (3 g) and 2 g of a 50/50 (v/v) mixture of Menhedan fish oil (Mistler) in ethanol. The bottle was shaken to dissolve the solid components. To this solution was added PZT-840 (196 g) as well as Bi_2O_3 and additive A in the same proportions used in the preparation of the ball milled powder. This was mixed by shaking and then poured into the grinding tank of a Szegvari attrition mill. To reduce the possibility of contamination the grinding tank was polyethylene and the agitator arms were polyurethane coated. The powders were milled with 3 mm spherical ZrO_2 media using a 5:1 weight ratio of media to PZT-840 powder.

Particle size distribution was measured by laser scattering with an Horiba LA-700 particle size distribution analyzer. A small amount of the ethanol suspension was dispersed in water with Darvan 821A and the suspension was ultrasonicated in the mixing chamber of the LA-700 to reduce agglomerates. An accurate determination of the distribution with the LA-700 requires that the ratio of the index of refraction (R.I.) of the suspended powder to the R.I. of the suspending fluid be known. The R.I. for PZT-840 has not been reported. However, R.I. for $PbTiO_3$ is 2.7 and that for PbO is 2.5. The R.I. for water is 1.33. Thus, for our measurements, a ratio of 2.0 was used for the measurement.

After homogenizing, the slurries were separated from the media and dried at 80°C. The powder cakes were crushed and the powders were sieved through a No.100 U.S.A. standard testing sieve (Tyler equivalent 100 mesh).

Disks 1.2 mm thick by 28.7 mm diameter were obtained by cold compaction of the powers in a steel die at 103 MPa. The organic binders were removed by heating in air to 600°C at 1°C/min. with a 1 hr hold at 300°C and a 2 h hold at 600°C. Dimensional and weight measurements showed that the samples after binder removal were about 57% of the theoretical density based on the reported value of 7.6 g/cm^3 for PZT-840.

Table 1. Results of Milling Study of PZT-840 and Doped PZT-840

Sample	Milling type	Milling time (h)	Mean (um)	Median (um)	S.D. (um)	Sw (cm^2/cm^3)
1[a]	Attrition	0.033	2.24	1.97	0.67	55352
1	Attrition	2	0.63	0.61	0.18	134247
1	Attrition	4	0.58	0.56	0.16	139845
1	Attrition	6	0.55	0.52	0.15	150432
2[b]	None	0	1.45	1.20	0.45	80409
2	Attrition	0.083	1.05	1.01	0.30	94909
2	Attrition	2	0.68	0.67	0.19	120945
2	Attrition	4	0.56	0.58	0.16	135512
2	Attrition	6	0.55	0.54	0.15	141063
2	Attrition	11.5	0.49	0.48	0.13	158845
2	Ball	24	0.70	0.66	0.20	124337

a. As-received PZT-840
b. PZT-840 Doped with sintering aids

The disks were sintered in closed alumina crucibles on a platinum setter with a mixture containing 10 wt % ZrO_2 and 90 wt % $PbZrO_3$ added to control the PbO vapor pressure above the samples. After sintering, the density was measured using the Archimedes method by immersion in ethyl alcohol. X-ray diffraction patterns (XRD) of the surface of the sintered disks were measured using CuK_α radiation from a Scintag PADV diffractometer. Analysis of the XRD spectra was done using the programs JADE and Shadow (Material Data Inc).

To measure the piezoelectric properties, Ag paste (Metech 3288) was screen printed on both sides of the sintered disks and the electrodes were cured at 600°C for 10 minutes. The disks were poled at 2.5 kV/mm for 10 minutes in a silicone oil bath at 120°C. The piezoelectric properties were measured at room temperature after a 24 h stabilization period. Capacitances were measured at 1 kHz and the resonant frequencies of the radial mode were measured using an impedance gain phase analyzer (Agilent 4194A). The piezoelectric constant, d_{33}, was measured using a Pennebaker model 8000 Piezo d33 tester (American Piezo Ceramics)

Results and Discussion

The rate of particle size reduction was followed during the attrition milling by measuring the particle size distribution in aliquots removed from the milled slurry. Table 1 gives the results of the milling study. The initial particle size in sample 1 was larger than that for sample 2 because different manufacturer production runs were used as starting material. It is apparent that the milling rate was similar for both manufacturer batches and that the addition of the sintering aids did not affect the milling behavior.

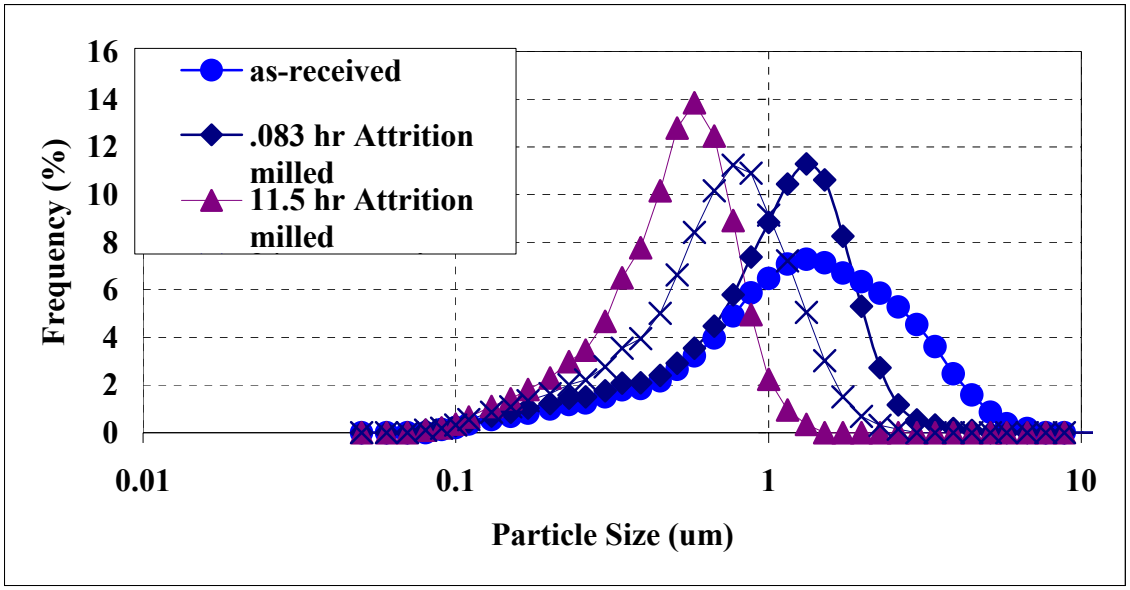

Figure 1. Effect of Milling on the Particle Size Distribution for ORNL Doped PZT-840 Powder

Figure 1 shows the change in the particle size distribution for the doped sample and is representative of that obtained with the undoped powder. The initial powder had a mean particle size of 1.5±0.5 um. Milling for 11.5 h reduced the mean particle size to 0.5±0.1 um. The particle size was quickly reduced from its initial value to about 0.55 um but then the rate of diminution decreased significantly (**Figure 2**).

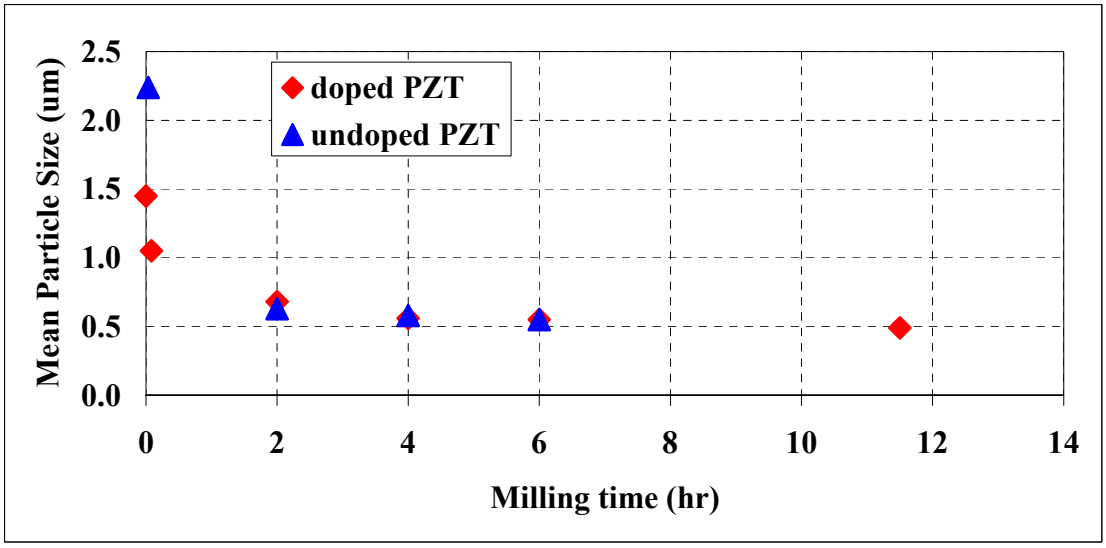

Figure 2. Effect of Attrition Milling Time on the Mean Particle Size for PZT-840

After milling, the powders were dried and the filter cakes were crushed and sieved through a 325-mesh screen. The dried sample 2 powder had a mean size of 0.53±0.15 um which shows that little, if any, agglomeration occurred during the drying process.

Uniaxially pressed disks were sintered at temperatures between 800°C and 1125°C. The density and the piezoelectric properties were measured on the sintered disks. The results are given in Table 2. The attrition milled powder sinters more rapidly to a higher density than does the ball milled powder. As-received powder does not sinter to full density at temperatures below about 1125°C, even when attrition milled. However, attrition milled powder containing the ORNL sintering aids reaches full density after 3 h at 850°C.

Table 2. Comparison of the Density and Piezoelectric Properties for Ball and Attrition Milled Doped PZT-840 Sintered Under Various Conditions

			Sintering Conditions			Piezoelectric Properties		
Id	Powder type[a]	milling type[b]	Temp (°C)	Time (h)	Density (% T.D)[c]	d_{33}[d]	Kr	Qm
172-A	1	None	1125	3	91.5	0.14	0.21	309
167-A	1	Attrition	1125	3	100.3	0.17	0.21	179
195-C	1	None	1125	12	96.6	0.17	0.28	280
195-D	1	Attrition	1125	12	101.2	0.21	0.35	195
259-C	1	None	1125	24	99.1	0.22	0.32	295
259-B	1	Attrition	1125	24	100.7	0.23	n.a.. sample broken	
175-C	1	None	960	3	64.1	Not poled – low density		
175-D	1	Attrition	960	3	63.5	Not poled – low density		
19-B	2	Ball	945	3	98.0%	0.32	0.59	805
44-A	2	attrition	945	3	101.5%	0.35	0.63	770
146-A	2	Ball	898	3	94.1%	0.31	0.54	961
200-B	2	Ball	898	24	98.9%	0.33	0.61	831
245-A	2	Attrition	898	3	101.6%	0.32	0.61	903
158-C	2	Ball	852	3	93.2%	0.26	0.47	848
250-B	2	Attrition	852	3	101.6%	0.28	0.58	977
205-B	2	Ball	852	24	98.2%	0.29	0.57	888
45-A	2	Attrition	852	24	101.5%	0.28	0.57	931
57-A	2	Attrition	800	3	100.1%	0.25	0.52	981
46-A	2	Attrition	800	24	101.0%	0.27	0.56	934

a. Type 1 is as-received powder; type 2 is doped with ORNL sintering aid A
b. Ball milled for 24 h; attrition milled for 11.5 h
c. Based on a theoretical density of 7.6 g/cm^3
d. x 10^{-9} m/V

The goal of this program is to develop a low cost actuator to be used in fuel injectors in diesel engines. Several factors in the design of the PZT active element must be considered. The cost and the size limitation on the actuator package and associated electronics are limiting. To lower the cost in the multi-layer actuator, the PZT active element must sinter to full density below the melting point of silver (960°C) so that costly Pd or Pd/Ag will not be needed as the interlayer

electrodes. To obtain the required movement of the actuator at an applied electric field suitable for use in a diesel powered vehicle, the piezoelectric strain constant (d_{33}) will need to be about 0.3 x 10^{-9} m/V and the electromechanical coupling coefficient (k_r) should be around 0.5. Furthermore, to lower the auxiliary cooling required to remove self heating of the element, a mechanical Q which is greater than 300 is desired.

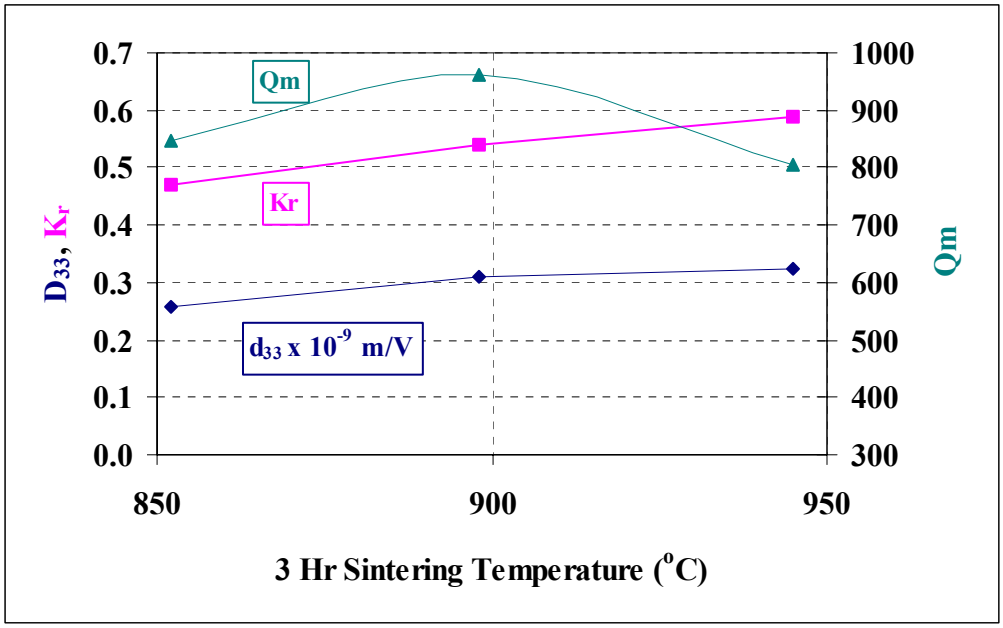

Figure 3. Electromechanical Properties for Disks of Ball Milled ORNL Doped PZT-840 Sintered for 3 h at Various Temperatures

Figure 3 and Figure 4 show the electromechanical properties of sintered disks fabricated from the ball milled and attrition milled powders doped with ORNL sintering aids. The d_{33} and the K_r increase with increasing sintering temperature, but Q_m reaches a maximum and then declines as the sintering temperature increases. Both milling techniques yield a powder that can be sintered and poled to satisfy the piezoelectric criteria described above. But, only the attrition-milled powder can be sintered to full density in 3 h at temperatures below the melting point of silver.

X-ray diffraction patterns were obtained from the surface of the sintered disks without pulverizing the disks into powders. Shown in Figure 5 is an overlay of the diffraction patterns from the disks prepared with the doped attrition milled powder. The PDF d-I line patterns for rhombohedral and tetragonal PZT and the Miller indices for some of the diffraction lines are given below the test samples patterns.

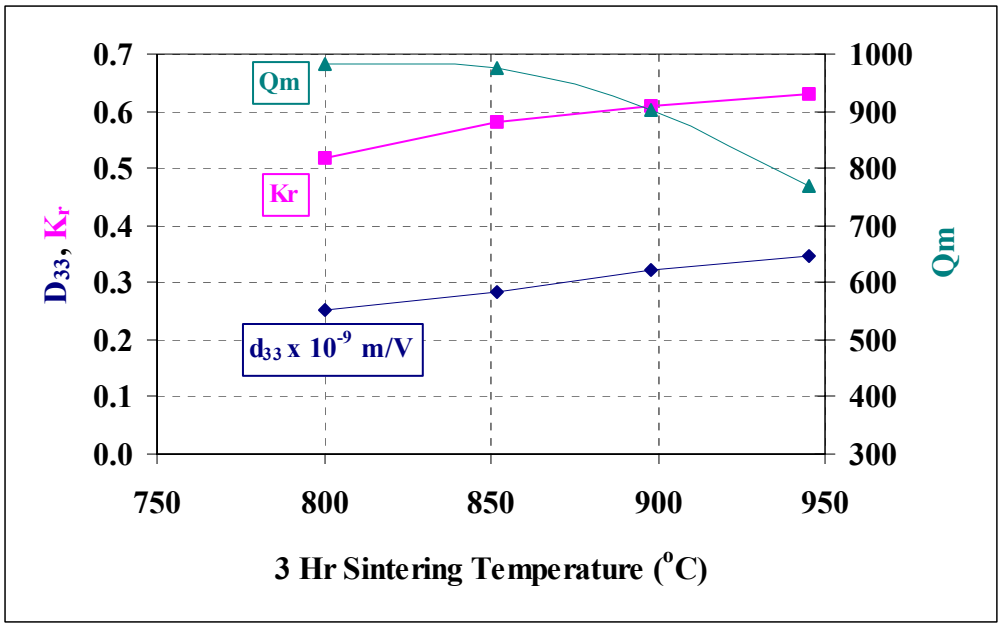

Figure 4. Electromechanical Properties for Disks of Attrition Milled ORNL Doped PZT-840 Sintered for 3 h at Various Temperatures

The small peaks at 2θ values of 29°, 37° and 43° are W_l lines caused by filament contamination on the XRD anode. The samples containing Additive A, which were sintered for only 3 h, have impurity phases present (2θ ≈16° and 27°) that has not yet been identified. This phase appears to be an intermediate compound formed during the liquid phase sintering, since it is not present in the starting powders. Furthermore, the amount of the intermediate phase decreases as the sintering temperature increases, or the dwell time at the sintering temperature is increased.

By examining the regions between the (001)/(100), (002)/(200), or the (112)/(211) diffraction lines of the tetragonal phase it is apparent that the sintering temperature is affecting the ratio of the tetragonal to rhombohedral structures. An estimate of the percentage of tetragonal PZT can be calculated from the (002) and (200) reflections of the tetragonal phase and the (202) reflection of the rhombohedral phase. The areas under these peaks were determined by deconvoluting the peak profile using a pseudo-Voigt function and the Shadow software for powder diffraction pattern analysis (Materials Data Inc.). The percent of tetragonal phase (F_t) was calculated from the following equation:[2]

$$F_t = 100 \times [A_t(002) + A_t(200)] / [A_t(002) + A_t(200) + A_r(020)]$$

Where $A_t(002)$ and $A_t(200)$ are the integrated peak areas of the tetragonal phase, and $A_r(020)$ is the integrated peak of the rhombohedral phase.

With an increase in the sintering temperature there is an increase in the rate of evolution of the tetragonal PZT phase. Between 850°C and 945°C, the amount of tetragonal phase formed in 3 h increases from around 55% to about 80%. As shown in Figure 6 the type of milling does not affect the rate of conversion to the tetragonal phase. The presence of both phases is thought to

reflect local compositional fluctuations. Examination of the $PbZrO_3$-$PbTiO_3$ phase diagram shows that the rhombohedral phase occurs in the Zr rich region and the tetragonal phase occurs on the Ti rich side of the morphotropic phase boundary. Several investigations of the phase transformations during synthesis of PZT from precursor powders have been reported. These studies have shown that the ratio of tetragonal/rhombohedral phases increases with the calcination temperature.[2] Zaghete attributes this to the fact that Pb^{2+} reacts more rapidly with compositions rich in Zr,$^{4+}$ thus preferentially yielding rhombohedral PZT.[3] As the temperature increases, Zr^{4+} ions diffuse toward the Ti^{4+} rich regions thus forming tetragonal PZT.

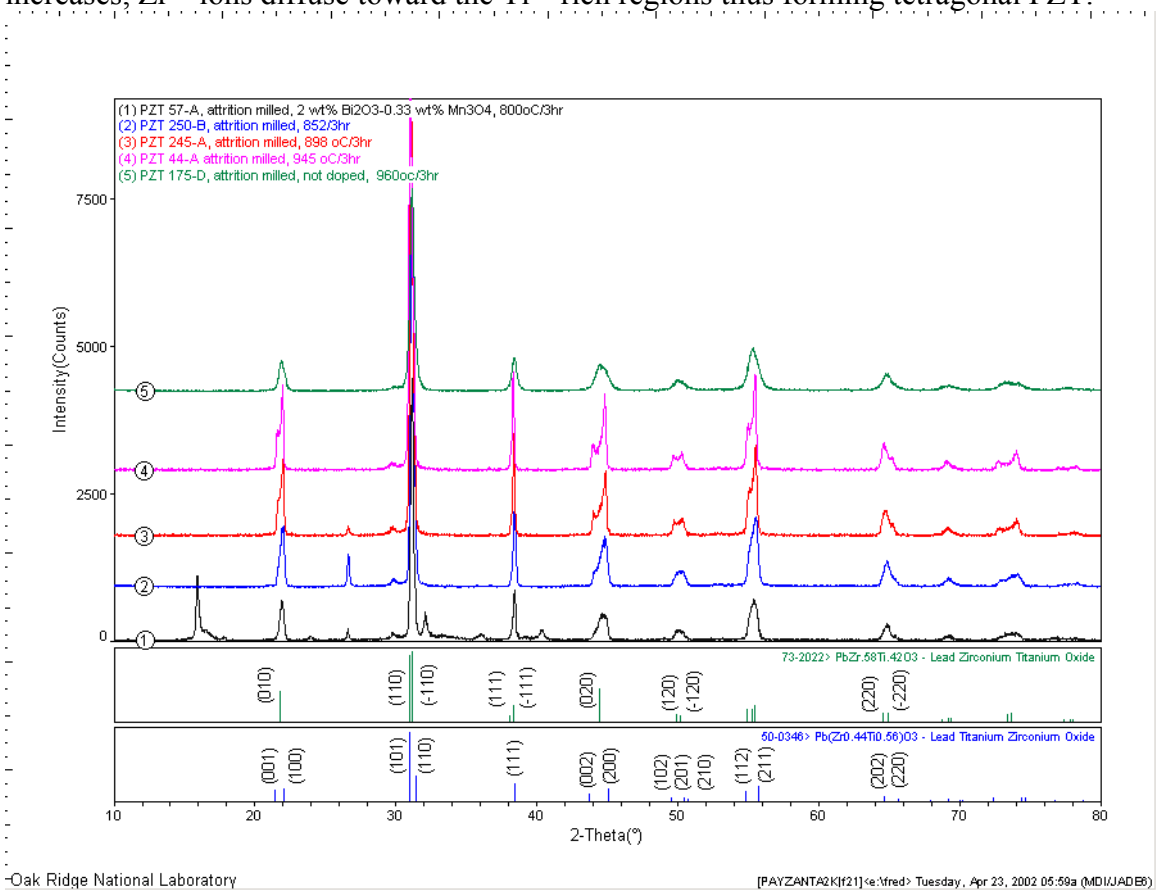

Figure 5. XRD Patterns for Attrition Milled PZT-840 Doped with ORNL Sintering Aids after Sintering for 3 h at Various Temperatures.

In ORNL doped PZT-840, the presence of the liquid from the sintering aid is crucial to forming the tetragonal phase at low sintering temperatures. In Figure 5, the top curve shows the XRD pattern obtained from a disk of attrition milled undoped PZT-840 powder that was annealed at 960°C for 3 h. Without adding a low temperature sintering aid, the rhombohedral phase predominates.

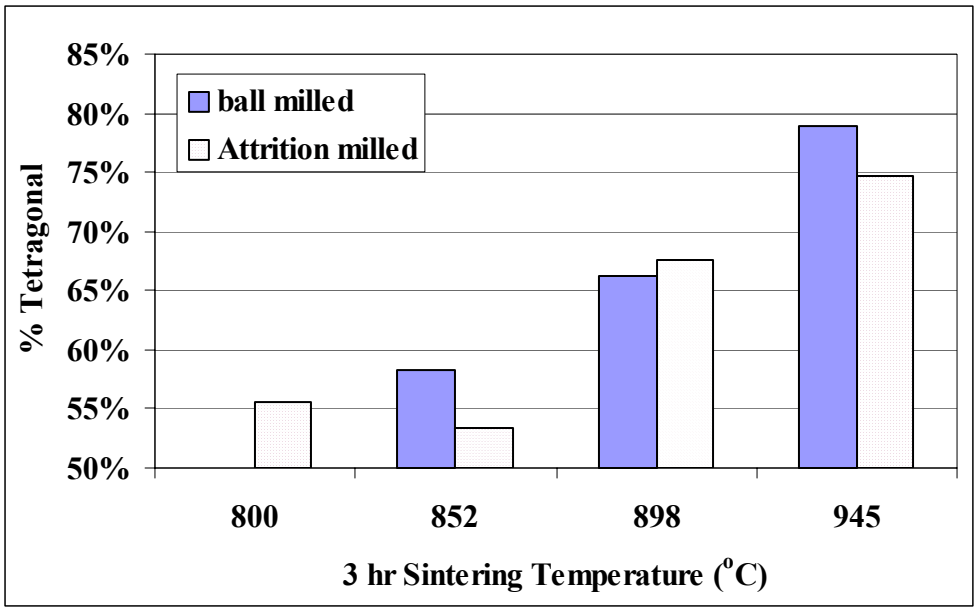

Figure 6. Percent of Tetragonal Phase in ORNL Doped PZT-840 after Sintering for 3 h at Various Temperatures

A study of the microstructure development in both ball milled and attrition milled PZT-840 powders is currently underway. Preliminary results are discussed here. The final results of the study will be reported in the next quarterly report. Figure 7 shows the microstructure of attrition milled powder after sintering. The average grain sizes were computed using the grain boundary intercept method. The average size was 2.0±0.2 um after sintering for 3 h at 850°C and it was 2.2±0.2 um after sintering 3 h at 900°C.

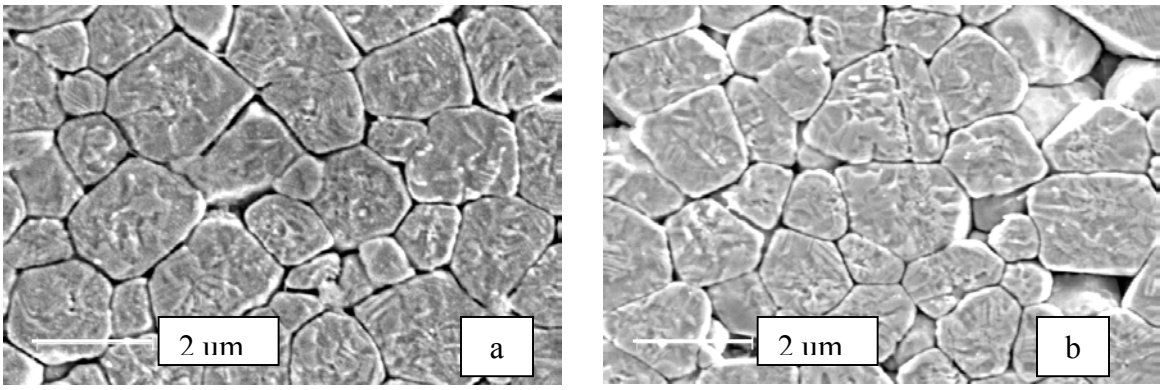

Figure 7. SEM Photomicrograph Showing the Microstructure of Attrition Milled ORNL Doped PZT-840 Sintered for 3 h at (a) 900°C and (b) 850°C.

Task 3. Static and dynamic testing of flexure amplified piezo stack actuator

A paper study is underway to compare amplifier designs, including both flexural and hydraulic-diaphragm types. There are no results to present in this report.

Status of Milestones

1) Evaluate and characterize commercially available PZT materials. Seek methods to improve the properties of these materials through alternative processing and forming methods. Fabricate new PZT compositions that allow sintering of the PZT materials at lower temperatures.
Status: The evaluations of new commercial materials and low temperature PZT materials are in progress.

2) Fabricate new PZT compositions to seek improvement in the electrical and mechanical properties. More specifically, research work will center on dopants that increase toughness of PZT materials.

Status: A literature search is underway regarding agents to help toughen and strengthen PZT materials. Biaxial strength tests have been performed on some low temperature sintered PZT materials.

3) Use ORNL expertise in motion amplifier devices to design and fabricate motion-amplifying fixtures for fuel injector assemblies. A paper study will be conducted to compare the advantages of fluid-mediated diaphragm amplifiers versus machined, bending structures.
Status: A paper study is in progress.

References

[1] D. W. Richerson, Modern Ceramic Engineering: Properties, Processing, and Use in Design, Boothroyd G, and G. E. Dieter, Eds., Marcel Dekker: New York, 1982, p163.

[2] Leite, E. R., Cerqueira, M., Perazoli, L. A., Nasar, R. S., Longo, E., and Jose Varela, "Mechanism of Phase Formation if Pb(ZrxTi1-x)O3 Synthesized by a Partial Oxalate Method," J. Am. Ceram. Soc., vol. 79 (6), 1563-68 (1996).

[3] Zaghete, M. A., Santos, C. O. P., Varela, J. A., Longo, E. and Y. P. Mascarenhas, "Phase Characterization of Lead Zirconate Titanate Obtained from Organic Solutions of Citrates," J. Am. Ceram. Soc., vol. 75 (8), 2088-2093 (1992).

Low-Cost Manufacturing Processes for Ceramic and Cermet Diesel Engine Components (SIU-C)

D. E. Wittmer
Southern Illinois University

Objective/Scope

The purpose of this work is to investigate the potential of low-cost manufacturing processes for ceramic and cermet diesel engine components. The primary task is to develop cost effective processing, forming and sintering methodologies for cermet and ceramic formulations, used by industrial diesel engine manufacturers.

Technical Highlights

Task 1. Collaboration with industrial partner(s).

This task involves the collaboration with industrial partners to assist them in processing and sintering of their diesel engine components. Our goal is to provide assistance in processing and sintering which may result in a reduction in surface reactions and part warping. Moreover, this may also provide an alternative sintering process that will allow improved throughput efficiency and manufacturing economy. Due to the proprietary nature of this task, any research data generated from this task is normally controlled by the terms of each specific confidentiality agreement. The reporting of this data and any results are the responsibility of the industrial partner(s).

Task 2. Cost Effective Processing and Sintering

Sintering

During this reporting period, work has continued on intermetallic bonded TiC with the primary objectives of comparing pre-alloying to reaction sintering, isopressing to not isopressing, and pre-sintering to no pre-sintering. Both batch sintering, with a vacuum-low pressure cycle (V-LPHIP), at ORNL and continuous sintering at SIUC continue to be used for sintering comparisons. The formulations were all 40 vol % intermetallic with 60 vol % TiC. For injection molding, the binder ratio was 55:44:1 (petroleum jelly:paraffin wax:stearic acid) and the injection molding temperature was 160EF at a pressure of 60 psi. The powder sources for this research are given in Table 1 and the formulations along with the composition identification are given in Table 2.

During this reporting period, several rods of reaction sintered, NA4RH and NA20F4RH were sintered at ORNL by the V-LPHIP method at 1450EC. The NA4RH in both the isopressed and non-isopressed state sintered to 100% of theoretical, while the NA20F4RH sintered to 99.5% of theoretical. The rods from these sintering trials have been sent out for machining. Problems were encountered in the continuous sintering of these same formulations due to a problem with the liquid Argon supplier. It is expected that continuous sintering trials will be completed during the next reporting period.

Low Pressure Injection Molding

Work is continuing to try to optimize low-pressure injection molding for processing simple shapes. Minimizing internal defects of injection-molded rods has be a goal from the start of this task. We have made significant improvements in elimination of voids that form near the centerline of the injection molded rods.

During this reporting period, new vendors and powder sources were selected for the nickel and chromium powders, primarily to improve the flow characteristics and to reduce the cost. The cost was reduced by a factor of about 10 for the Cr powder from ACu Powder International and for the spherical Ni powder produced by Novamet. In addition the use of these powders has allowed the binder content to be reduced by about 3 vol %, thereby increasing the solids loading of the injected parts. By reducing the binder volume, it was also possible to burn out the binder following the same 24 h cycle used previously, without the presence of the sand bed. These alterations have lead to improved injection properties and reduced burnout defects, compared with previous trial results.

Extrusion

During this reporting period preliminary extrusion trials were conducted using the same binder system as that used for low-pressure injection molding. The hot-water supply provided an inconsistent temperature control over a long period of time. Increasing the water temperature to the highest control temperature failed to allow proper flow of the feedstock. Changes in the feedstock binder and the hot water supply are being investigated. The extruder is shown in Figure 1.

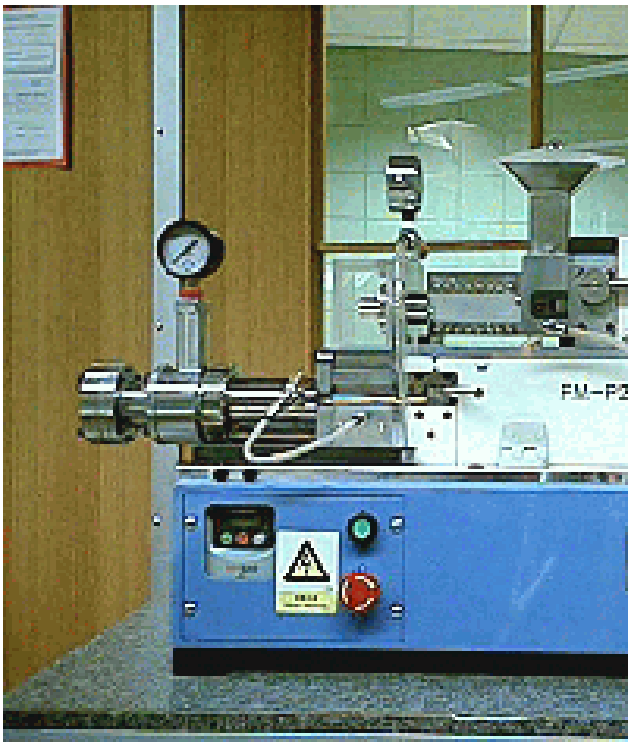

Table 1. Source and description of powders used.

	Manufacturer	Product ID	Particle Size (μm)
TiC	H.C. Starck	CAS	1.2-1.5
Ni_3Al	Homogeneous Metals Inc.	IC50 -325 mesh	<44
NiAl	Xform	-325 mesh	<44
Ni:Cr:Fe	Alfa Aesar	36604	<44
Ni:Cr	Alfa Aesar	13108	44-106
Ni	Novamet	type 123	3.6
Cr	Alfa Aesar	41797	<10
Fe	Alfa Aesar	00170	<10
B	Cerac	B-1119	<1.0

Table 2. Formulations of cermets investigated by constituent.

	Powders								
	TiC	**Ni_3Al**	**NiAl**	**Ni:Cr:Fe**	**Ni:Cr**	**Ni**	**Cr**	**Fe**	**B**
NA4PH	60	40	-	-	-	-	-	-	-
NA4RH	60	-	21	-	-	18.9	-	-	0.1
NA20F4PH	60	20	-	-	-	-	-	20	-
NA20F4RH	60	-	10.4	-	-	9.4	-	20.1	0.1
NC4PH	60	-	-	-	40	-	-	-	-
NC4RH	60	-	-	-	-	30.5	9.5		-
NCF4PH	60	-	-	40	-	-	-	-	-
NCF4RH	60	-	-	-	-	29	7.6	3.4	-

Status of Milestones

1. Collaboration with Industrial Partners — On Schedule
2. Cost Effective Processing and Sintering — On Schedule

Communications/Visits/Travel

D. E. Wittmer to ORNL to participate in meeting with Cummins and CoorsTek.

Problems Encountered

Problems with liquid Ar supplier.

Publications and Presentations

J. Hazelwood and D. Wittmer, "Low-Pressure Powder Injection Molding of Ceramic-Metallic Composites," Research Day at Southern Illinois University, Sigma Xi,
March 25, 2002 (poster session)

Low Cost-High Toughness Ceramics

T. N. Tiegs, F. C. Montgomery, and P. A. Menchhofer
Oak Ridge National Laboratory

Objective/Scope

Significant improvement in the reliability of structural ceramics for advanced diesel engine applications could be attained if the critical fracture toughness (K_{Ic}) were increased without strength degradation. Currently, the project is examining toughening of ceramics by incorporation of ductile intermetallic phases.

Technical Highlights

Previous studies have shown that the properties of the aluminide-bonded ceramics are attractive for diesel engine applications and consequently, development of these materials was started. At the present time, TiC-based composites with 40-60 vol % Ni_3Al are being developed because they have expansion characteristics very close to those for steel. Preliminary wear testing indicated that improved wear resistance could be achieved by decreasing the grain size of the TiC. Achieving fine grain size with the high binder contents is difficult because of the large inter-grain distances. In addition, it was thought that changing the TiC grain shape from a highly faceted one to a more rounded equiaxed grain would reduce localized stress at sharp corners. This, in turn, would improve abrasion resistance from any wear debris. Consequently, grain size refinement is presently being studied. Several approaches can be used to control the final TiC grain size. The methods studied in the present report include: (1) use of additives to change the interface behavior of the growing TiC grains, and (2) reduction of the initial TiC particle size. The development effort is being done in collaboration with CoorsTek, Inc.

Large Batch Processing of TiC-Ni_3Al Composites - The series of large batches (≥2 kg) discussed in the previous progress report to investigate batch-to-batch variations, milling conditions, use of alternate binders/dispersants, and addition of grain growth inhibitors was continued.

In the past reporting period, approximately 10 kg of milled composite powder (Composition #10 in Table 1) were supplied to CoorsTek, Inc. for fabrication into long rod shaped specimens. After isopressing into shape, the specimens were bisque fired and returned to ORNL. The bisque firing was necessary to provide adequate strength to survive shipping back to ORNL. These were sintered at ORNL using the standard vacuum/low-pressure hot-isostatic pressing cycle used on all previous batches. A total of 10 sintering runs were preformed to provide enough material for component testing. After sintering, the samples that had high densities (≥ 98% T. D.) were sent out for machining into test components.

To complete the study on effects of additives on the wear properties, additional large batches of compositions were fabricated (#14 and #15). The compositions are given in Table 1. The Mo additions have been utilized in the past to improve the flexural strength. The TaC addition has been shown in previous small batches to improve the hardness of the cermets. B_4C has also been shown to improve the hardness of the cermets and boron is a known additive to increase the ductility of the Ni_3Al. Previous work has shown that Fe additions increase the room temperature

strength, but more importantly Fe has been shown to be very effective at changing the shape of the TiC grains. These compositions are currently being sintered.

Grain Refinement by Multiple Additives - Based on the previous results which showed the effects of individual additives, more samples are being fabricated that will examine the behavior of multiple additives. The compositions are shown in Table 2. The ZrC addition is used to refine the grain size, round the grains, and to improve the strength. The DC-2002-4 composition uses just Ni and Al for the reaction synthesis of the Ni_3Al. All previous work used a combination of Ni and NiAl for the Ni_3Al. Because the costs of the starting raw materials for Ni and Al are low, this avenue for fabricating the cermets is of interest.

Status of Milestones
On schedule.

Communications/Visits/Travel
Travel by T. N. Tiegs to Cocoa Beach, FL, Jan. 13-17 to attend American Ceramic Society Conference on Ceramics and Composites and present paper.

Travel by T. N. Tiegs to Seattle, WA, Feb. 17-21 to attend TMS Society Conference on Advanced Materials and present paper.

Problems Encountered
None.

Publications
None.

Table 1. Summary of large batch processing variables for different TiC- Ni_3Al composites.

Batch No.	Ni_3Al Content (vol %)	Grain Growth Inhibitor (w. %)	TiC Milling Time (min.)	Metal Milling Time (min.)
#10	50	2% Mo*	90	30
#14	50	4% TaC	90	30
#15	50	1% Mo*, 2% TaC*, 0.1% $B_4C^{\dagger}$, 1% $Fe^{\dagger}$	90	30

* Percent based on TiC content.
† Percent based on Ni_3Al content.

Table 2. Summary of processing variables for different TiC- Ni_3Al composites that will examine the effects of multiple additives.

Batch No.	Ni_3Al Content (vol %)	Additives (w. %)*	TiC Milling Time (min.)	Metal Milling Time (min.)
2001-1	50	2 Mo, 2 TaC	60	20
2002-2	50	2 Mo, 2 TaC, 2 Fe	60	20
2002-3	50	2 ZrC	60	20
2002-4	$50^{\dagger}$	2 Mo	60	20

* Percent based on TiC content.
† Ni_3Al derived from reaction of Ni and Al precursors.

Synthesis of Powders TiC and Nickel Aluminide

Alan W. Weimer, PI
University of Colorado

Task 1: Synthesis of Titanium Carbide

TiC Kinetics Modeling:

The carbothermal reduction of titania with carbon black had previously been studied in a prior ORNL supported project using a thermogravimetric analyzer (TGA) capable of monitoring the weight change of a sample with microgram sensitivity. In an effort to characterize the reaction, those data were used to develop a kinetic model of the reaction that could be useful for TiC/Ni_3Al (or TiC/NiAl) composite synthesis. Other researchers have modeled the synthesis of carbides and other ceramics using a variety of kinetic expressions, including product layer diffusion control, phase boundary reaction control, nuclei growth control and order of reaction[1].

For the TGA data, an Avrami kinetic model (nuclei growth control) was chosen due to the physical model of particle growth inherent in the equations. The Erofeyev form of Avrami kinetics is given in Equation 1.

$$-(kt)^m = \ln(1-X) \qquad (1)$$

In this expression, k represents an Arrhenius rate constant, t is the time, and X is the conversion. The Avrami constant, m, indicates the order of the time dependence of the nucleation and the number of growth directions.[2] The data were fit by minimizing the sum of squared error using a 4th order Runge-Kutta scheme on the differential form of the kinetic expression (Equation 2).

$$\frac{dX}{dt} = (1-X)km(kt)^{m-1}\left[1 + t\frac{E_a}{RT^2}\frac{dT}{dt}\right] \qquad (2)$$

The variables in Equation 2 have the same meaning as those in Equation 1, with E_a representing the activation energy associated with the rate constant, k, and R being the gas law constant. One mathematical limitation of the Avrami-Erofeyev expression is that the derivative of temperature with respect to time must be positive for the model to make mathematical sense. When it is negative, the model will predict that the reaction proceeds in the reverse direction.

Figures 1 – 8 show the modeling results for eight TGA runs. All experiments were conducted at a nominal heating rate of 30 K/min, although the actual heating rates varied slightly. The variables during each experiment were the excess carbon content of the feed (either 65, 100, or 135%) and the maximum temperature (either 1623, 1773, or 1923 K). Since excess carbon content does not figure into the reaction model, those runs served as replicates for the model. The vertical lines represent the point at which the time derivative of temperature is no longer positive, and therefore where the model is no longer applicable. The model results are represented by the triangles. The modeled data is based on the average of the best-fit kinetic constants found for each run. The best-fit Arrhenius pre-exponential is $3.5 \times 10^{-7}\ s^{-1}$, and the value of E_a/R is 2200 K.

In most cases, the model predicts the light-off time for the reaction fairly well. The best fits are obtained when the maximum reaction temperature is 1923K, and the worst are obtained at a maximum reaction temperature of 1623 K (recall that the model is only mathematically applicable when the derivative of temperature with respect to time is positive). For the purposes of modeling, therefore, experiments should be run with an increasing temperature profile over the course of the reaction. The model does not do well with any changes in the heating rate.

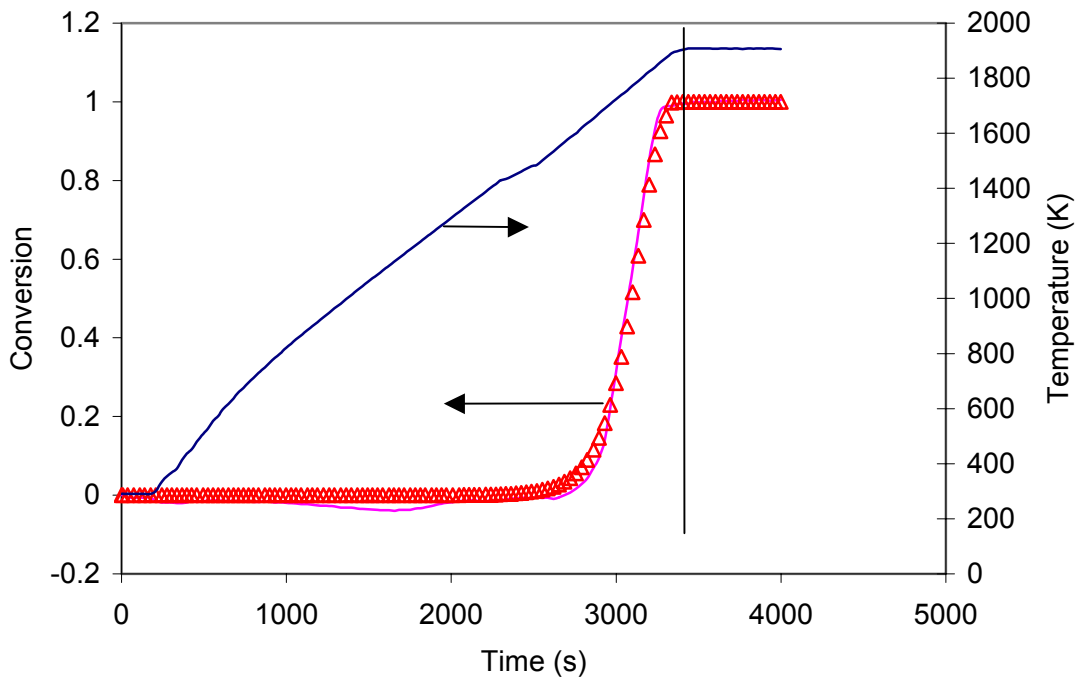

Figure 1. Model fit for 65% excess carbon and T_{max} = 1923 K

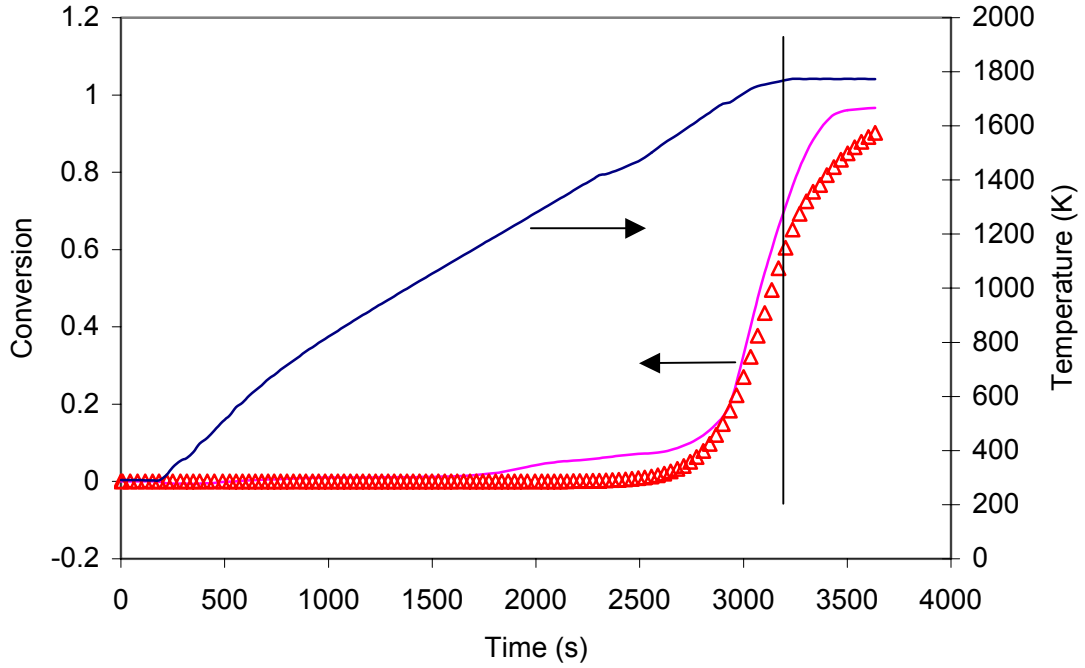

Figure 2. Model fit for 65% excess carbon and T_{max} = 1773 K

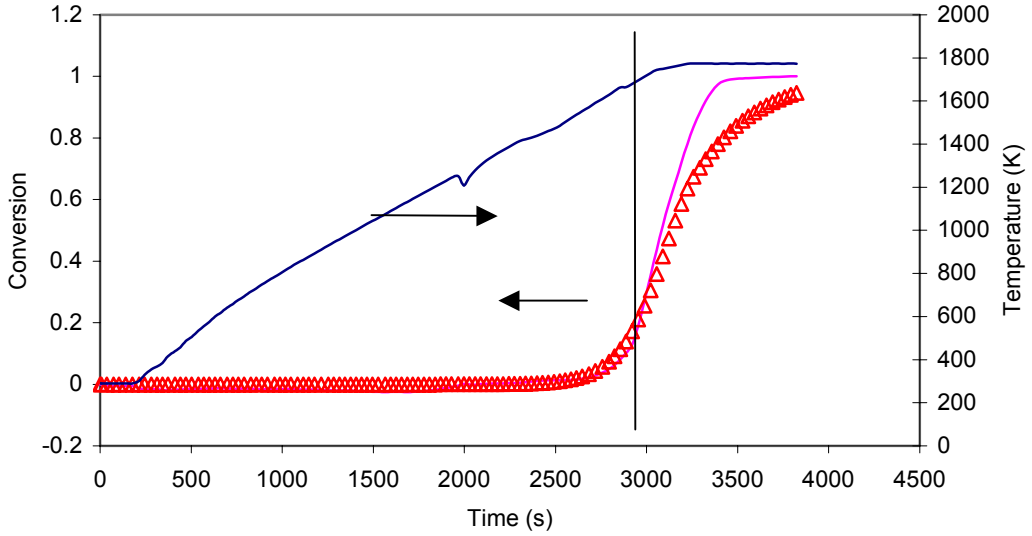

Figure 3. Model fit for 65% excess carbon and T_{max} = 1773 K

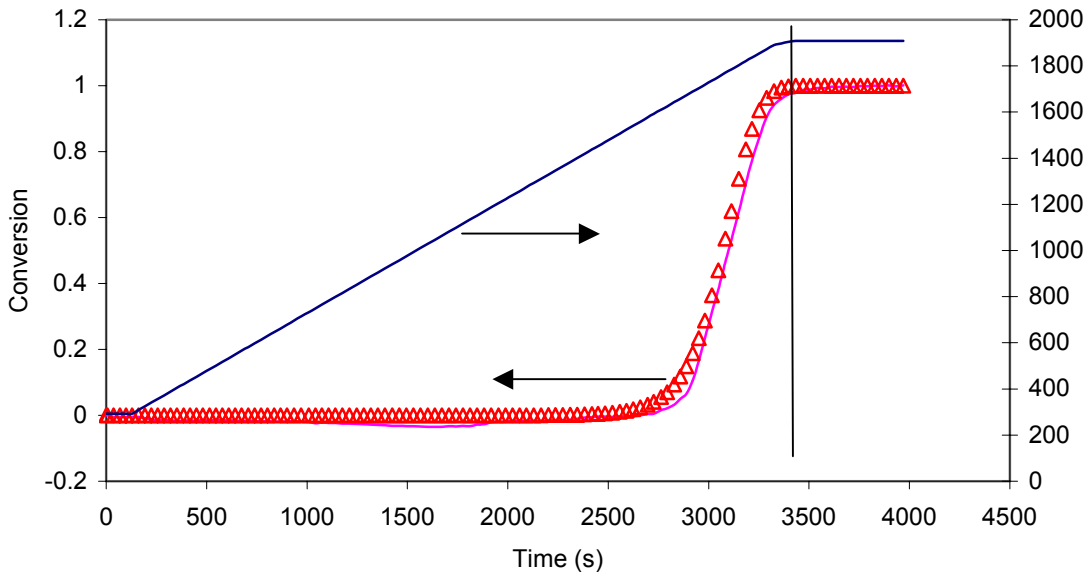

Figure 4. Model fit for 100% excess carbon and T_{max} = 1923 K

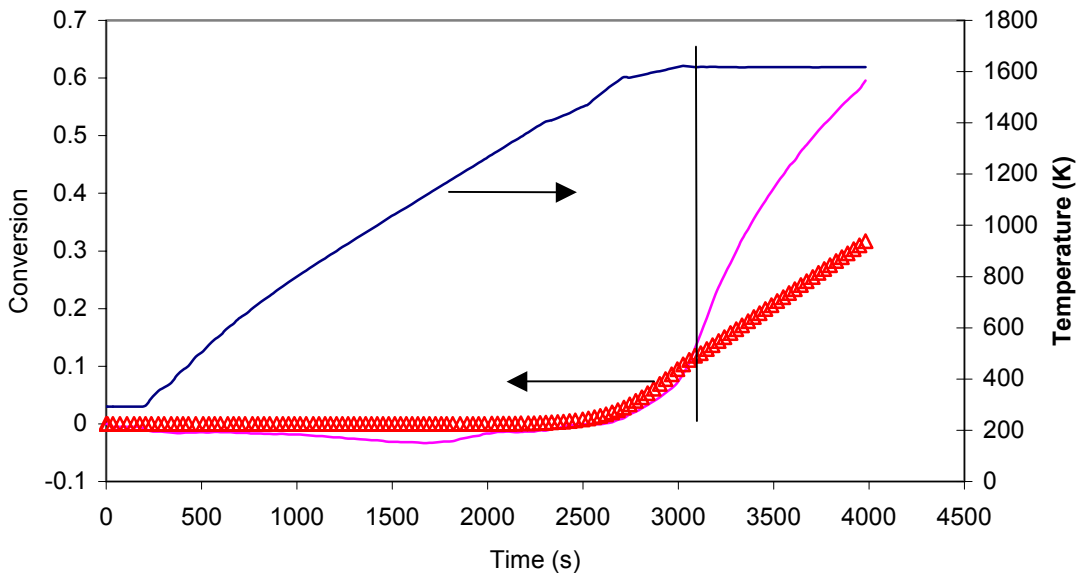

Figure 5. Model fit for 100% excess carbon and T_{max} = 1623 K

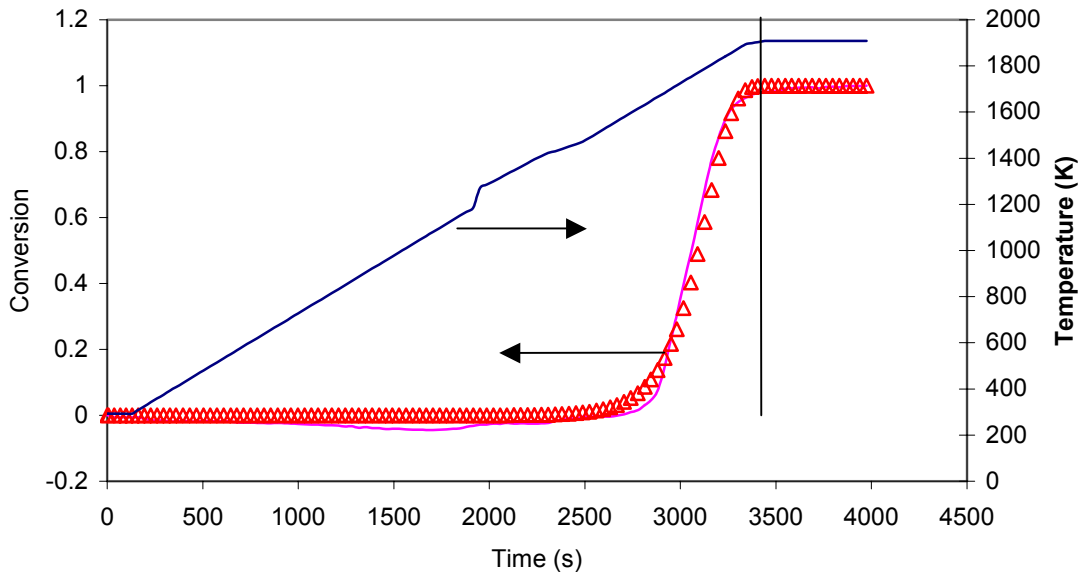

Figure 6. Model fit for 135% excess carbon and T_{max} = 1923 K

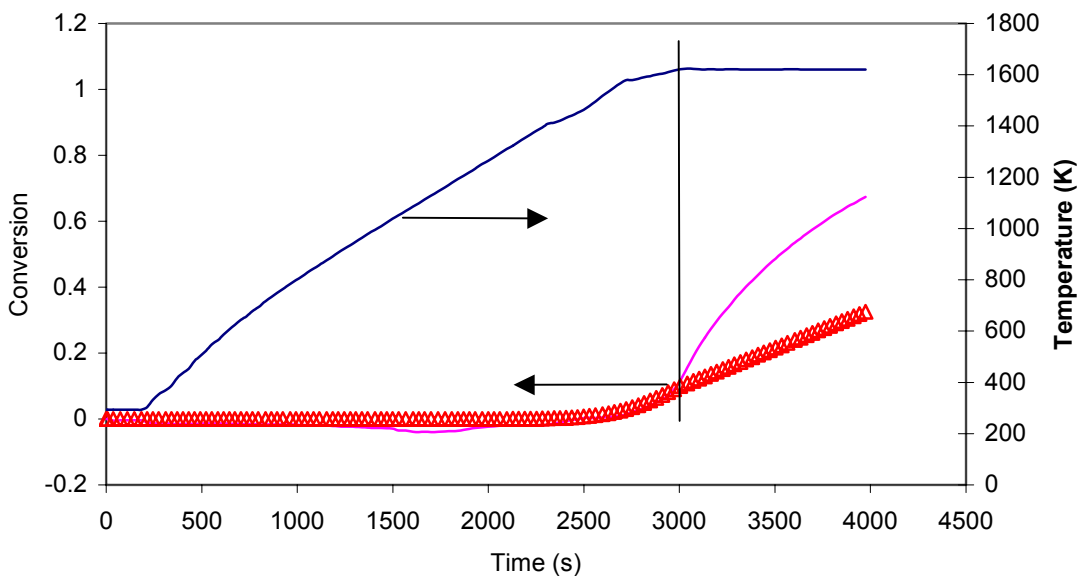

Figure 7. Model fit for 135% excess carbon and T_{max} = 1623 K

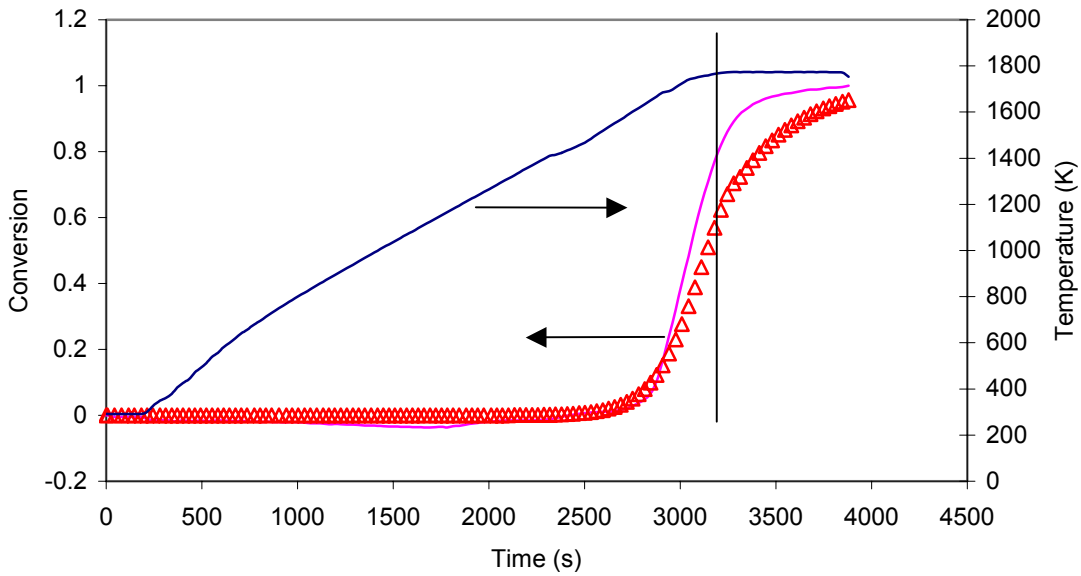

Figure 8. Model fit for 135% excess carbon and T_{max} = 1773 K

Task 2: Synthesis of Nickel Aluminide

Nickel Aluminum TGA experiments:

Introduction

Intermetallics often possess new and useful physical properties for the realms of industry and engineering, including greater strength, higher melting points, and better corrosion resistance than common alloys. While alloys are a simple mixture of metals, intermetallics are comprised of definite atomic formulas, such as Ni_3Al. Some intermetallics are even dubbed "superalloys" because of their extraordinary strength and their high thermal and electrical conductivity. However, their heat resistance and low ductility are similar to ceramic materials[3].

As a superalloy, nickel aluminum (NiAl or Ni_3Al) is a desired intermetallic for a variety of applications, including die-casting and glass making molds, superconductor substrates, diesel engine inserts/pre-burner chambers, incinerator liners, heat exchangers and high temperature/oxidation resistant coatings[4]. Hot pressing these parts requires a fine powder of nickel aluminum. The current method of synthesis (the Exomelt process) produces a solid brick of nickel aluminum that must be milled into a fine powder[5]. Due to the cost and time associated with this process, it is desirable to develop a process for directly synthesizing powdered nickel aluminum.

Powdered synthesis of nickel aluminum is currently difficult due to the low melting point of aluminum. When powdered aluminum is heated to its melting point to start a nickel aluminum reaction, the aluminum particles often gather and coalesce into relatively large droplets of aluminum metal and can remain unreacted. The use of diluents may combat the coalescence of aluminum. The purpose of this research was to investigate whether a nickel aluminum diluent can be used to make powdered synthesis feasible.

Background

Nickel aluminum is currently used for many facets of industry, the driving reason being its unique combination of properties. Current methods of production involve reacting liquid nickel and aluminum metals. The aluminum melts first, at around 660°C, and then proceeds to react with the nickel. The heat released during the reaction then melts the remaining nickel in the mixture. As the reaction approaches completion, the new intermetallic compound cools to a solid. While this process is very successful in the synthesis of nickel aluminum, it results in a solid brick of NiAl that must be milled into powder.

A carrier material acting as a diluent solves this problem. Union Carbide Corporation[6] developed a way of dealing with such heat and melting issues when synthesizing aluminum nitride from powders. Union Carbide uses 30-50% diluent in their processes. A similar method and amount of diluent may be applicable for nickel aluminum. By adding a small amount of nickel aluminum powder to the nickel and aluminum reactant mixture, a desirable effect is achieved. The nickel aluminum already in the mix provides a surface for the molten aluminum to coat, as opposed to the aluminum coalescing into droplets. The added nickel aluminum also serves to absorb some of the heat from the exothermic reaction.

Methods

Reactions were performed in a Theta Industries thermogravimetric analyzer (TGA). Reactant powders were prepared in both stoichiometric variations of NiAl and Ni_3Al, with powder ratios of 1:1 and 3:1, nickel to aluminum, respectively. The proper diluent (NiAl or Ni_3Al) was added to each powder reactant ratio. Diluent effect was tested with three amounts of diluent, 10, 30, and 50 mass percent. Each experiment was run twice, giving a total of 12 experiments, run in random order. Four runs were done without diluent, two of each NiAl and Ni_3Al.

Powders were prepared by first calculating all needed masses for powders of proper ratios and diluent concentrations. These amounts were measured to milligram accuracy and placed in vials. Each vial was then vigorously shaken for a period of a few minutes. An alumina crucible was used to hold the sample in the TGA. To prevent cracking of the crucible from thermal expansion during the course of the reaction, a small bed of powdered alumina was placed in the crucible. In addition to preventing cracking, it was hoped that the alumina would prevent the nickel aluminum from sintering to the crucible.

For each run, approximately .09 grams of reactant was heated at 30°C per minute. Heating stopped when the furnace reached 700°C, and then cooling began, at 30°C per minute. The reasoning behind this heating scheme is to provide just enough heat for the aluminum to melt. Once the aluminum melts, it coats and comes in close contact with the nickel and reacts. Aluminum melts at 660°C, therefore 700°C is a sufficient temperature to reach and ensure melting of all the aluminum reactant.

Products were then placed in individual vials and stored for analysis. Products were analyzed by x-ray diffraction (XRD) and scanning electron microscopy (SEM). XRD was taken to ensure the abundance of nickel aluminum in the product. SEMs were gathered to examine particle sizes and morphology. Because of the small samples sizes for the product nickel aluminum, standard

particle sizing techniques like BET surface area or particle size distribution measurements were not feasible.

Results and Discussion

A dramatic effect on particle size through use of diluent was observed through SEM. Images showed that particles synthesized with diluent particles were two orders of magnitude smaller than particles synthesized without diluent. The reaction of NiAl with no diluent produced very round particles that appear to have formed through coalescing (Figure 9). This is what was expected to happen if powders were simply heated. The aluminum most likely coalesced with other molten aluminum to produce somewhat spherical particles ranging from 50 to 150 microns. The physical appearance of this product also supported what appears in the SEM. The product resembled small metal spheres, some large enough to gauge their size by the human eye, upwards of 400 microns. The size difference can be attributed to the amount nickel the aluminum encountered: the larger the particle, the more aluminum that came in contact before reacting.

Nearly the same result is true for the 3:1 ratio product of Ni_3Al. Figure 10 shows the SEM for Ni_3Al with no diluent. Particle sizes are mainly around 50 microns in this sample. This is explained by the increased amount of nickel in the sample. With three times as much nickel as the previous sample, the nickel acts somewhat as a diluent by providing a surface for molten aluminum to coat instead of coalesce. The mass seen in the middle of Figure 10 is just an agglomerate of smaller, 50-micron particles.

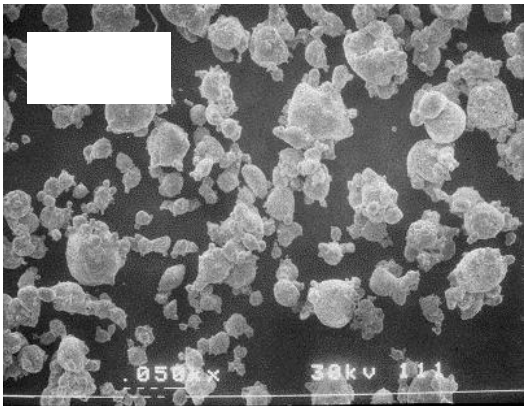

Figure 9. (NiAl without diluent)

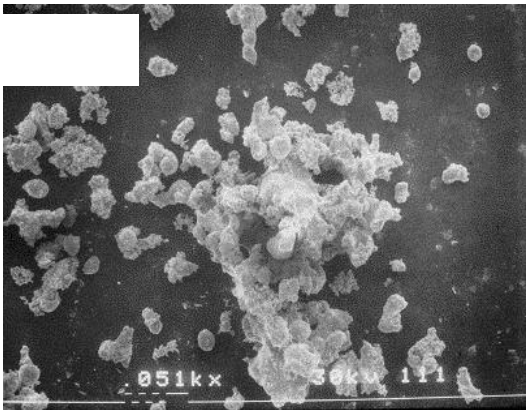

Figure 10. Ni_3Al without diluent

Diluent made a drastic difference on the size and appearance of the samples. When diluent was added to 1:1 NiAl the physical appearance changed from small metal spheres to that of a powder. When removed from the crucible, each product was in a small clump. Once a clump was transferred to a vial and shaken gently it was quickly broken up. When NiAl with diluent was shaken it reduced to a fine powder, and the SEM image confirms this (figure 11). In the SEM a much smaller group of particles is observed. The diluent has done what was intended and reduced the particle size.

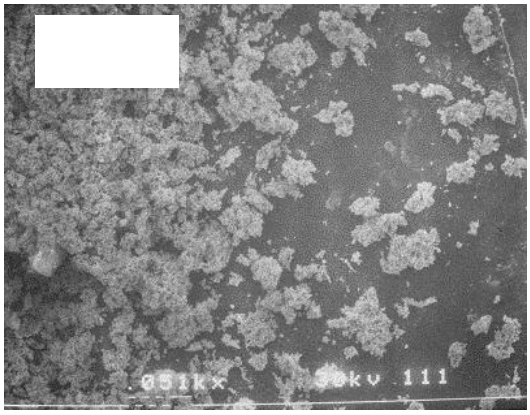

Figure 11. (NiAl with 30% diluent)

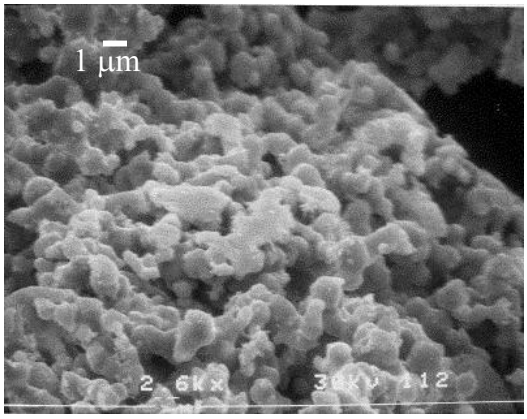

Figure 12. (NiAl with 30% diluent zoom)

Figure 12 illustrates just how much particle size was reduced. This SEM is a taken at 2600x magnification of the same sample as figure 11. With this SEM it can be seen that most particles in the agglomerate are about 1 micron in size. XRD analysis for this sample confirmed the identity of nickel aluminide. XRD also indicates some unidentified species. Further investigation will be done to discover the identity of this unknown.

Nickel aluminum in a 3:1 ratio exhibited identical behavior to that of its 1:1 counterpart. When diluent was added to Ni_3Al, particle size was reduced. Figures 13 and 14 show Ni_3Al with 10% diluent added at 50x and 2600x magnification. These agglomerated particles are about 1 micron in diameter as well. This sample was also easily reduced to a fine powder by a series of quick shakes while in a vial.

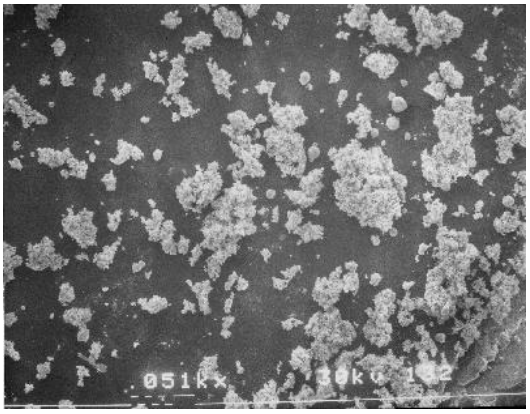

Figure 13. (Ni_3Al with 10% diluent)

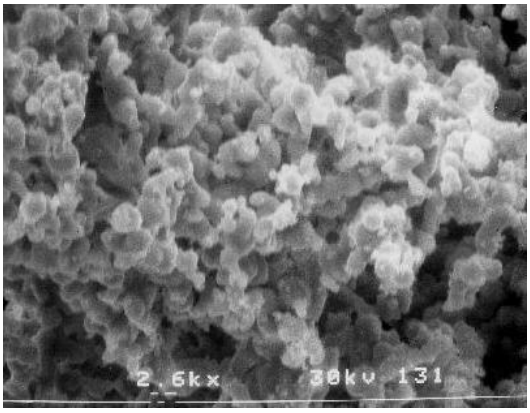

Figure 14. (Ni_3Al with 10% diluent zoom)

SEM micrographs of the remaining samples (Figs. 15 – 18) indicate similar sizing patterns except for 1:1 NiAl with 10% diluent. In that sample it appeared that the amount of diluent added was not enough to overcome coalescing effects of the aluminum. This

coalescing is not seen in 3:1 NiAl with 10% diluent, however, and is most likely attributed to the extra surface area provided by the nickel.

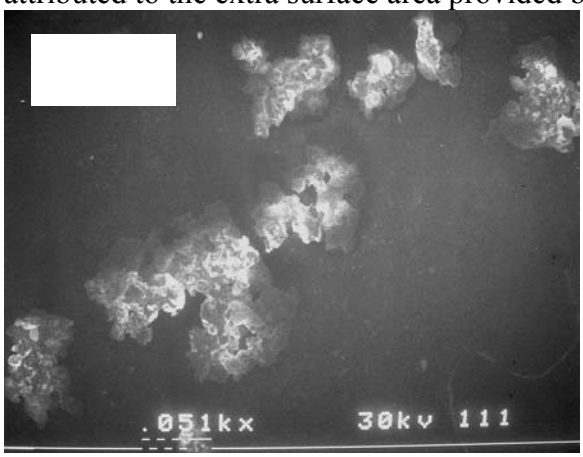

Figure 15. (NiAl 10% diluent)

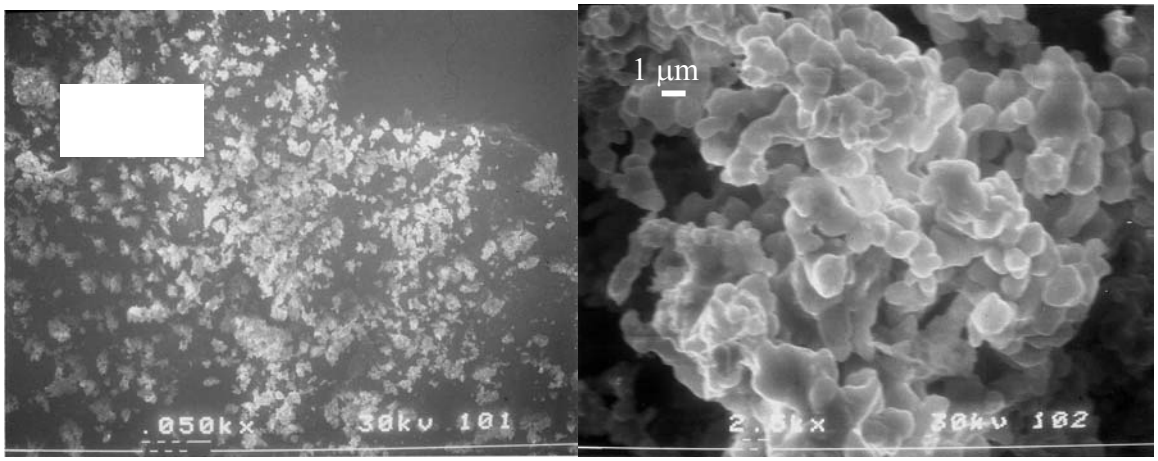

Figure 16. (Ni_3Al 30% diluent)

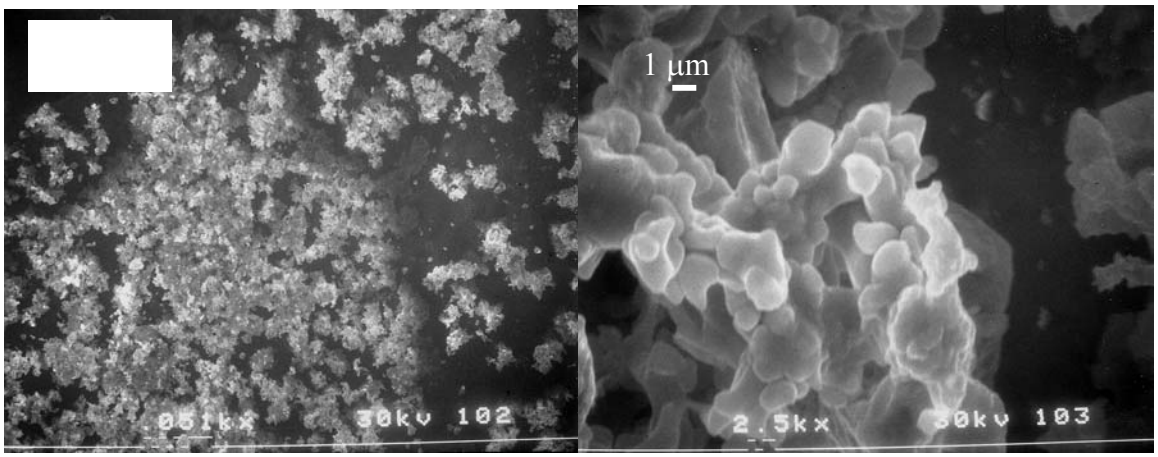

Figure 17. (NiAl 50% diluent)

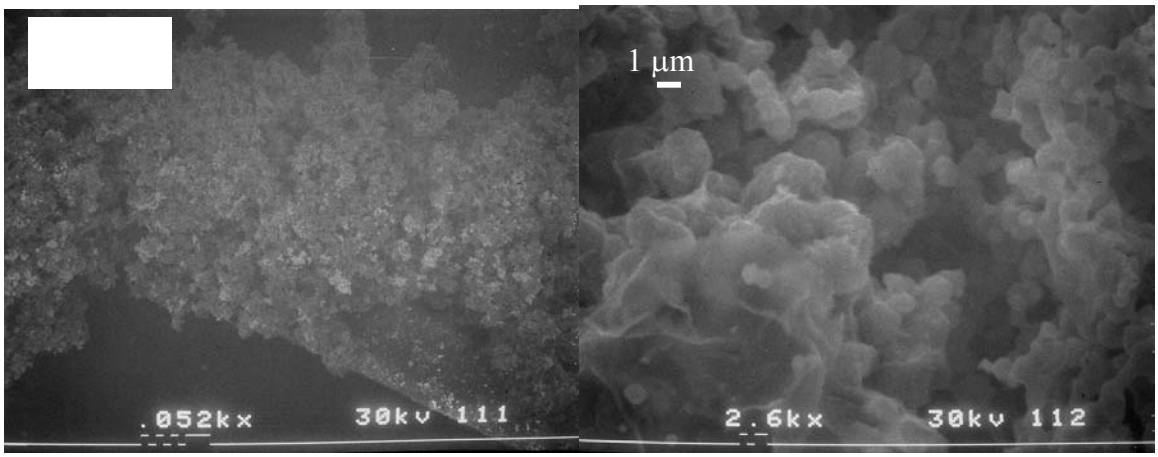

Figure 18. (Ni_3Al 50% diluent)

Figure 19 shows the DTA data collected during a sample experiment. The graph shows furnace temperature and DTA thermocouple microvoltage as a function of time. A reading is gathered by comparison of a reference cup to a sample cup. If an exothermic reaction takes place in the sample cup, thereby heating it, a positive difference in microvoltage will be observed. Broad, asymmetrical peaks are usually due to temperature lag between the two cups. Sharp, symmetrical peaks result from the rapid release or absorption of heat associated with a phase change or a chemical reaction. One such peak is observed at about 700°C (near the melting point of aluminum). This peak is most likely the heat released by the reaction of the molten aluminum with the nickel. The negative peak that would be associated with the melting of the aluminum cannot be resolved from this large exothermic peak.

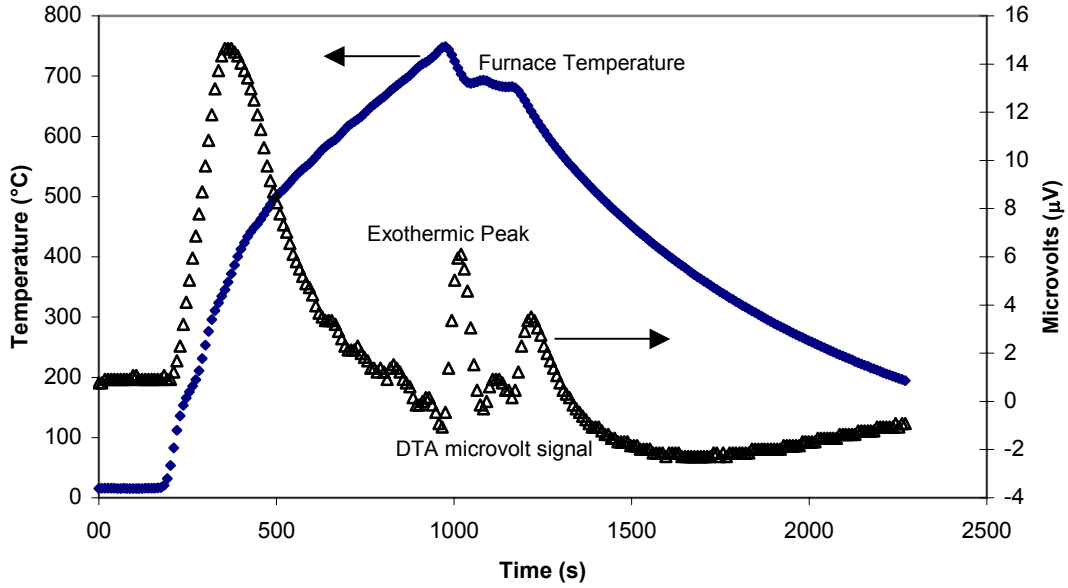

Figure 19. (Sample DTA data)

Conclusions

The effect of diluent on the nickel aluminide powder reaction was tested. The use of a diluent drastically changed the physical outcome of the product, reducing its size by nearly two orders of magnitude. SEM pictures were used to confirm particle sizes and shapes. XRD analysis confirmed the product as nickel aluminide. Further analysis remains to be done on experimental data to determine what affect the percent diluent in the mixture has on final product. In conclusion, instead of forming the molten beads with the simple powder synthesis, a fine powder can be formed with an addition of a diluent material.

References

(1) Weimer, A. *Carbide, Nitride and Boride Materials Synthesis and Processing*; Chapman & Hall: London, 1997.

(2) Strnad, Z. *Glass-Ceramic Materials: Liquid Glasses*; Elsevier: New York, 1986.

(3) Cortie, M.; http://www.mintek.ac.za/Physmet/intermet/intro.htm ed.; Council for Mineral Technology, 2002; Vol. 2002.

(4) Ritzert, F.; http://technology.grc.nasa.gov/tech/tops/ms/MS0701.PDF ed.; NASA, 2002; Vol. 2002.

(5) Dunand, D. *Mat. and Manuf. Proc.* **1995**, *10*, 373.

(6) Mandorf, V.: US, 1967.

Intermetallic-Bonded Cermets

P. F. Becher, T. N. Tiegs, and S. B. Waters
Oak Ridge National Laboratory

Objective/Scope

The goal of this task is to develop materials for diesel engine applications, specifically for fuel delivery systems and wear components (e.g., valve seats and turbocharger components). This will require materials that have a minimum hardness of 11 GPa and a thermal expansion coefficient of between 10 to 15 x 10^{-6}/°C. The material should also have excellent corrosion resistance in a diesel engine environment, flexure strength in excess of 700 MPa, and fracture toughness greater than 10 MPa√m to ensure long term reliability. The material should also be compatible with steels and not cause excessive wear of the steel counter face. The upper temperature limit for fuel delivery systems applications is 200°C, and for the other wear applications, the limit is 815°C. Finally, the total material processing costs for these advanced materials should be competitive with competing technologies such as TiN or other ceramic coatings on high-speed tool steels.

Technical Highlights

Studies of the influence of composition of the intermetallic phase on the linear thermal expansion coefficients of the intermetallic phase bonded TiC cermets have continued. The driving force is the need to match thermal expansion coefficients of metallic alloy components as closely as possible. Samples of TiC cermets containing 60 vol % binder phases of NiCrFe, Ni_3Al+Fe, and NiCr were provided by Prof. D. Wittmer of Southern Illinois University. The results are compared to expansion coefficients for TiC-Ni3Al cermets in Table I. The intermetallic alloying does not offer a distinct advantage over the use of Ni_3Al, especially in view of the fact that the Ni_3Al binder phase can plastically deform and provides significant toughening of the cermet.

Table I. Comparison of Linear Thermal Expansion Coefficients.

Cermet Composition	Linear Thermal Expansion Coefficients (α) 10^{-6}/°C 22° - 622°C
TiC (2 wt. % Mo) + 40 vol % Ni_3Al	9.68
TiC + 50 vol % Ni_3Al	10.40
TiC + 60 vol % NiCrFe	9.60
TiC + 60 vol % (Ni_3Al + Fe)	10.0
TiC + 60 vol % NiCr	10.5
TiC (2wt. % Mo) + 60 vol % Ni_3Al	11.25

Status of Milestones

On Schedule

Communication/Visits/Travel

Meeting held at ORNL on March 26, 2002, to discuss progress on processing and evaluation of cermets for engine applications with T. Yonushonis, R. Stafford and M. Naylor of Cummins Engine, J. Stephan of AMT/CoorsTek, D. Wittmer of Southern Illinois University, and D. R. Johnson, T. Tiegs and P. Becher of ORNL.

Publications

None

Cylindrical Wire Electrical Discharge Machining (EDM) and Temperature Measurement

Albert Shih
North Carolina State University

Objective/Scope

To develop precise, efficient, and cost-effective cylindrical Wire Electrical Discharge Machining (WEDM) process for cermet and other electrically conductive advanced engineering materials, and temperature measurement methods for grinding and diesel exhaust aftertreatment devices.

Technical Highlights

Two highlights in this quarter are the abrasive waterjet machining of cylindrical Ti-6Al-4V parts and the temperature measurement of diesel engine exhaust aftertreatment filters.

1. Abrasive Waterjet Machining of titanium alloys

The Abrasive WaterJet (AWJ) machining process has a wide range of applications in industry [1]. As a non-traditional machining process, AWJ offers a productive alternative with high material removal rate and flexibility. Both electrically conductive and nonconductive materials can be machined by AWJ. The cylindrical abrasive waterjet cutting has been explored but not studied in detail for cutting epoxy carbon-fiber composite [2-4]. There is still lack of research of applying this technology for cutting cylindrical parts made of titanium alloys. An exploratory research in this area was conducted. The Ti-6Al-4V alloy, provided by Cummins, was cut in a Flow International Integrated Fine Bridge abrasive waterjet machine, as shown in Fig. 1(a).

1.1. Abrasive Waterjet Turning

In this study, similar to cylindrical wire EDM [5], a rotary spindle is added to the AWJ machine to cut cylindrical shape titanium alloy parts. Figure 1(b) shows the close-up view of the spindle and the abrasive waterjet turning of a cylindrical Ti-6Al-4V part. Sparks can be observed during waterjet machining. The machine setup and process parameters of AWJ machining and wire EDM are listed in Table 1.

Table 1. Machine setup for the AWJ turning experiments.

Type of abrasive waterjet machine	Flow International Integrated Fine Bridge
Nozzle diameter (mm)	1.0
Water pressure (ksi)	50
Abrasive metering orifice diameter (mm)	6.0
Abrasive average size (mm)	0.32
Feed rate v_f (mm/min)	7.2, 21.6, 36

1.2. Experimental results and discussion

Three Ti-6Al-4V parts cut by the cylindrical AWJ with three cutting configurations are shown in Fig. 2. Figure 2(a) shows the capability to cut an angle with varying material removal rate. Figure 2(b) illustrates a part cut by AWJ turning with a straight cut along the axial direction (parallel to the centerline) at three different feed rates. The change in feed rate creates slightly

varying diameters and different levels of roughness on the AWJ machined surface. Figure 2(c) shows a part cut by AWJ turning with the same straight cut and three different feed rates as in Fig. 2(b). The spindle speed was reduced from 60 rpm in Fig. 2(b) to 10 rpm in Fig. 2(c). A screw shape workpiece was machined at the two high feed rates, 21.6 and 36 mm/min. The surface roughness and waviness, R_a and W_a, of the three sections in Fig. 2(b) was measured, and results are shown in Fig. 3. Higher feed rate generates higher surface waviness.

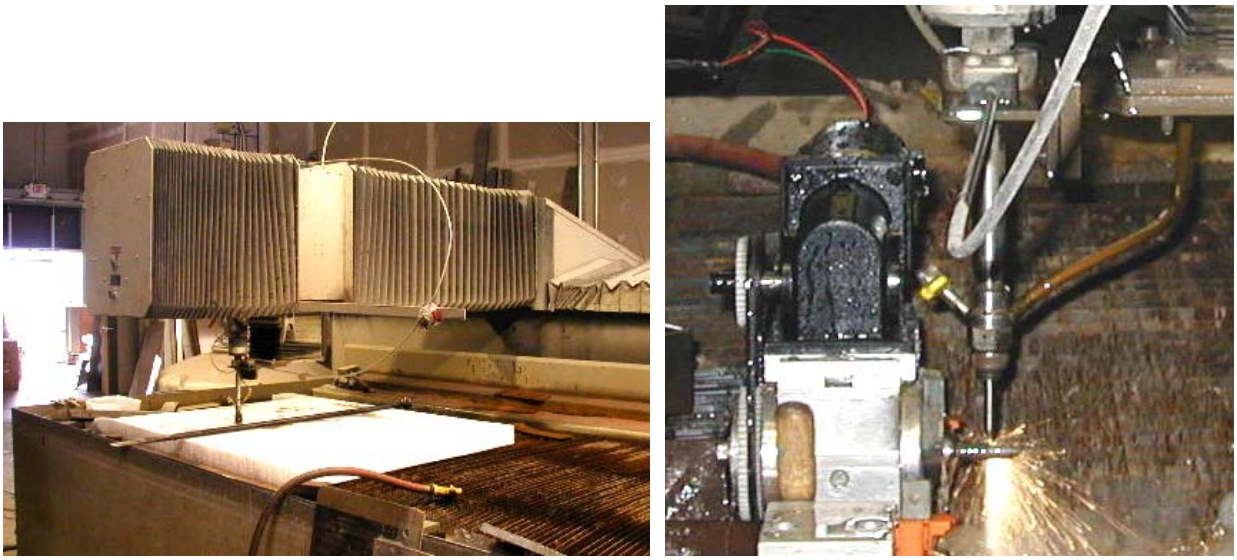

(a) (b)

Fig.1. Abrasive waterjet cutting of cylindrical titanium workpiece (a) overview of the Flow International Integrated Fine Bridge waterjet machine and (b) close-up view of abrasive waterjet cutting of a rotating Ti-6Al-4V part.

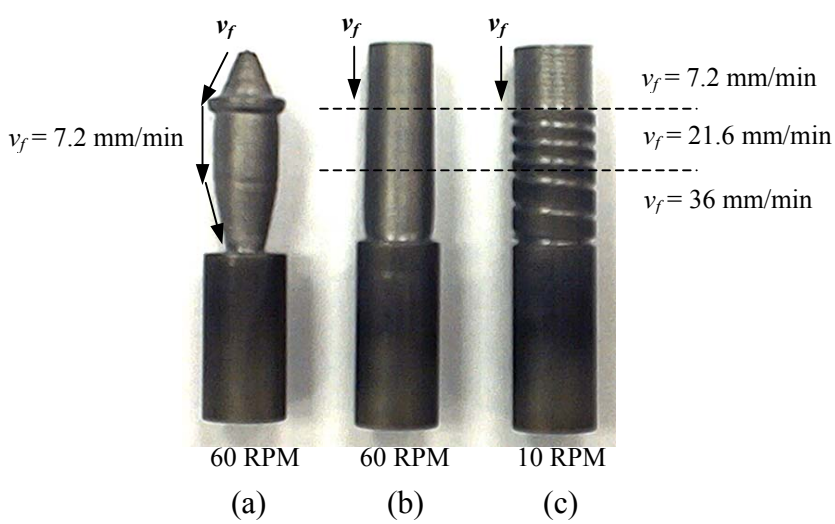

Fig. 2. Cylindrical parts machined by AWJ cutting

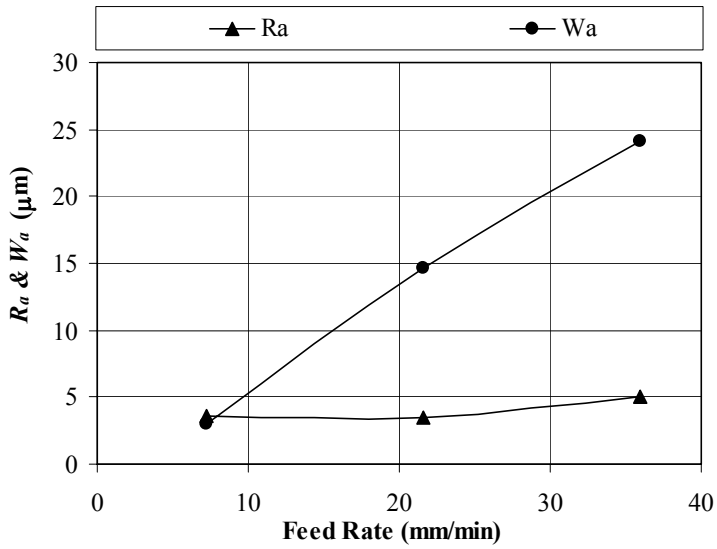

Fig. 3. Surface roughness and waviness at different feed rate.

In conclusion, the feasibility of cylindrical abrasive waterjet machining of titanium alloy is demonstrated. This AWJ machining process is especially feasible for machining parts without tight tolerance requirements. More test are planned for the near future when the new graduate student to replace Jun Qu is on board. Jun Qu has received his Ph.D. degree in April 2002 and will be working as a post-doctoral researcher at Oak Ridge National Lab.

2. Temperature Measurement in Diesel Engine Exhaust Aftertreatment Filters
As introduced in the last quarterly report, a 0.425 mm diameter single crystal sapphire optical fiber was used to transmit the infrared signal from the filter cavity to a two-color PbS and PbSe sensor to diesel exhaust filter temperature measurement. The highlight achievements in this quarter are:

- The thermal-electrically cooled PbS and PbSe sensor was tested. A mechanical chopper was implement. An optical connection was build without using complicated lens to transmit the infrared signal from the sapphire fiber to the sensor.
- The gain for individual PbS and PbSe detectors in the two-color sensor was tested. Results showed that there are needs to be adjusted the gain to improve the ratio of voltage output from two detectors for temperature measurement in the 400 to 800 K range.
- The proposed calibration method to use an oven to generate the required filter calibration curve has been explored and proven feasible.
- Theoretical calculation of the effective aperture, end surface losses, parasitic radiation effect, and influence of the fiber self-emission for an angled sapphire fiber in the infrared range has been conducted.
- Investigation is continuing to find feasible infrared lamp in the 400 to 800 K range for the study of parasitic radiation effect.

Status of Milestones

Milestone 1: Develop process technology to achieve high material removal rate in cylindrical WEDM of advanced engineering materials.

Status: Two journal and two conference papers have been published or accepted on this research.

Milestone 2: Determine the level of form tolerances and surface finish achievable by the cylindrical WEDM.

Status: Nothing to report. The surface finish was as low as 0.68 μm Ra, comparable to rough grinding, for the carbide materials.

Milestone 3: Prototype needles, armature pins, and plungers for diesel engine fuel injectors.

Status: Several prototype diesel injector plungers were manufactured. Exploratory experiments to machine miniature shafts about 0.06 mm in diameter were conducted on sub-μm TiC grain bonded in Ni and NiAl matrix.

Milestone 4: Develop mathematical models for material removal rate and surface finish of the cylindrical WEDM.

Status: Noting to report. The mathematical models for material removal rate and surface finish have been derived. These results have been summarized in a technical paper.

Milestone 5: Characteristics of the recast layer after WEDM and cylindrical WEDM and the surface condition after abrasive blasting.

Status: Nano-indentation tests have been applied to quantified mechanical properties of cylindrical wire EDM surface layers on WC-Co workpiece. Micro SiC abrasive blasting of the recast layer was demonstrated to improve the surface finish of WC-Co by about 40%~60%.

Milestone 6: Development of optical fiber based temperature measurement method, with applications for grinding process and diesel exhaust aftertreatment filters.

Status: A system for infrared-based temperature measurement of diesel exhaust aftertreatment filters was designed and tested. The system setup is undergoing further adjustment.

Communications/Visit/Travel

Albert Shih and Mustafa Bakkal visited Porvair and Oak Ridge National Lab. on March 14 and 15, 2002.

Publications

- A.C. Curry, A.J. Shih, R.O. Scattergood, and S.B. McSpadden, "Grinding Temperature Measurements in MgO PSZ Using Infrared Spectrometry," *J. Am. Ceram. Soc*. (accepted)
- J. Qu, L. Reister, A.J. Shih, R.O. Scattergood, E. Lara-Curzio, "Nanoindentation Characterization of Surface Layers of Electrical Discharge Machined WC-Co," Materials Science and Engineering: A. (submitted)
- J. Qu and A. J. Shih, "Analytical Surface Roughness Parameters of an Ideal Profile Consisting of Elliptical or Circular Arcs," *Precision Engineering*. (submitted)

References

[1] Kovacevic, R., Hashish, M, Mohan, R., Kim, T.J., and Geksin, E.S., 1997, "State of the Art of Research and Development in Abrasive Waterjet Machining," Journal of Manufacturing Science and Engineering, Vol. 119, pp. 776-785.

[2] Sheridan, M. D., Taggart, D. G., and Kim, T. J., 1994, "Screw Thread Machining of Composite Materials using Abrasive Waterjet Cutting," Manufacturing Science and Engineering, ASME PED-Vol. 68-1, pp. 421-432.

[3] Sheridan, M. D., Taggart, D. G., Kim, T. J., and Wen, Y., 1995, "Microstrucral and Mechanical Characterization of Threaded Composite Tubes Machined using AWJ Cutting," Proceedings of 8th American Water Jet Conference, Houston, TX, August 26-29, pp. 245-258.

[4] Ansari, A. I. and Hashish, R., 1992, "On the Modeling of Abrasive Material Turning," Jet Cutting Technology, A. Lichtarowicz, ed., Kluwer, Academic, Boston, pp. 555-576.

[5] Qu, J., Shih, A.J., and Scattergood, R., "Development of the Cylindrical Wire Electrical Discharge Machining Process, Part II: Surface Integrity and Roundness," *ASME Journal of Manufacturing Science and Engineering* (to appear).

NDE/C Technology for Heavy Duty Diesel Engines: Fuel Delivery and Insulating Materials

W. A. Ellingson, C. Deemer
Argonne National Laboratory
In cooperation with A. Parikh, Illinois Institute of Technology, and
N. Moryls, Illinois Math and Science Academy

Objective/Scope

The objective of the work in this task, part of the Testing and Characterization research area of the Heavy Vehicle Propulsion System Materials Program, is to develop enabling nondestructive evaluation/characterization (NDE/C) technology for lower cost and high performance materials. Specifically, this project addresses development of advanced NDE/C technology for; a)-advanced fuel delivery systems (including injector nozzles) and b)-insulating materials for reducing heat losses in the combustion zone. Fuel delivery systems for heavy-duty diesel engines are complex, very expensive and represent a significant portion of the cost of a heavy vehicle diesel engine. High pressures inside these fuel delivery systems contribute to poor fuel delivery and hence poor emissions. Materials development is part of Goal 3 of the heavy vehicle propulsion materials program. Insulating materials are also a significant materials development area because of the improvement in engine efficiency if reduced heat losses can be obtained. NDE/C technology that can provide information for reliable cost production and engine component surveillance would be of benefit to reaching the goals.

Technical Highlights

There is one main highlight this period. That is that we successfully obtained polarized laser back-scatter data on several fuel-injector plungers with a totally automated set up. As noted last period, we have continued in our efforts to develop an analytical model for the back-scattered laser effort so that we might begin to be able to predict effects of different subsurface defects on the resulting back-scattered laser data.

Technical Progress

All work this period again focused on NDE technology for the oxide monolithic ceramic fuel metering plungers under development by Cummins Engine Company of Columbus, IN. The effort this period focused on advancing the fiber-optic experimental set up.

Fuel Delivery Systems

Fuel delivery systems are critical and impact many engine performance parameters. Higher pressures required for advanced fuel systems are driving new designs and as with any design, material trade-offs become an area for evaluation. Ceramic materials provide many advantages but only if there is a reduced cost with the same or better reliability of a metal component. High pressures and potential for erosion inside fuel metering systems usually call for hard tool steels in the design and thus costs immediately become a factor. Ceramics offer a desirable option because they offer high hardness and erosion resistance. As noted the last two reporting periods, Cummins Engine Company has optioned in their CELECT^{TM} fuel injector system to use MgO materials in the metering plunger.

Experimental Set up

The experimental laser back-scattering system we are developing is shown in Fig. 1.

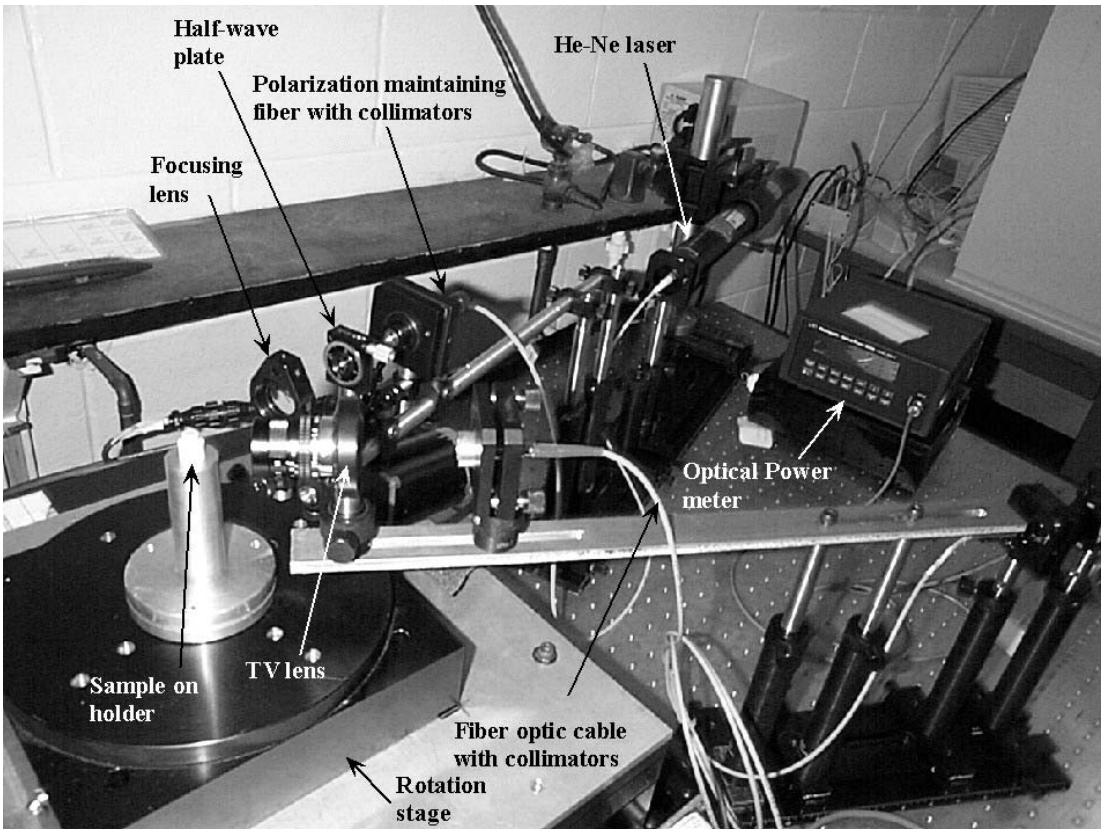

Fig. 1. Photograph of the angle laser back-scatter experimental set up

The angle optical scatter NDE system consists of: a Uniphase 1135P 20 mW He-Ne laser (wavelength of 632.8 nm), a Newport power meter, a Newport detector, Newport polarization-maintaining optical fiber on the incident side, and Thorlabs non-polarization-maintaining optical fiber on the detector side. The optical elements in the transmission leg consist of a collimator, polarization maintaining fiber optic cable, a collimator and a focusing lens that focuses on the ceramic part. The detector side consists of a wide Angle TV lens, a collimator, a non-polarization maintaining fiber optic cable, and a Newport low power optical detector. The optical power meter is connected to the Data acquisition computer running Labview™. The Labview™ program automatically controls the position of the sample, acquires the output of the optical power, stores and displays the data. A schematic of the setup is shown below in Figure 2.

The ceramic fuel injector nozzle is mounted in a custom-made clamping device mounted on a rotational stage that is controlled by the Labview™ program. The laser was determined to be originally vertically polarized. Using the wave plates, the polarization angle can be changed on both the incident and detector side of the setup. The program to acquire data from the power meter and control the stages was locally written using Labview™.

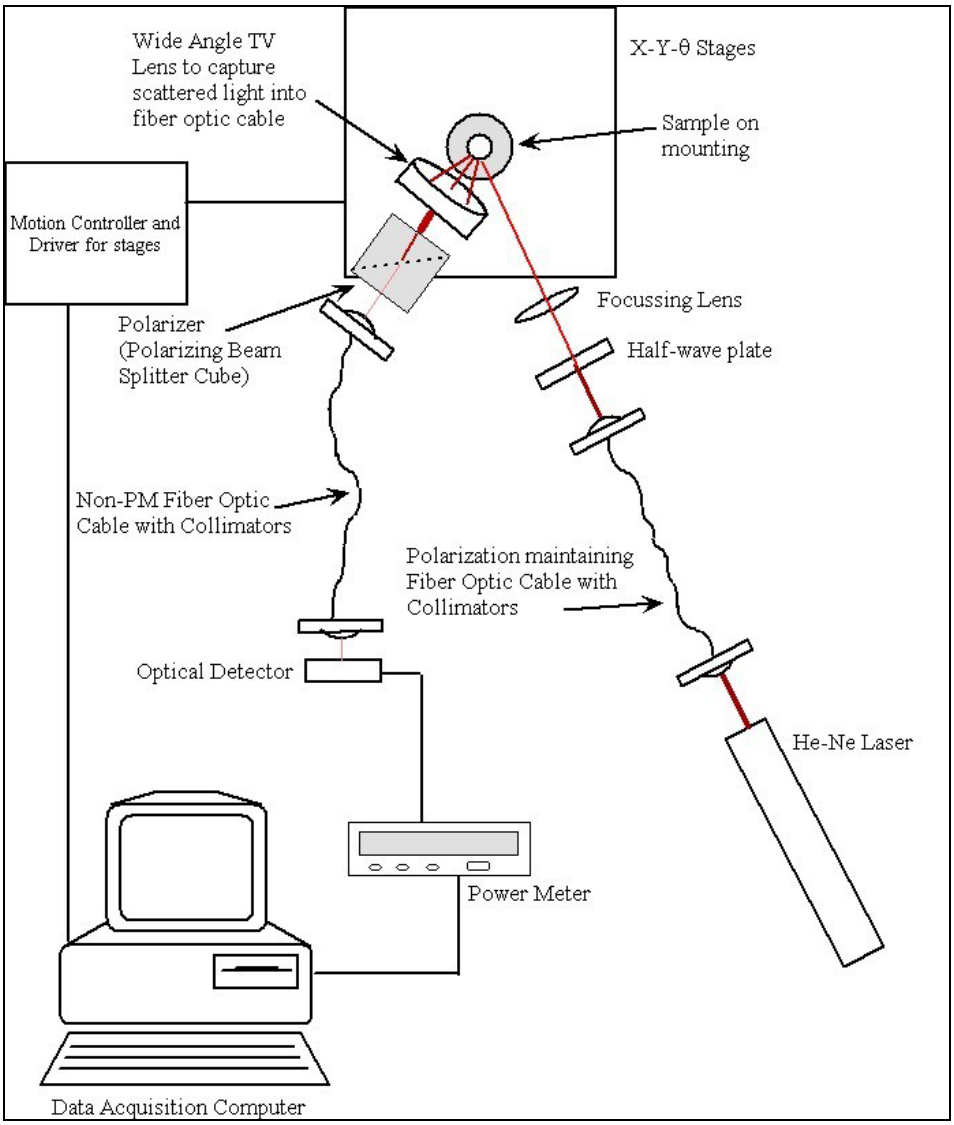

Fig. 2. Schematic of the angle laser back-scatter system at Argonne

To run an experiment, the user needs to define how many data points are needed for the scan, and the program automatically adjusts the rotation angle for each interval. During the scan, the computer reads data from the optical power meter, rotates the stage the specified amount and repeats these steps for the full circumference. A graph is produced by Labview™ and the data points are saved into a file. This file can be opened in Excel to view details about the data points or to re-graph the results.

Tests were conducted this quarter using various input and output laser polarization states on a set of fuel injector plungers. The backscattered light was analyzed without any polarization filtering as well as with filtering (indicated by the polarizer in Fig. 2). An optical photomicrograph of the top face of one such plunger is shown in Fig. 3 below and shows one surface-breaking crack and two detection cracks that do not break the surface. Resulting graphs clearly indicated the

detection of the surface-breaking crack. Further work on data analyses can yield important information about subsurface cracks and probably about the depth of the cracks.

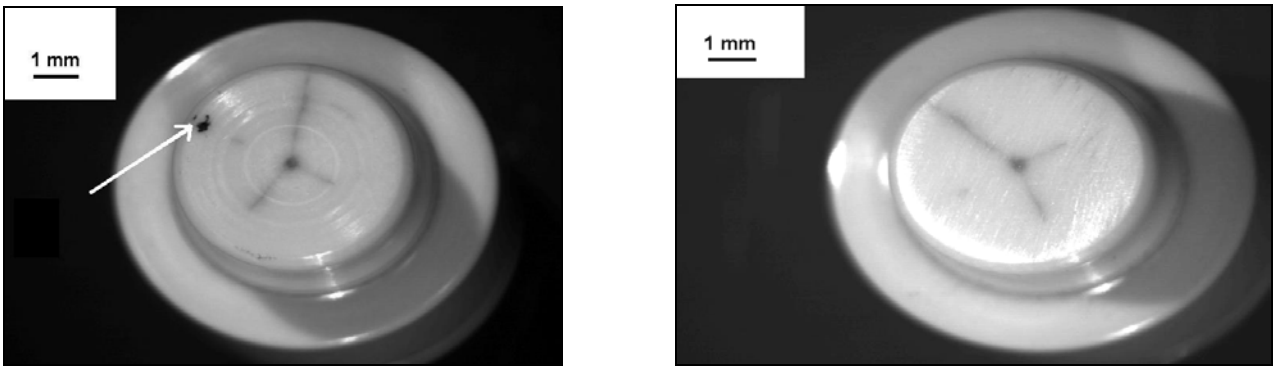

(a) (b)

Fig. 3. Optical photomicrographs of top surface of MgO high pressure fuel injector nozzle (a) photograph in the 'as-received" condition; (b) photograph after light polishing. (Note the surface-breaking crack and the two subsurface cracks.)

Several parametric scans are shown in Figs. 4 and 5. These are plots of detected back-scattered light intensity as a function of the rotation angle and show the presence and the location of the surface-breaking crack in the sample.

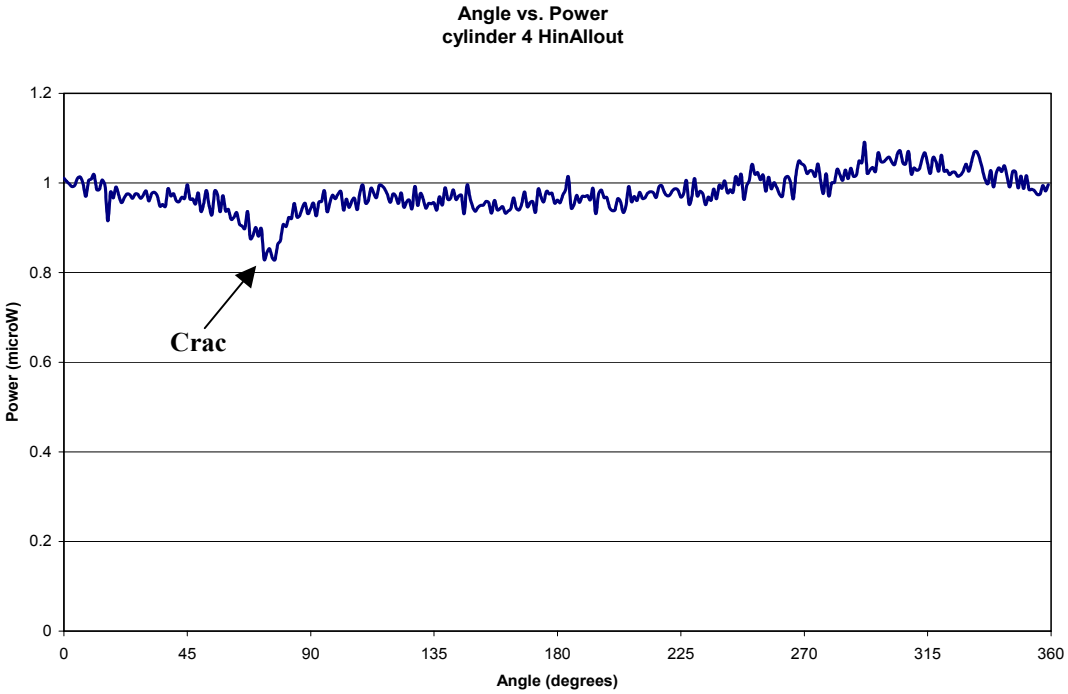

Fig. 4. Plot showing the position of the surface-breaking crack in the region 72° from the start position. The incident light is horizontally polarized.

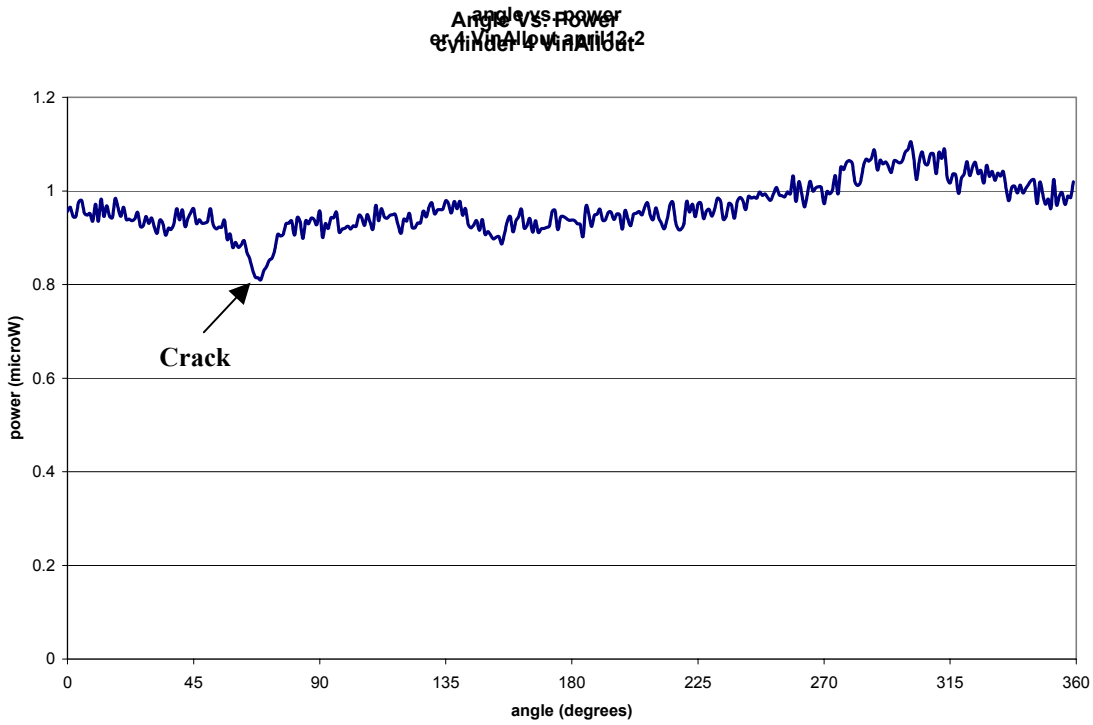

Fig. 5. Plot showing the position of the surface-breaking crack in the region of 70° from the start position. The incident light is vertically polarized in this case.

As can be seen from the data and the optical photomicrographs, this method detects the surface-breaking cracks and can reliably locate the crack. Because of the high optical transmission in these materials, detection of the subsurface cracks will require additional analysis of the back-scatter data.

There are two main conclusions that can be arrived at from the results of this experiment. First, the ability to use angle scatter to detect surface-breaking cracks in the fuel injector parts has been demonstrated. Second, polarization maintaining fiber optic cables can be used for launching the incident laser light to the part, which in future can have complex geometries not possible to reach using conventional set-ups. Further work on this project will include analyzing the different output polarization states of the scatter to find out more about subsurface defects, effect of different polarization maintaining fibers and related optics, use of powerful and more tightly focused lasers.

NDE for Insulating Materials

We continue work on developing this aspect of this effort.

Meetings, Trips, Communications

Meetings

None

Trips

None

Communications

Additional discussions were held with staff of Cummins Engine in Columbus, IN.

NDE Development for Ceramic Valves for Diesel Engines

J. G. Sun, W. A. Ellingson
Argonne National Laboratory

and M. J. Andrews
Caterpillar, Inc.

Objective/Scope

Emission reduction in diesel engines designated to burn fuels from several sources has lead to the need to assess ceramic valves to reduce corrosion and emission. The objective of this work is to evaluate several nondestructive evaluation (NDE) methods to detect defect/damage in structural ceramic valves for diesel engines. One primary NDE method to be addressed is elastic optical scattering. The end target is to demonstrate that NDE data can be correlated to material damage as well as used to predict material microstructural and mechanical properties. There are three tasks to be carried out: (1) Characterize subsurface defects and machining damage in flexure-bar specimens of NT551 and SN235 silicon nitrides to be used as valve materials. Laser-scattering studies will be conducted at various wavelengths using a He-Ne laser and a tunable-wavelength solid-state laser to optimize detection sensitivity. NDE studies will be coupled with examination of surface/subsurface microstructure and fracture surface to determine defect/damage depth and fracture origin. NDE data will also be correlated with mechanical properties. (2) Assess and evaluate subsurface damage in ceramic valves to be run in bench test and in a single-cylinder-engine test. All valves will be examined at ANL prior to test, during periodic scheduled shut downs, and at the end of the planned test runs. (3) Evaluate healing of subsurface damage by laser glazing on machined surfaces of GS44 ceramics. ANL will perform laser-scattering characterization on machining surfaces at before and after glazing treatment. NDE data will be correlated with glazing parameters and mechanical properties.

Technical Highlights

Work during this period (January-March 2002) focused on measuring optical transmission property of new Si_3N_4 step-wedge samples, studying microstructure of fracture origins, and developing laser scatter system for full-valve scans.

1. Elastic Optical Scattering NDE for Machining Damage

The 3 step-wedge specimens described in the previous report (for period Oct.-Dec. 2001) were found to have large thickness variations in all steps and, therefore, were not suitable for transmission property measurement. New step-wedge specimens of SN235P, L-M C99091, and NT551 Si_3N_4 ceramics were prepared in this period. Figure 1 shows a comparison of photomicrographs at the edges of L-M C99091 step-wedge specimens machined from the first and the second set. It is apparent that the thickness in each step is uniform in the second step-wedge set. Similar results were obtained for SN235P and NT551 step wedges as the same machining tool was used for preparing each step-wedge set. Average thickness for each step was determined from the photomicrographs.

The transmission property of these ceramics was measured using a similar setup as that illustrated in our April-May 1999 report and the data are plotted in Fig. 2. Because the detection sensitivity of laser-scattering signal for defect identification is typically in the order of 1%, we can estimate that the penetration depth for He-Ne laser (at wavelength of 633 nm) is about 100 µm for SN235P, 250 µm for NT551, and 500 µm for L-M C99091 Si_3N_4 ceramic. It should be noted that the penetration depth can be increased with longer optical wavelengths by using the Ti:Sapphire tunable laser (wavelength range in 700-960 nm) in our laboratory.

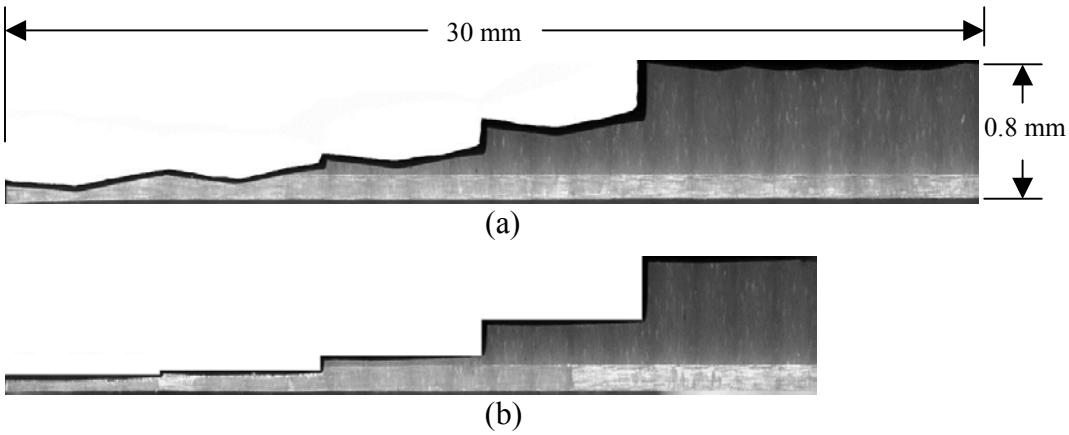

Fig. 1. Photomicrographs at the edge of L-M C99091 step-wedge specimens from (a) first and (b) second machined set (note the uniform thickness in the second machined set).

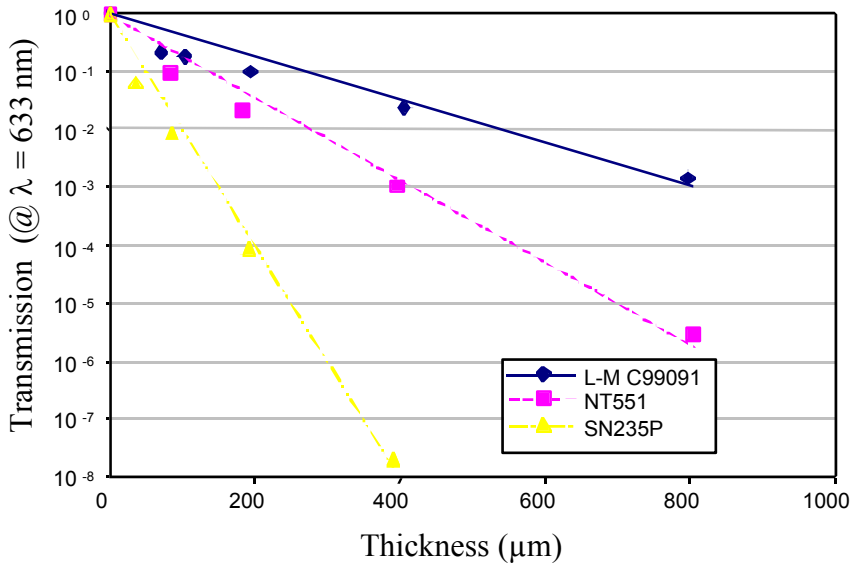

Fig. 2. Optical tramsnission properties for step-wedge specimens of NT551, L-M C99091, and SN235P ceramics.

During this period we continued correlating laser-scattering data with higher-magnification photomicrographs on fracture surfaces to identify fracture origins in AS800, GS44, and SN235 Si_3N_4 flexure-bar specimens. Figure 3 shows correlation of photomicrographs with laser-

scattering sum images on the tensile surfaces and high-magnification photomicrographs on fracture surfaces at the two fracture locations in AS800 flexure-bar specimen #5. The fractures appear to start from higher-porosity defects near the tensile surface.

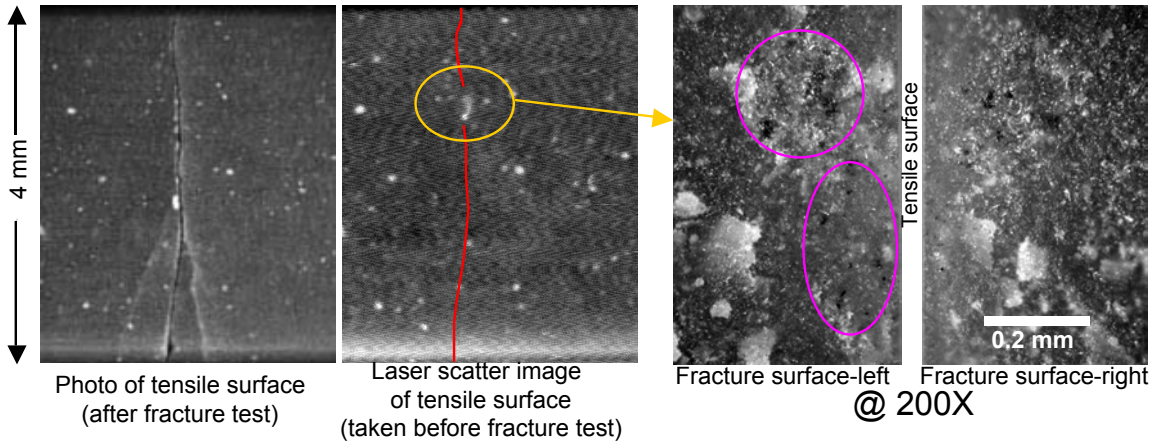

(a) fracture location 1

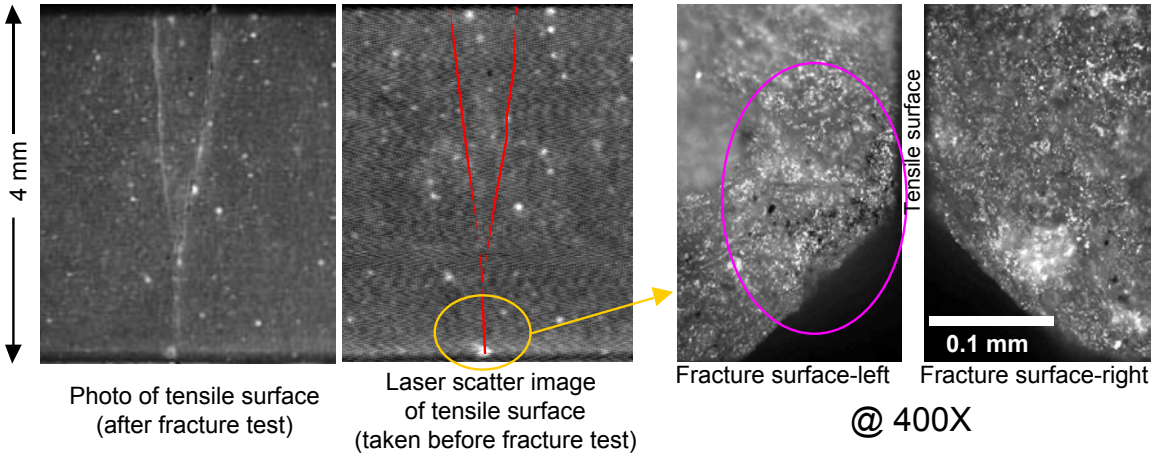

(b) fracture location 2

Fig. 3. Photomicrographs and laser-scattering sum images on tensile surface and photomicrographs on fracture surfaces at two fracture locations of AS800 specimen #5 (note higher porosity at the fracture origins).

2. Laser-Scattering System Development for Si_3N_4 Valves

During this period we continued development of the laser-scattering system suitable for scanning an entire valve. Figure 4 shows the schematic diagram of the system setup. It consists of two translation and two rotation stages controlled by a four-axis stage controller that are currently available in our laboratory. One optical detector is illustrated for initial setup. However, the detector train can be easily modified to our standard setup with two optical detectors. The hardware and software development will continue in the next period.

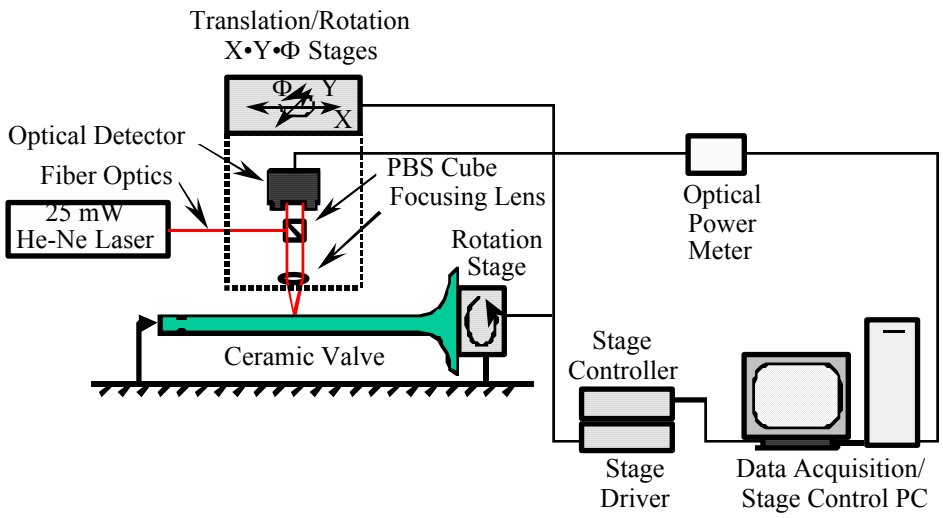

Fig. 4. Schematic diagram of laser-scattering system for scanning an entire valve.

Status of Milestones

Current ANL milestones are on or ahead of schedule.

Communications/Visits/Travel

J. G. Sun will attend the American Ceramic Society's 104th Annual Meeting & Exposition in St. Louis, MO, April 28-May 1, 2002, and make a presentation entitled "Laser Scattering Detection of Subsurface Defects as Fracture Origins in Silicon-Nitride Ceramics."

J. G. Sun will meet M. J. Andrews of Caterpillar Inc. to discuss project issues during the American Ceramic Society's 104th Annual Meeting & Exposition in St. Louis, MO, April 28-May 1, 2002.

Problems Encountered

None this period.

Publications

None this period.

Processing and Characterization of Structural and Functional Materials for Heavy Vehicle Applications

J. Sankar, Z. Xu, and S. Yarmolenko
North Carolina A & T State University

Objective/Scope

Continue to investigate the combustion chemical vapor deposition technique of fully stabilized zirconia (YSZ) thin films for solid oxide fuel cells.

Task

Investigate the effects of more controlling parameters on the growth of the YSZ thin films.

Technical Highlights

In the previous report, the development of the experimental set-up was presented, as well as the results of the studies on some controlling processing parameters. In this report, more effects of some of the significant processing parameters on the properties of the deposited YSZ films will be discussed. These parameters are Y/Zr ratio in the solutions, substrate position with respect to the flame and the substrate material. The Y/Zr ratio is expressed in mole percent. The substrate position is expressed by the substrate-to-nozzle distance in millimeter. The materials used for substrates are mirror-polished Si(100) and MgO(100). The as-deposited YSZ thin films were characterized with scanning electron microscope (SEM), transmission electron microscopy (TEM), X-ray diffraction (XRD), and energy dispersive spectrum (EDS).

Results and Discussion

Y/Zr Ratio in the Solution

The experiments to study the effect of Y/Zr ratio on the deposited YSZ thin films were conducted on MgO(100) substrates. The range of the ratio is from 6 mol % to 20 mol %. In the XRD spectra shown in Figure 1, there are only three X-ray characteristic peaks obtained for each film. Two of them are for YSZ(111) and YSZ(200), the other one for the substrate MgO(100). This phenomenon indicates fully stabilized zirconia was obtained in all the cases. When the film was characterized with TEM, the electron diffraction pattern and high-resolution image reveal the existence of superstructure (Figure 2) in the YSZ film, which means the presence of a long range atomic ordering due to the doping by Y^{+3} cations. Compositional analysis of the films with EDS showed that the Y/Zr ratios in the deposited films are linear to that in the source.

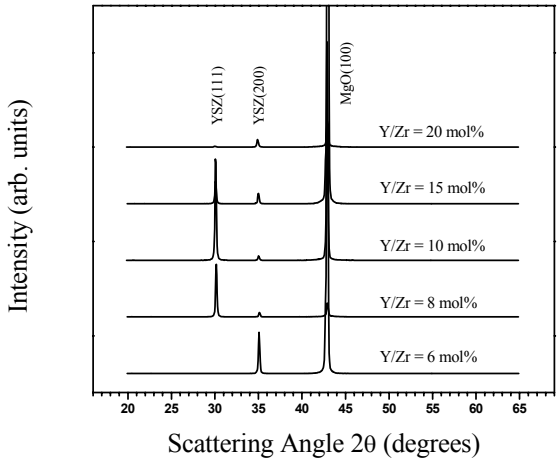

Figure 1. XRD spectra of Zirconia films deposited at different ratios of Y/Zr

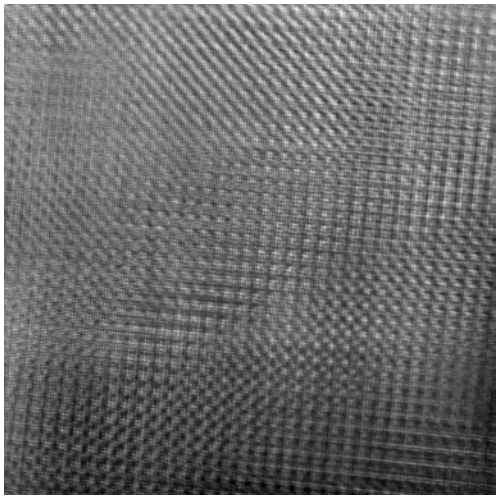

Figure 2. High-resolution TEM image of an YSZ film

Substrate Position

To study the film growth at different substrate-to-nozzle distances, six film depositions were carried out at different distances between 83 mm (out of the visible end of the flame) and 51 mm (far into the flame). Other constant conditions are 1.25×10^{-3} M for the total-metal-concentration, 1200°C for the substrate temperature, and Si(100) for substrate material. SEM experiment showed a general tendency that with the decrease in the substrate-to-nozzle distance, the size of the crystals increase from about 60 nm to as large as 200 nm. Another feature is that the film grown at larger substrate-to-nozzle distance has more uniform sized crystals, while the crystals on the films grown at smaller substrate-to-nozzle distances are more irregularly sized. In the latter case, a great amount of secondary nucleation was also found.

From the cross-sectional SEM images the average thickness of each film was measured. When the thickness data were plotted as shown in Figure 3 (line 1), they can be well fitted by an exponential equation. With the increase of the substrate-to-nozzle distance, precursor concentration in the flame will be attenuated because of the expansion of the flame. The film thickness was normalized with the precursor concentration and plotted as line 2 in the graph. The growth rate of the film still follows the exponentially decaying mode with the substrate-to-nozzle distance.

Substrate Material

Thin films deposited on Si(100) and MgO(100) have different morphologies. Film has a three-dimensional growth feature on Si(100) substrate, while film has two-dimensional growing feature or domain epitaxial growth on Mg(100) substrate.

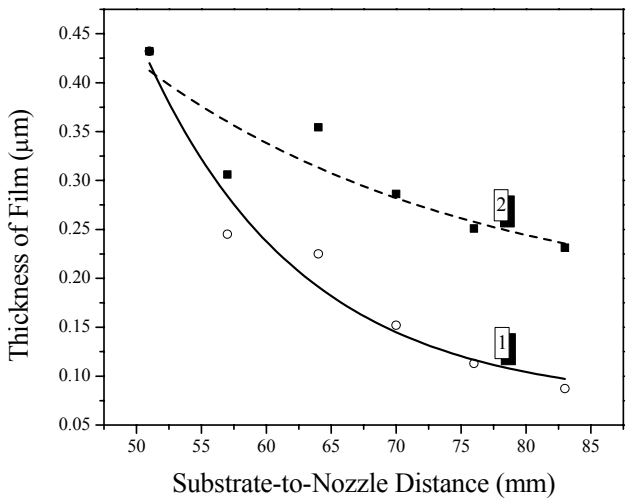

Figure 3. Film thickness as a function of substrate-to-nozzle distance

Status of Milestones
On Schedule

Communications/Visitors/Travel
None

Problems Encountered
None

Publications

1. "Liquid Fuel Chemical Vapor Deposition of YSZ Thin Films For Fuel Cell Applications", PhD Dissertation (Z. Xu), May, 2002, North Carolina A&T State University, Greensboro, NC 27411.
2. "Preparation And Properties of YSZ Electrolyte Thin Films Via Liquid Fuel Combustion Chemical Vapor Deposition", To be published in Proceedings of The 26th Annual International Conference On Advanced Ceramics & composites, Jan. 18, 2002, Cocoa Beach, FL.
3."Combustion Chemical Vapor Deposition of YSZ Thin Films for Fuel Cell Applications," published in proceedings of ASME 2001 ASME International Mechanical engineering Congress and Exposition, New York, " Processing and Understanding of Structural and Electronic Ceramic Materials"(Full Peer Reviewed Proceeding) ASME publication, MD-Volume 95, 2001.

Life Prediction of Diesel Engine Components

H. T. Lin, T. P. Kirkland, M. K. Ferber
Oak Ridge National Laboratory

and M. J. Andrews
Caterpillar, Inc.

Objective/Scope

The valid prediction of mechanical reliability and service life is a prerequisite for the successful implementation of structural ceramics as internal combustion engine components. There are three primary goals of this research project which contribute toward that implementation: the generation of mechanical engineering data from ambient to high temperatures of candidate structural ceramics; the microstructural characterization of failure phenomena in these ceramics and components fabricated from them; and the application and verification of probabilistic life prediction methods using diesel engine components as test cases. For all three stages, results are provided to both the material suppliers and component end-users.

The systematic study of candidate structural ceramics (primarily silicon nitride) for internal combustion engine components is undertaken as a function of temperature (< 900°C), environment, time, and machining conditions. Properties such as strength and fatigue will be characterized via flexure and rotary bend testing.

The second goal of the program is to characterize the evolution and role of damage mechanisms, and changes in microstructure linked to the ceramic's mechanical performance, at representative engine component service conditions. These will be examined using several analytical techniques including optical and scanning electron microscopy. Specifically, several microstructural aspects of failure will be characterized:

(1) strength-limiting flaw-type identification;
(2) edge, surface, and volume effects on strength and fatigue size-scaling;
(3) changes in failure mechanism as a function of temperature;
(4) the nature of slow crack growth; and
(5) what role residual stresses may have in these processes.

Lastly, numerical probabilistic models (i.e., life prediction codes) will be used in conjunction with the generated strength and fatigue data to predict the failure probability and reliability of complex-shaped components subjected to mechanical loading, such as a silicon nitride diesel engine valve. The predicted results will then be compared to actual component performance measured experimentally or from field service data. As a consequence of these efforts, the data generated in this program will not only provide a critically needed base for component utilization in internal combustion engines, but will also facilitate the maturation of candidate ceramic materials and a design algorithm for ceramic components subjected to mechanical loading in general.

Technical Highlights

Microstructural characterization of SN84 silicon nitride after 1000 h exposure in an oil ash environment was carried out during this reporting period. Mechanical testing results at 850°C and 0.003 MPa/s in air reported in the previous quarterly report indicated that the SN84 silicon nitride exhibited no properties degradation after 1000 h exposure, suggestive an excellent corrosion resistance to the simulated diesel engine environment. Polished cross sections of selective samples were prepared for SEM analysis in order to understand the effect of diesel engine environment on the chemistry and microstructure of secondary phase(s) as well as silicon nitride. Figure 1 shows the SEM micrographs taken from the exposed surface region. SEM observations indicated there is change in microstructure; i.e., intergranular cracking near the subsurface region, after 1000 h exposure. Note that similar change in microstructure was also observed for NGK SN88 tested at 850°C. Also, no oil ash elements were detected via EDAX in the silicon nitride grains as well as secondary phase pockets, indicative of no inward diffusion of elements during exposure. Therefore, the presence of intergranular cracking could possibly be due to the transformation of secondary phase, but not due to the oil ash exposure. Nonetheless, it could be expected that the generation of extensive cracking during the operation would probably lead to the loss of long-term mechanical reliability and, thus, lifetime of engine components.

Studies of dynamic fatigue properties of SN84 silicon nitride ceramic, which were transversely machined per ASTM C116 standard, were completed during this reporting period. The objective of this study is to provide an understanding on the effect of grinding orientation on the mechanical properties. Mechanical tests for transversely machined bend bars would be more representative of strength obtained for the ceramic valves, which would be transversely machined in the component production lines. Also, the study would provide a complete database for component design and lifetime prediction of diesel engine companies. Dynamic fatigue tests were conducted in four-point bending using 20mm/40mm, α-SiC semi-articulating fixtures at 850 and 1000°C in air. Stressing rates of 30 and 0.003 MPa/s were employed to evaluate the fatigue effect. Load was continuously measured as a function of time, and flexure strength was calculated using ASTM C1161. Mechanical results at room temperature showed that transversely machined SN84 bend bars exhibited strength, which was ~ 13% lower than those obtained for bend bars longitudinally machined, as shown in Table 1. Similar strength difference between transversely and longitudinally machined specimens has also been previously reported for candidate silicon nitride materials evaluated under this subtask. However, the effect of machining orientation on the measured mechanical strength became less significant at elevated temperatures, as shown in Table 1 and Figs. 2-5. The insensitivity of mechanical properties to machining orientation could be due to the healing of surface machining flaws by oxidation. On the other hand, flexure strength versus stressing rate curves at 850 and 1000°C revealed high fatigue exponents, indicative of no fatigue effect (Fig. 6). However, the strengths obtained at 1000°C and at 0.003 MPa/s for both machining orientation were 5-10% higher than those obtained at 1000°C and at 30 MPa/s, suggestive of the possible onset of SCG processes.

Status of Milestones

All milestones are on schedule.

Communications / Visitors / Travel

Dynamic fatigue results of transversely machined SN84 bend bars at 850 and 10000°C at 30 and 0.003 MPa/s were communicated with M. J. Andrews at Caterpillar.

Update of the status of initial bench test on Norton NT551 exhaust valves was held with M. J. Andrews at Caterpillar.

Communication with M. J. Andrews at Caterpillar on the failure of SN84 silicon nitride designed for use as a mechanical load pin for a thermal-mechanical test apparatus

Problems Encountered

None.

Publications

H. T. Lin and T. P. Kirkland, A. A. Wereszczak, and M. J. Andrews, "Effect of Long-Term Oil Immersion Test on Mechanical Reliability of Candidate Silicon Nitride Ceramics for Diesel Engine Applications," to be presented in the 2002 American Ceramic Society Annual Meeting, April 28-May 1, 2002.

References

[1] H. T. Lin, T. P. Kirkland, M. K. Ferber, and M. J. Andrews, "Life Prediction of Diesel Engine Components," Heavy Vehicle Propulsion System Materials Program Bimonthly Technical Progress Report to DOE Office of Transportation Technologies, Apr. 2001 – June 2001.

[2] H. T. Lin, T. P. Kirkland, M. K. Ferber, and M. J. Andrews, "Life Prediction of Diesel Engine Components," Heavy Vehicle Propulsion System Materials Program Bimonthly Technical Progress Report to DOE Office of Transportation Technologies, Oct. 2001 – Dec. 2001.

[3] A. A. Wereszczak, and T. P. Kirkland, M. J. Andrews, M. K. Ferber, and R. Tandonl, "Life Prediction of Ceramic Diesel Engine Components," *Heavy Vehicle Propulsion System Materials Program Semiannual Technical Progress Report to DOE Office of Transportation Technologies*, Oct. 1998 - Mar. 1999.

Table 1. Summary of uncensored Weibull strength distributions for NGK SN84 specimens, longitudinally and transversely machined per ASTM C1161.

Material	# of Spmns. Tested	Stressing Rate (MPa/s)	Temp. (°C)	± 95% Uncens. Weibull Modulus	Uncens. Uncens. Weibull Modulus	± 95% Uncens. Chrctstic Strength (MPa)	Chrctstic Strength (MPa)
SN84 (Long.)	20	30	20	10.59	7.06, 15.00	858	818, 898
SN84 (Long.)	20	0.003	20	9.61	6.52, 13.80	754	716, 792
SN84 (Tran.)	15	30	20	12.52	7.59, 18.24	758	723, 793
SN84 (Tran.)	15	0.003	20	10.10	6.67, 14.02	659	662, 697
SN84 (Long.)	15	30	850	25.14	15.58, 37.35	818	718, 803
SN84 (Long.)	15	0.003	850	10.27	6.51 15.06	761	718, 803
SN84 (Tran.)	15	30	850	20.38	13.12, 29.25	810	787, 832
SN84 (Tran.)	15	0.003	850	18.13	11.75, 25.85	781	756, 805
SN84 (Long.)	15	30	1000	20.59	13.49, 29.45	777	757, 796
SN84 (Long.)	15	0.003	1000	14.71	9.63, 20.85	863	829, 896
SN84 (Tran.)	15	30	1000	15.80	9.63, 23.69	780	752, 809
SN84 (Tran.)	15	0.003	1000	11.72	7.58, 16.81	816	776, 855

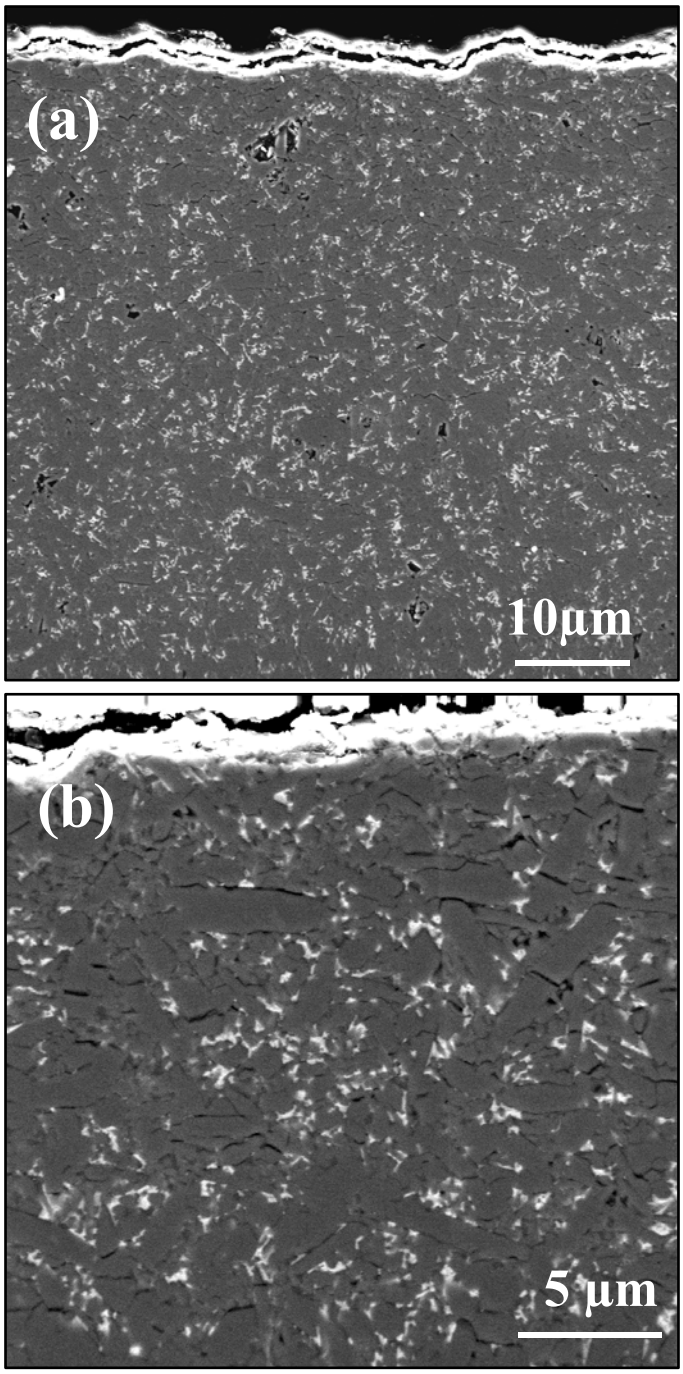

Figure 1. SEM micrographs of polished cross sections of SN84 silicon nitride after 1000h exposure in an oil ash environment at 850°C in air.

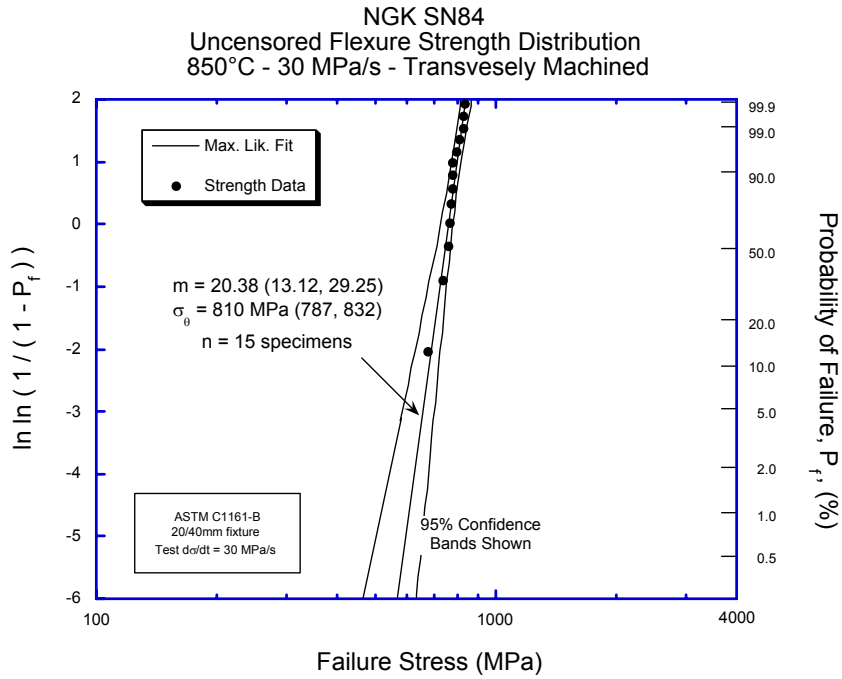

Figure 2. Characteristic strength of NGK SN84 silicon nitride machined transversely and tested at 850°C and 30 MPa/s. Note that the dimension of bend bar has been scaled down to unit size in the analysis.

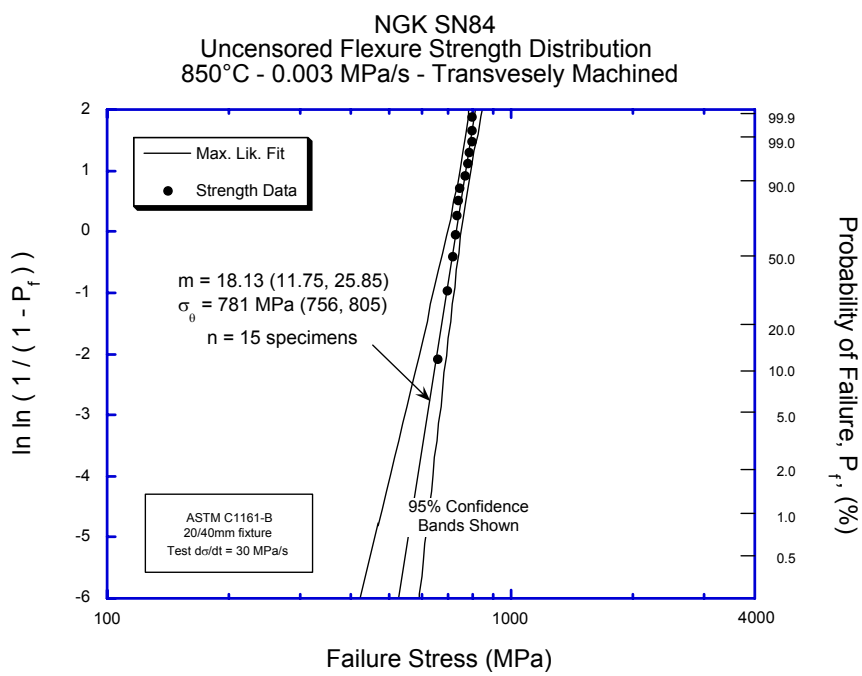

Figure 3. Characteristic strength of NGK SN84 silicon nitride machined transversely and tested at 850°C and 0.003 MPa/s. Note that the dimension of bend bar has been scaled down to unit size in the analysis.

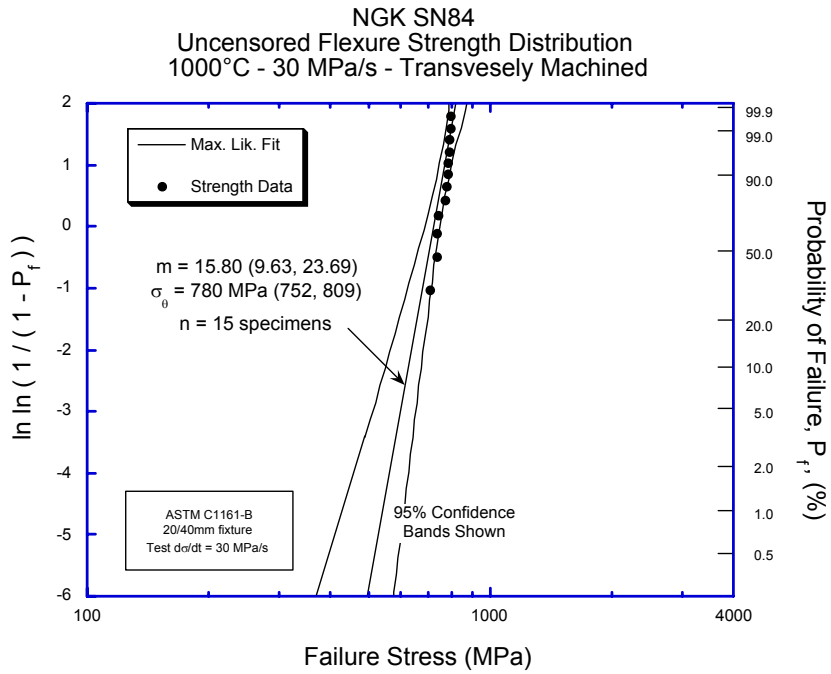

Figure 4. Characteristic strength of NGK SN84 silicon nitride machined transversely and tested at 1000°C and 30 MPa/s. Note that the dimension of bend bar has been scaled down to unit size in the analysis.

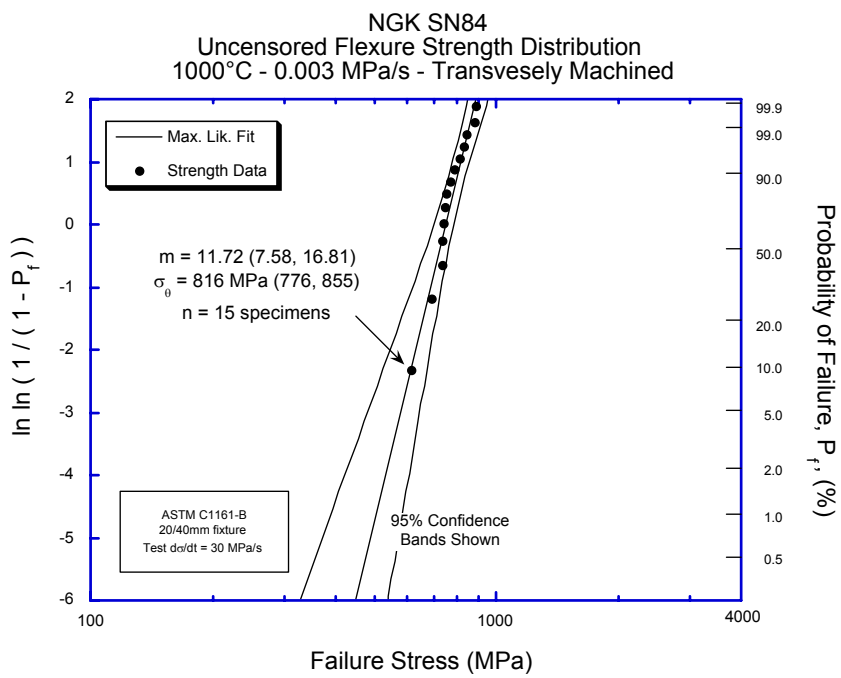

Figure 5. Characteristic strength of NGK SN84 silicon nitride machined transversely and tested at 1000°C and 0.003 MPa/s. Note that the dimension of bend bar has been scaled down to unit size in the analysis.

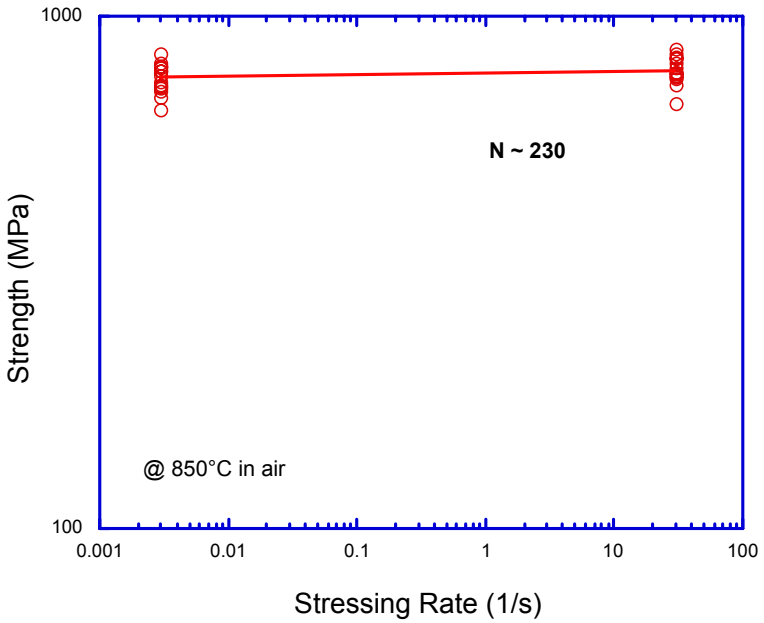

Figure 6. Fatigue exponent of transversely machined NGK SN84 silicon nitride tested at 850°C.

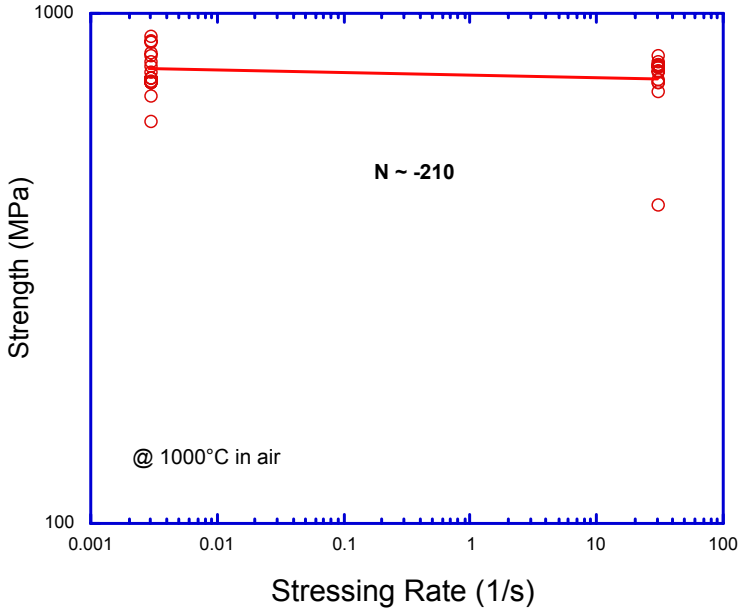

Figure 7. Fatigue exponent of transversely machined NGK SN84 silicon nitride tested at 1000°C.

Durability of Diesel Engine Component Materials

Peter J. Blau and Ronald D. Ott
Oak Ridge National Laboratory

Objective/Scope

The objective of this effort is to enable the development of more durable, low-friction moving parts in diesel engines for heavy vehicle propulsion systems by conducting friction, lubrication, and wear analyses of advanced materials, surface treatments, and coatings. The scope of materials and coatings is broad and includes any metallic alloy, intermetallic compound, ceramic, or composite material which is likely to be best-suited for the given application. Parts of current interest include scuffing-critical components, like fuel injector plungers and EGR waste gate components. Hot scuffing is a primary surface damage mode of interest. Bench-scale simulations of the rubbing conditions in diesel engine environments are used to study the accumulation of surface damage, and to correlate this behavior with the properties and compositions of the surface species. The effects of mechanical, thermal, and chemical factors on scuffing and reciprocating sliding wear are being determined. Results will be used to refine material selection strategies and suggest materials for durability-critical engine components.

Technical Highlights

High-Temperature Scuffing Tests. Using the testing procedures described in previous reports, additional high-temperature (600° C) scuffing tests were conducted on two additional material combinations: Stellite 6B on Custom 465™ and Stellite 6B on Pyromet 80™. The two new tile materials were heat-treated according to the supplier's recommendations

During this quarter, a new ranking method was employed to help identify which of the selected material couples had the best overall response. Previously, the data for each couple were tabulated under the six headings: (1) average initial torque (N-mm), (2) standard deviation in initial torque (N-mm), (3) average final torque (N-mm), (4) standard deviation in final torque (N-mm), (5) pin specimen wear volume, based on wear scar width (mm^3), and (6) arithmetic average surface roughness of the tile specimen (μm). Then the values under each heading were ranked from best to worst, and a numerical order was assigned. Values within a narrow range were given the same rank order. For example, two or three material pairs could be tied for ranking #2 if their average initial torque was within normal experimental scatter. Finally, the rankings in each of the six categories were added and given a composite final score. While useful, the composite ranking method did not include an effective measure of how much better one was from the other within a category, just what the order was.

The limitations of the previous method were overcome by instituting a weighted ranking system. In that case, the best ranking in each category was used to normalize the other values to a maximum score of 100. The best received 100 and the others were a fraction of that. On this basis, the results of the high-temperature scuffing test matrix, including the two most recently evaluated material pairs, are given in Table 1.

Table 1. Weighted Rankings of High-Temperature Scuff Test Pairs
[Top score in each category is in **bold face** font]

Pin	Tile	Index 1	rating 1	Index 2	rating 2	Index 3	rating 3	Index 4	rating 4	Index 5	rating 5	Index 6	rating 6	**Sum**
St6	P80	120.57	47.8	33.92	35.2	46.25	71.6	17.21	57.5	0.33	9.1	4.70	6.8	227.9
Zr	304	107.57	53.6	28.36	42.1	69.48	47.6	16.25	60.9	0.18	16.7	4.14	7.7	228.5
St6	304	116.78	49.3	32.40	36.8	58.81	56.3	13.73	72.0	0.16	18.8	5.62	5.7	238.9
303	304	99.35	58.0	27.06	44.1	45.01	73.5	12.35	80.1	2.70	1.1	4.15	7.7	264.5
T20	IC	73.24	78.7	13.66	87.3	44.95	73.6	14.41	68.6	0.11	27.3	0.90	35.6	371.1
Zr	SN	95.04	60.6	19.32	61.7	96.18	34.4	48.58	20.4	**0.03**	**100.0**	**0.32**	**100.0**	377.2
St6	465	58.76	98.1	13.23	90.2	47.77	69.3	18.89	52.4	0.04	75.0	2.05	15.6	400.5
St6	IC	80.84	71.3	13.14	90.8	41.93	78.9	10.18	97.2	0.09	33.3	0.88	36.4	407.9
GT	GT	**57.63**	**100.0**	14.54	82.0	**33.10**	**100.0**	10.35	95.6	0.15	20.0	2.62	12.2	409.8
Zr	IC	74.36	77.5	**11.93**	**100.0**	41.48	79.8	**9.89**	**100.0**	0.05	60.0	0.73	43.8	**461.1**

Material codes:
St6 = Stellite 6B, 303SS = 303 stainless steel, 304SS = 304 stainless steel, GT = GallTough stainless, Zr = TTZ zirconia, IC = alloy IC 221M, 465 = Custom 465 alloy, SN = silicon nitride ceramic, P80 = Pyromet 80 alloy, T = Tribonic 20 alloy

Table Index codes:
(1) Average of initial torque (N-mm)
(2) Standard deviation in intial torque (N-mm)
(3) Average of final torque (N-mm)
(4) Standard deviation in final torque (N-mm)
(5) Pin specimen wear volume (mm3)
(6) Tile specimen roughness, Ra (μm)

Overall, the combination of zirconia on IC 221M intermetallic alloy provided the highest rating (461). Note that the zirconia on silicon nitride couple gave the best wear behavior, but the final torque values (Indexes 3 and 4) were the worst of any couple. The new combinations tested this period (Stellite 6B on heat-treated Pyromet 80 and Stellite 6B on heat-treated Custom 465) did not perform better than the leading material combinations that were evaluated during the previous quarters.

Future Plans

1. Continue metallurgical studies of scuff-tested specimens, and conduct additional tests to examine the effects of intermittent operation on the durability and frictional torque behavior of the four leading material pairs. A newly developed coating process, based on technology from the Former Soviet Union, will be evaluated and compared with uncoated material pairs.

2. Conduct cylinder-on-twin cylinder tests on fuel injector plunger materials under diesel fuel-lubricated conditions.

Travel

None.

Status of FY 2002 Milestones

1) Complete design and construction of fixtures to adapt existing ORNL friction and wear testing machine for fuel injector plunger materials. (December 15, 2001 – completed.)

2) Complete elevated temperature scuffing tests of leading candidate materials and coatings. Submit report. (March 31, 2002 – uncoated material evaluations are completed, but these will be supplemented with additional work on novel coatings in the next quarter.)

3) Complete tests of candidate ceramic materials and cermets for fuel injector applications. Submit report. (September 30, 2002)

Publications

None this period.

Implementing Agreement For A Programme Of Research And Development On Advanced Materials For Transportation Applications

M. K. Ferber
Oak Ridge National Laboratory

Objective/Scope

The International Energy Agency (IEA) was formed via an international treaty of oil consuming countries in response to the energy crisis of the 1970s. A major objective of the IEA is to promote secure energy supplies on reasonable and equitable terms. The governing board of the IEA, which is composed of energy officials from each member country, regularly reviews the world energy situation. To facilitate this activity, each member country provides energy experts who serve temporary staff assignments at IEA headquarters. These staff or secretariat support the governing board by collecting and analyzing energy data, making projections in energy usage, and undertaking studies on specialized energy topics. The governing board is also assisted by several standing groups; one being the committee on energy research and technology (CERT), which encourages international cooperation on energy technology. Implementing agreements (IAs) are the legal instruments used to define the general scope of the collaborative projects. There are currently 40 active implementing agreements covering research topics such as advanced fuel cells, coal combustion science, district heating and cooling, enhanced oil recovery, fluidised bed conversion, fusion materials, solar heating and cooling, pulp and paper, hydropower, heat pumping technologies, hybrid and electric vehicles, high temperature super conductivity, wind turbines, and high temperature materials. A complete listing can be found at the IEA website, www.iea.org.

This progress report summarizes recent activities in the implementing agreement entitled, "Implementing Agreement For A Programme Of Research And Development On Advanced Materials For Transportation Applications." This implementing agreement currently consists of one active annex entitled," Annex II: Co-Operative Program on Ceramics for Advanced Engines and Other Conservation Applications". The motivation for this IA is the development of new and improved ceramic materials, brittle material design methods, and life prediction methodology. The objective of Annex II is coordinated R&D on advanced ceramics leading to standardized methods for testing and characterization.

The Executive Committee for the IA on Advanced Materials is also exploring the possibility of adding new efforts (Annex III and Annex IV). Annex III focuses on the characterization of contact damage (fatigue) while Annex IV deals with materials for hydrogen storage.

Technical Highlights

The minutes from the annual executive committee meeting recently held in conjunction with the PAC RIM IV meeting on 4-8 November 2001 were distributed to the various participants. In addition a fax vote was distributed to the executive committee members in early February to address the following issues:

1. Agreement to the validity of this written procedure (faxvote) as an Executive Committee decision (all Contracting Parties to vote; unanimous decision needed).

2. Approval of the minutes from the executive committee meeting held in Sweden in 2000.

3. Approval of the minutes from the executive committee meeting held in Hawaii in 2001.

All three issues were approved.

Acting under a subcontract funded by the IEA program, Gateway Materials Technology completed a project to assess the current requirements for ceramic coating tests in the diesel engine community and to develop a standards development strategy. The major goal was to determine the needs and priorities for test standards for ceramic coatings in the U.S. Diesel engine community. To this end a ceramic coatings e-mail survey was sent to over 230 individuals in the engine, coating producer, and research communities in the summer of 2001. With a 10% reply rate, the survey responses covered a wide range of engine components -- fuel injectors, piston rings, valves, engine heads; gears, wristpins, cylinders, rocker arms, and seals; turbine shrouds, blades, vanes, nozzles, and combustion components.

Ceramic oxides, nitride/carbides, and diamond-like carbon (DLC) were the coating compositions of primary interest. 2. The great majority (80%) of the respondents felt strongly that test standards were needed. The primary performance and durability requirements were – contact damage and sliding wear, spallation, erosion, cracking, and impact, oxidation, phase change, and hot corrosion. The "TOP FOUR" tests in the survey with a high priority for standardization are - adhesion, wear, thermal conductivity, and microstructural analysis.

Status of Milestones
All milestones are on track.

Communications/Visits/Travel
None.

Publications
None.

References
None

Standards For Reliability Testing Of Heavy Vehicle Propulsion Materials

Said Jahanmir and William Luecke
National Institute of Standards and Technology

Objective/Scope

The objective of this project is to develop international standard test methods for assessing the reliability of ceramic components used in diesel engines and other heavy vehicle propulsion systems. Advanced ceramics such as silicon nitride offer a unique combination of properties that include light weight, excellent high-temperature strength, and resistance to wear and corrosion. These properties make them particularly attractive for diesel engines, where their use as key engine components will allow the higher operating temperatures that lead to higher thermal efficiencies and environmentally cleaner propulsion systems. Reliability and cost-effectiveness are critical issues in implementing ceramics in the valve train of diesel engines. Ceramic valve train components are subjected to demanding conditions that include high contact loading, elevated temperatures, and corrosive environments. To ensure a reliable service life, standard test methods are needed to evaluate the performance of potential ceramics in highly loaded rolling and sliding contacts. This project will develop test methods for evaluating the contact damage behavior of ceramics under rolling and sliding conditions that simulate the cam roller followers, valves and valve seats. In support of this goal we will pursue four research thrusts: 1) fundamental issues in the relation between ceramic microstructure and performance reliability, 2) basic mechanisms that lead to formation and propagation of contact damage and the effect on reliability of residual stresses developed during machining and by contact, 3) effect of machining damage on contact reliability as well as the interactions between machining and contact damage that may lead to premature failure, 4) development of international standards for assessing contact damage.

Technical Highlights

IEA Annex III Activities

During this reporting period, NIST circulated a draft of a new Annex under the Implementing Agreement for a Programme of Research and Development on Advanced Materials for Transportation Applications. The draft is currently under review by NIST, DOE, and representatives from Germany and Japan. NIST will act as Operating Agent for the Annex.

The objective of the proposed Annex III (Co-operative program on Contact Reliability of Advanced Engine Materials) is to conduct co-operative research and development on contact reliability of advanced engine materials, leading to the standardization of testing and characterization methods for these new materials. Activities under this Annex shall include various forms of contact damage relevant to the implementation of advanced materials in different types of engines. It may include rolling contact fatigue, sliding and fretting wear, fretting fatigue, and other mechanical performance phenomena that control the reliability of contacts in advanced engines. Materials under consideration may include structural ceramics, composites, and coatings, as well as nanostructured friction/wear coatings.

There will be two subtasks under the annex. One is concerned with Technical Information Exchange. The other will compare currently available test methods for characterizing rolling contact fatigue of ceramics.

Pre-Standards Research for Rolling Contact Fatigue

Although early grades of silicon nitride exhibited rolling contact fatigue (RCF) failures by spalling, similar to bearing steels in various laboratory tests,[1,2] modern grades typically do not fail by RCF[3,4,5] in laboratory testing. Effectively, the newer materials have outstripped the ability of the test method. Although several test geometries exist for evaluating RCF in the laboratory (thrust washer, ball-on-3-balls, twin-disc-on-rod), the 3-ball-on-rod (Federal Mogul test) is the most common in the United States. We are researching extensions to this test method that will enable it to again yield RCF data on modern grades of silicon nitride. We are also examining the its potential for ASTM standardization. The 3-ball-on-rod test[1], see Figure 1, uses a 9.52 mm diameter rod approximately 75 mm long, held in a precision chuck and driven at 3600 rpm. A special test head clamps 3 (or 5) specially prepared AISI 52100 steel balls against the rod at a known, fixed load. An accelerometer mounted on the test head detects the vibration produced as the balls drop into a developing spall on the rod, and shuts the test down when that vibration reaches a prescribed level.

During this reporting period research focused on three areas of the 3-ball-on-rod test using Ceradyne Ceralloy 147-31N test rods. The first extended the work on failure due to excessive wear or spalling of the rods when tested with silicon nitride balls. The second examined the wear and deformation of the special AISI 52100 test balls during testing with silicon nitride test rods, to quantify the potential stress drop during the test. The third area examined the relation between rolling contact fatigue performance and resistance to damage under spherical indentation.

Table 1 summarizes the rolling contact fatigue/wear data to date. We have tested two types of surface finish: commercially finished (CF) as well as CF rods that have been further polished by hand (HP). Visually, the HP rods have a finer finish than the CF rods, but the surface roughness, measured by profilometry is nominally the same ($R_a \approx 0.08$ μm). The commercially finished rods (CF) fail primarily by spalling along 1/2 to 1/3 of the circumference. These spalls are typically 20-30 μm deep. In contrast, the rods that are further hand-polished (HP) wear excessively and uniformly around the circumference instead of spalling. These wear tracks are up to 90 μm deep. Figure 2 shows the results of special interrupted tests to characterize the wear rate at 7.3 GPa and 6.3 GPa. Rods tested using silicon nitride test balls at both 7.3 GPa and 6.3 GPa wear significantly. In contrast, silicon nitride rods tested at 6.3 GPa with AISI 52100 steel balls show insignificant wear over the same life. (See Table 1 and Figure 2.)

Research in other laboratories [6,7] has asserted that during the test, even with AISI 52100 balls on AISI 52100 rods, the stress drops, from an initial 5.4 GPa -6.3 GPa to 4 GPa or less, due to wear and deformation of the AISI 52100 ball. We have tested this assertion by characterizing the wear and deformation of silicon nitride rods and steel test balls tested at 6.3 GPa (the stress produced by the standard test load) using the standard steel balls. Table 2 summarizes the results. Note that the balls do not lose appreciable mass, and the wear scar on the ball represents only a very small change in diameter during the test. Figure 3 plots the diameter change, δd, as a function of rod (not ball) stress cycles. It also has additional data from tests that ended by spalling of the ball, rather than suspension. Unlike the suspended tests, balls from tests where one ball spalled have

flattened substantially on the wear scar. Apparently, most of the flattening occurs when the balls spall, rather than during the test. The reduction in stress from the flattening of the steel ball during the test must be much less than the reduction in stress from the formation of the deep wear scar in the rod during tests using silicon nitride balls. Even so, the wear of the rods in silicon nitride ball tests is significantly greater.

The third research area focused on correlating the indentation response of silicon nitride to rolling contact fatigue and wear. Typical RCF tests require special equipment and long test times, while single or cyclic spherical indentation is a simple technique with relatively simple analysis. Correlating the performance of candidate materials could help to reveal important microstructural parameters for contact reliability. A number of different silicon nitrides were indented using 6.35 mm and 3.175 mm diameter WC balls and the diameter and depth of the residual impression measured using profilometry. The different silicon nitrides are grouped into three basic types: bearing grade materials, HIP'ed, creep resistant materials, and higher-toughness, gas-pressure-sintered (GPS) materials. Table 3 shows a number of parameters for each silicon nitride: the approximate diameter of the residual impression, *w*; the depth, *dmax*, of the residual impression; the occurrence of acoustic emission (AE) during the indentation; and the occurrence of ring cracks (Crack) surrounding the residual impression. Note that these loads and stresses are substantially larger than those in the RCF tests.

As expected, the bearing-grade materials (Ceralloy 147-31N, Ceramics for Industry N8201, and NBD-100) have an excellent resistance to distributed damage under the indent, as revealed by the high critical loads for formation of a residual impression. The N8201 and Ceralloy 147-31N silicon nitrides form neither ring cracks nor residual impressions at the lowest load with 6.35 mm balls. The NBD-100 forms ring cracks at all loads, unlike the other two bearing-grade materials. Furthermore, the residual impressions are not hemispherical, as in all the other silicon nitrides. Instead, the center of the indent is flat-bottomed, as if it had just been punched below the surface. The coarser-grained gas-pressure-sintered materials generally have deeper residual impressions. The creep-resistant, HIP'ed silicon nitrides have residual indentation depths between the other two types.

Table 3 reveals several contradictory and surprising results. The existence of acoustic emission during indentation is not uniquely correlated with the formation of ring cracks. It may be, however, that the AE equipment is not sensitive enough to detect the formation of the some of the ring cracks. Interestingly, although the depths of the residual impressions vary by a factor of five at some loads, the diameters vary by only about 15 %, which is probably within the uncertainty of the measurement. Cross-sectioning of the residual impression should reveal the extent of shear-faulting damage under the impressions. Generally, ring cracks do not form in the higher-toughness GPS silicon nitrides. One exception is the SN88, which has the typical elongated microstructure of GPS materials, but has shallower impressions and more ring cracks than the other GPS silicon nitrides.

Status of Milestones

1. Propose to the IEA Executive committee the formation of a new subtask under Annex II to study contact damage (December 2001): complete.

2. Compare the nature of failure mechanisms in single-cycle ball-on-flat contact damage to those in rolling contact fatigue for silicon nitride. (March 2002) complete

3. Compare the nature of failure mechanisms in multi-cycle contact damage to those in rolling contact fatigue for silicon nitride. (July 2002) on schedule

4. Explore the feasibility of standardizing the 3-ball-on-rod rolling contact fatigue (RCF) test and assemble a team of users of the 3-ball-on-rod RCF test to conduct an interlaboratory study of RCF of engine ceramics. (September 2002) on schedule.

Communication/Visits/Travel

A draft research agreement (RA) was sent to potential members of the Contact Reliability Working Group for comments. NIST approvals have been obtained and the RA has been sent to those that have expressed an interest to join.

A draft agreement for Annex III (Co-operative program on Contact Reliability of Advanced Engine Materials) was sent to potential participants in Germany and Japan. The draft is currently awaiting approvals from DOE and NIST before it is submitted to the IEA Executive Committee for balloting. National representatives for Japan and Germany have been selected.

A symposium on contact reliability is being planned for October 2002 to assess the standardization needs in participating countries.

Publications

None this period

References

[1] Douglas Glover, "A Ball-rod Rolling Contact Fatigue Tester," pp 107—124 in *Rolling Contact Fatigue Testing of Bearing Steels*, J. J. C. Hoo, ed. ASTM STP 771, American Society for Testing and Materials, Philadelphia, Pa, (1982)

[2] Harold L. Burrier Jr. "Optimizing the Structure and Properties of Silicon Nitride for Rolling Contact Bearing Performance," *Trib. Trans.*, **39**[2], 276—285 (1996)

[3] L.-Y Chao, R. Lakshminarayanan, N. Iyer, G.-Y. Lin, and D. K. Shetty, "Transient Wear of Silicon Nitride in Lubricated Rolling Contact," *Wear*, **223**, 58-65, (1998).

[4] Vimal Pujari and William Collins, "All Ceramic Bearing", United States Patent 6158894,December 12, 2000.

[5] Deborah L. Allen, "Effect of Composition and Physical Properties of Silicon Nitride on Rolling Wear and Fatigue Performance," *Trib. Trans.*, **37**[2], 410—414, (1994)

[6] John W. Lucek, "Rolling Wear of Silicon Nitride Bearing Materials," Paper 90-GT-165, 1990, American Society of Mechanical Engineers ``Presented at the Gas Turbine and Aeroengine Congress and Exposition, June 11--14, 1990 Brussels, Belgium.

[7] Mary-Jo Liston, "RCF Life Comparision of Bearing Steels at Two Stress Levels," Lub. Eng., **55**[6], 12-19, (1999).

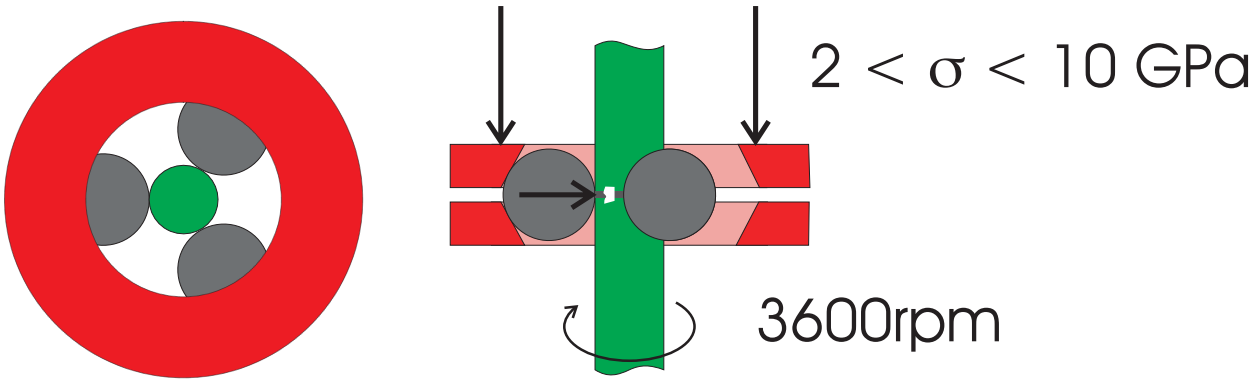

Figure 1. Schematic of the RCF test rig

Table 1 Summary of RCF Tests to date						
Rod-Track	Initial Stress (GPa)	Ball Mat'l	# Cycles	Wear track depth (μm)	Spall size	Notes; why shutdown
HP1-0	6.3	AISI 52100	1.3E7	0.2	no spall	ball spall
HP1-4	6.3	AISI 52100	5.8E6	0.4	no spall	ball spall
HP1-5	6.3	AISI 52100	5.2E7	3.0	no spall	3 restarts, all ball spalls
HP5-1	6.3	AISI 52100	3.1E7	0	no spall	suspended test
HP1-1a	6.3	AISI 52100	2.3E7	0.4	no spall	
CF6-1	6.3	AISI 52100	<3.5E7	0	19.3 μm deep	suspended test
CF6-2	6.3	AISI 52100	6.27E7	0	2 μm deep	ball spall
CF6-14	6.3	AISI 52100	5.8E7	0	no spall	suspended test
CF6-3	7.3	Si_3N_4	3.6e5	0	19.6 μm ¼ circumference	rod spall
CF6-4	7.3	Si_3N_4	3.1E5	0	27.9 μm ¼ circumference	rod spall
CF4-1	7.3	Si_3N_4	4.6E5	2.2	16.5 μm 1/3 circumference	rod spall
CF6-5	7.3	Si_3N_4	8.8E5	0.2	33.3 μm ¼ circumference	rod spall
CF6-2a	6.3	Si_3N_4	7.5E7	56.3	no spall, uniform wear	test suspended
CF6-3a	6.3	Si_3N_4	1.1E6	0.9	10.9 μm ½ circumference	rod spall
HP5-2	7.3	Si_3N_4	2.3E8	58.6	no spall	uniform, deep wear; suspended test
HP5-3	7.3	Si_3N_4	1.2E7	86.3	no spall,	machine failure
HP5-6	6.3	Si_3N_4	9.8E7	62.7	no spall	test suspended
HP1-6	6.3	Si_3N_4	8.4E7	48.5	no spall	test suspended
Wear Rate Tests						
HP5-4	7.3	Si_3N_4	4.1E5	0.7	no spall	test suspended
HP5-5	7.3	Si_3N_4	9.8E5	5.6	no spall	test suspended
HP5-6	7.3	Si_3N_4	2.2E6	22.0	no spall	test suspended
HP1-7	6.3	Si_3N_4	5.2E5	0.3	no spall	test suspended
HP1-8	6.3	Si_3N_4	1.0E6	0.5	no spall	test suspended
HP1-9	6.3	Si_3N_4	2.4E6	25.2	no spall	test suspended

Table 2 AISI 52100 Ball wear data (6.3 GPa)					
t (h)	Rod Stress cycles	ball wear scar (mm)	δm/ball (g)	δd (mm)	Notes
0.61	3.1E5	0.917±0.004		+0.000	
6.71	3.5E6	0.925±0.001	+0.0001	-0.002	
23.71	1.2E7	0.943±0.002	-0.0010	-0.005	
66.60	3.4E7	0.971±0.002	-0.0002	-0.004	

Table 3 Residual impressions during spherical indentation of silicon nitride										
		Bearing Grade			HIP'ed creep-resistant		Gas-pressure sintered			
Material Manufacturer		147-31N Ceradyne	N8201 CFI	NBD100 St. Gobain	NT164 St Gobain	GN10 Allied-Signal	AS800 Allied-Signal	SN88 NGK	GS44 Allied-Signal	Yb-Al MPI/ Stuttgart
6.35 mm WC Ball										
Pmax (N)	2796									
dmax (µm)	14 GPa	0.26	0.18	Note 1	0.23	0.33	0.77	0.37	0.60	1.07
w (mm)	(note 3)	0.50	0.62	n/a	0.55	0.67	0.68	0.66	0.68	0.66
AE		yes	yes	yes	yes	no	no	yes	no	no
Crack		yes	yes	yes	yes	no	no	yes	no	no
Pmax (N)	2239									
dmax (µm)	13 GPa	Note 2	0	Note 1	0.17	0.13	0.42	0.10	0.36	0.79
w (mm)		Note 2	0	Note 1	0.56	0.59	0.64	0.57	0.59	0.68
AE		yes	no	yes	no	no	no	no	no	no
Crack		yes	yes	yes	no	no	no	yes	no	no
Pmax (N)	1761									
dmax (µm)	12 GPa	0.0	0.0	note 1	0.10	0.10	0.25	0.08	0.19	0.47
w (mm)		0.0	0.0	note 1	0.50	0.52	0.55	0.58	0.50	0.62
AE		yes	no	yes	no	no	no	no	no	no
Crack		no	no	yes	no	no	no	yes	no	no
3.175mm WC ball										
Pmax (N)	1044			note 1						
dmax (µm)	16 GPa	0.52	0.29	note 1		0.28	0.75	0.37	0.67	
w (mm)		0.44	0.36			0.40	0.35	0.33	0.39	
AE		no	yes	no		no	no	no	no	
Crack		no	no			no	no	yes	no	
Pmax (N)	860									
dmax (µm)	15 GPa	0.41	0.13	note 1		0.17	0.55	0.29	0.35`	0.65
w (mm)		051	0.32	note 1		0.38	0.38	0.34	0.33	0.37
AE		no	no	yes		no	no	no	no	no
Crack						no	no	yes	no	no
Pmax (N)	699									
dmax (µm)	14 GPa	0.11	0.05	note 1	0.05	0.11	0.15	0.16	0.29	0.46
w (mm)		0.24	0.27		0.32	0.34	0.36	0.30	0.33	0.43
AE		no	no	no	no	no	no	no	no	no
Crack		no	no	yes	no	no	no	no	no	no
Note 1	Residual indentations in NBD100 were not spherical, but rather were flat-bottomed and surrounded by numerous ring cracks									
Note 2	Polishing scratches made it impossible to assess the depth of the residual indentation									
Note 3	Residual indentation diameters have uncertainties of +/-0.1 mm									

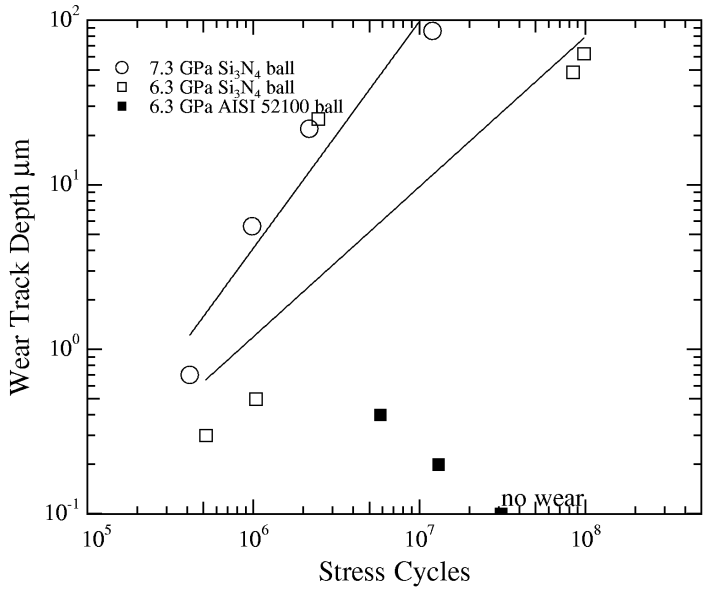

Figure 2. Wear of silicon nitride test rods during rolling contact with silicon nitride and AISI 52100 balls

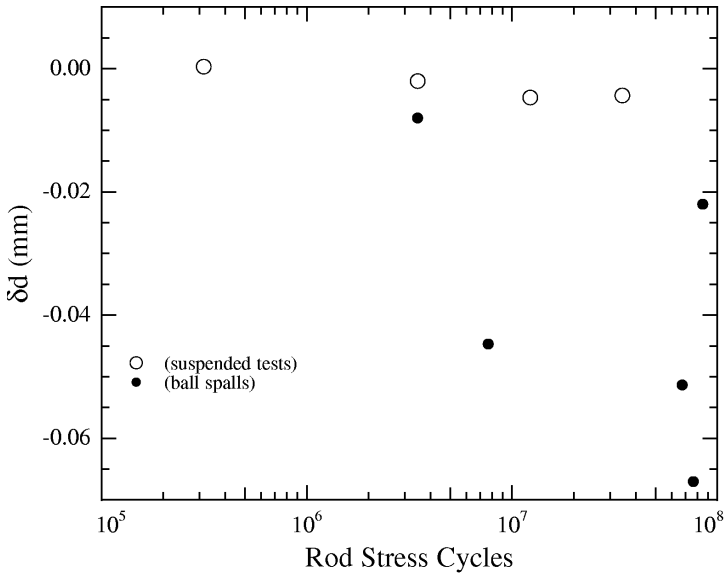

Figure 3. AISI 52100 Ball diameter change during RCF testing on silicon nitride rods

Mechanical Property Test Development

George Quinn
Ceramics Division
NIST

Objective/Scope

This task is to develop mechanical test method standards in support of the Propulsion Systems Materials Program. Test method development should meet the needs of the DOE engine community but should also consider the general USA structural ceramics community as well as foreign laboratories and companies. Draft recommendations for practices or procedures shall be developed based upon the needs identified above and circulated within the DOE engine community for review and modification. Round robins will be conducted as necessary. Procedures will be standardized by ASTM and/or ISO.

Technical Highlights.

1. General

Work on flexure testing of cylindrical rods specimens resumed this quarter. Emphasis was on firming up a fascinating trend of ***machining damage characteristics*** versus grinding wheel grit size in Ceradyne's SRBSN material. To that end, we reexamined two full sets of ground bend bars in order to compare the damage depths in the bars to what had been measured in rods.

A second round of follow up revisions to the ***ASTM C 1161 flexural strength standard*** were balloted. A series of bulletins, announcements, and direct letters to companies have been sent out heralding the changes to this important standard.

A comprehensive set of 19 major revisions to the ***ASTM fractography standard C 1322*** was balloted.

2. Fracture Toughness

a. ASTM C 1421 No activity this period. Major changes to ASTM C 1421 standard were accomplished in the last quarterly period.

b. ISO SCF method DIS 18756

In early February 2002, many editorial and clarifying changes were made to the draft International Standard as a result of the input received in the TC 206 meeting in Maui in November. In addition, an investigation into the terminology "width" and "thickness" was conducted when the Korean delegation pointed out inconsistencies in the document. The inconsistencies occurred not only in this document, but also in many of the ISO standards in development in TC 206. A proof copy from the secretariat was reviewed in late March 2002. This document is nearing completion. It will be voted on as a formal DIS = "Draft International Standard" in mid 2002.

3. Flexural Strength of Advanced Ceramics – Rectangular Specimens

a. ASTM C 1161 Revisions

After 11 years on the books, ASTM standard C 1161 was overhauled in the fall of 2001. Twenty-six revisions were approved. Four follow on revisions were balloted in late January 2002, in response to input received from several balloters including Jeff Swab, Sung Choi, Jonathan Salem, and Vic Tennery. One of these revisions is a new scratch inspection procedure (which was summarized in the last quarterly report.) This is the first such scratch inspection procedure of its type in the world for strength test specimens, flexural, tensile, or disk. Announcements and articles in trade journals have been sent out. Approximately 100 letters to key machine shops were also sent out on February 5th, announcing the revisions. The new engineering drawing of a standard bend bar (Figure 1) has been distributed widely and requests

for copies are coming by email. We are distributing free copies via email. Inquiries are welcome.

We received feedback from Bomas Machine Specialties that the change to final finishing of 400 – 600 grit (as opposed to the former 320 – 500 grit) was very timely. Some of their discriminating customers had shifted to finer finishes and new cost effective grinding wheels are now available. This feedback echoed comments from Chand Technical Ceramics that we received in mid 2001. In other words, the timing of the shift to the flexural strength standard was just about right.

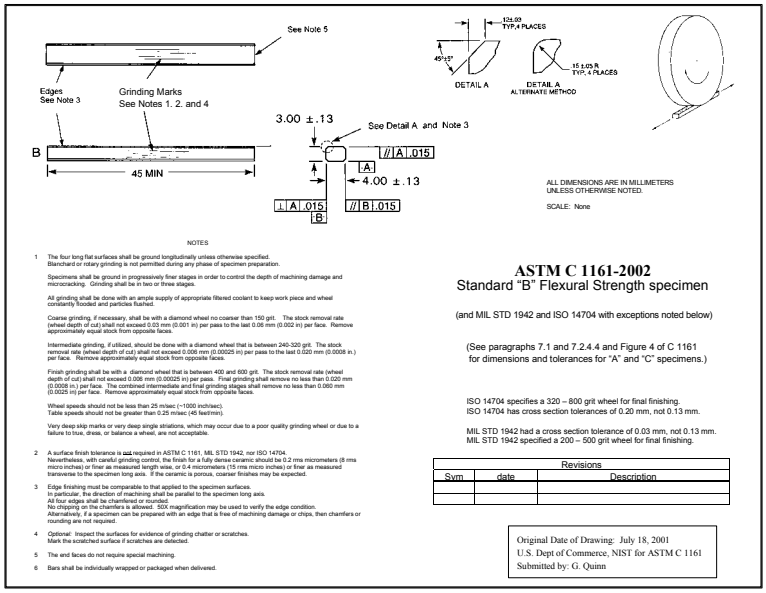

Figure 1. The new engineering drawing for standard flexural strength specimens. Free full sized copies are available upon request: Contact:. **george.quinn@nist.gov**.

The new revised **C 1161-02** has been posted by ASTM as of March 2002, but unfortunately it will be distributed only as "separates." The printed 2002 Annual Book of Standards volume 15.01 will still have the 1996 version of the standard. Worse, the version posted on the ASTM Web site contains numerous editorial mistakes. The ASTM editor has been informed but we are disappointed that the faulty rendition is still posted as of this writing (April 11, 2002).

The original version C 1161 was a good standard when adopted, but years of new experience by the ceramics and engineering community especially at ORNL and NIST warrant the major overhaul.

b. ASTM C 1211, Elevated Temperature Flexural Strength Revisions

This standard, the elevated temperature version of C1161, is also due for an overhaul. The changes will be much less extensive since C 1211 was already revised in 1997. We will propose that this standard be shortened considerably and the users referred back to C 1161. When this standard was created in 1994, the ASTM committee wanted it to be a stand-alone document. Unfortunately this led to a lot of unnecessary redundancy with C 1161. A list of proposed changes and the proposal to shorten C 1211 has been prepared for the April 2002 meeting of Committee C-28 in St. Louis.

c. ISO 17565, Elevated Temperature Flexural Strength

Fourteen editorial revisions were recommended for this standard. It began its 5-month worldwide balloting period at the end of October 2001.

4. ASTM Standard C 1322, Fractographic Analysis of Advanced Ceramics
This ground breaking standard was due for renewal. It was the first standard in the world to set a course of action for normal fractographic analysis and interpretation of fractured strength-test specimens. In late December, the author in cooperation with Mr. J. Swab of the U.S. Army Research Laboratory, compiled a group of 19 revisions to C 1322. They were balloted by ASTM in late January- mid March 2002.

Many of the revisions were intended to shorten the document and make it easier for users to understand. For example, the tables comparing the merits and drawbacks of various specimen cleaning solvents will be deleted since most users are already familiar with the cleaning agents. The extensive bibliography was eliminated.

C 1322 was expanded in some areas. More guidance is given on component failure analysis. A simple flowchart was added that illustrates the logical order of the common fractographic analysis.

A new, vastly expanded appendix of fracture mirror constants was added. The full list was in the previous quarterly report. We also added many more examples and illustrations of machining damage cracks, based on the lessons we have learned in this program in the last few years.

A host of comments and negative ballots were received on the ballot, and these will have to be dealt with at the upcoming meeting of committee C-28 in St. Louis at the end of April. Nor surprisingly, many of the negatives were on some of the definitions. Definitions always seem to arouse concern.

5. Flexural Strength Testing of Cylindrical Ceramic Specimens
In December 2001, the NIST Ceramic Machining Consortium program was completed. A final meeting was held at NIST with important representatives from ORNL (Sam McSpadden), Chand, Ford, and Ceradyne among others in attendance. We reviewed all the fractographic findings to date and the final data collected on Ceradyne sintered reaction bonded silicon nitride 220 grit transversely ground rods. As expected, the 220 grit specimens had severer machining damage cracks than the 320 and 600 grit ground specimens. Our experience in detecting machining cracks in this material was helpful and the new machining cracks were easy to detect.

We had reached the point that we could detect machining damage fairly easily in this material. This was quite an achievement, since at the beginning of the study, the machining cracks seemed very elusive! This exercise underscores a key tenet of fractographic analysis in general. Fractography often is pattern recognition. Once an observer recognizes the key elements of a pattern and how to detect the markings, then interpretations come faster and easier. We are now able to not only detect the machining damage, but to measure its size, shape and depth. One goal of this project has been to transfer this know how to a more general audience. To this end, the ASTM standard C 1322 was revised as described above (with numerous illustrations and general schematics). Papers and poresentations on this topic will also be prepared.

In December, we detected a trend of size of machining cracks versus grinding wheel grit size. This trend is shown below as Figure 2. The trend was sketchy, and not too surprising, since it has been well known that coarser grits produce coarser damage. A <u>full quantification</u> of the trend has never been published, however. Numerous papers have plotted *strength versus grit size*, but very few have ever plotted *crack size versus grit size*. The crack size plot is more useful since it provides a direct indication of how deep the machining damage extends.

The practical ramifications of such a figure are enormous. Machinists and users will now know exactly how much material need be removed to eliminate the machining damage, if they so choose. This is especially important in instances where the direction of the grinding and hence the damage,

cannot be favorably controlled. Parts that must have transverse grinding, or parts which are biaxially loaded cannot escape the worst effects of subsurface machining damage.

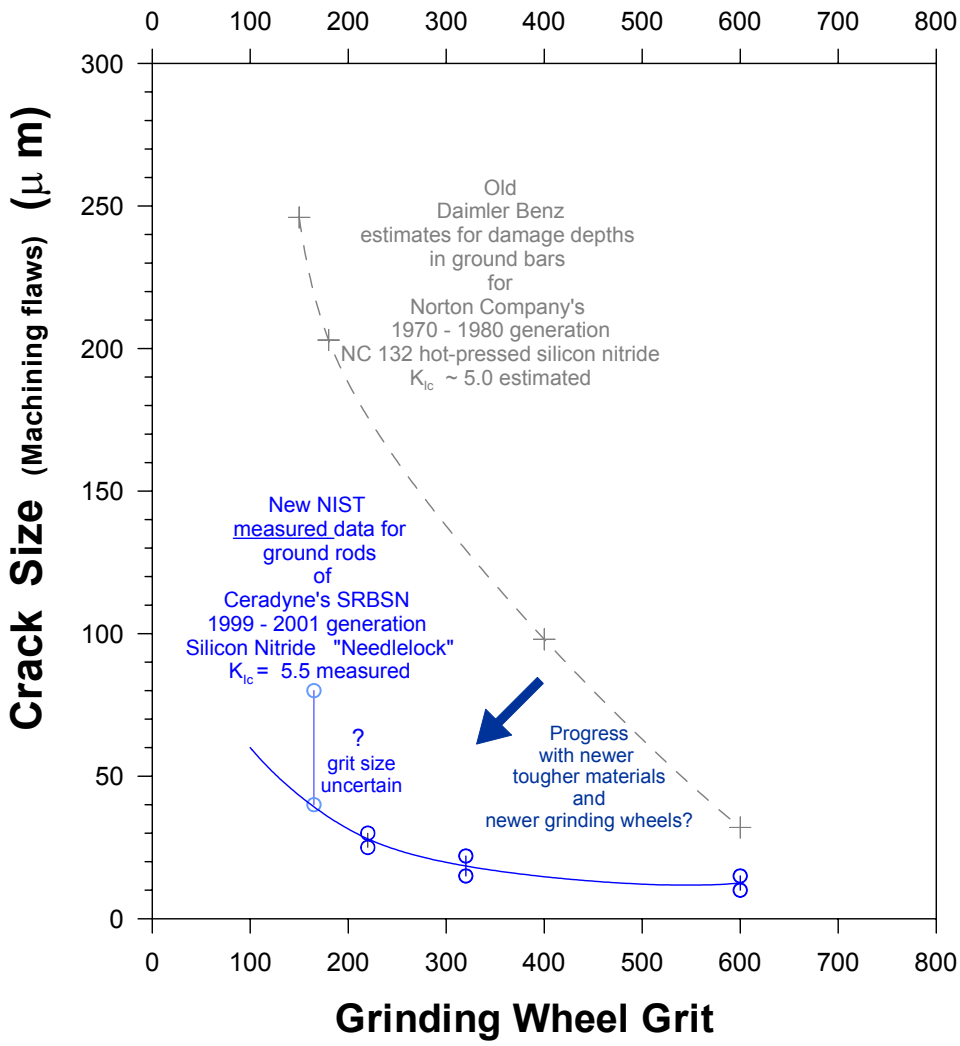

Figure 2 Depth of machining damage cracks as a function of grinding wheel grit for Ceradyne sintered reaction bonded silicon nitride (SRBSN) **rods**. For comparison, a set of Daimler Benz recommendations in 1982 is shown. The Daimler Benz crack depth estimates were based on calculations from flexural strength data from a variety of ground **bars** and the then estimated fracture toughness (~5.0 MPa√m) of hot pressed silicon nitride, Norton grade NC 132. The new NIST data taken for the Ceradyne SRBSN shows the actual machining damage depths are much smaller. Is this because the SRBSN has greater fracture toughness, or some other factor?

Recognizing the significance of these results, and the availability of our new expertise to accurately measure the heretofore-elusive machining damage, we launched a major thrust into firming up this graph. We added data for ground bars as well as rods. Old bar specimens with 80 grit and 150 grit transverse grinding were evaluated. We also reviewed the technical literature and government program progress reports for comparable data. The results are in Figure 3.

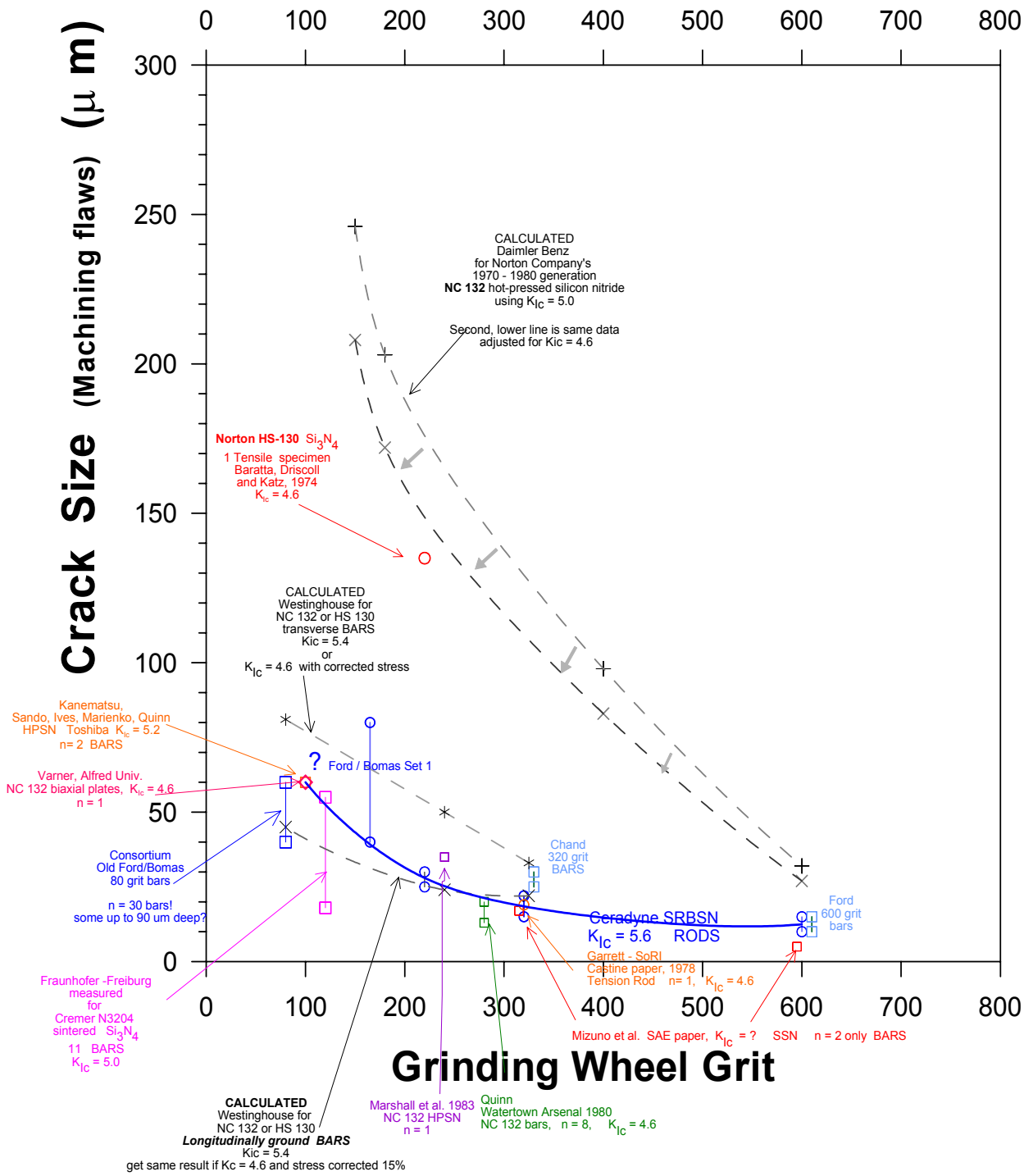

Figure 3. Graph of crack size (depth) versus grinding wheel grit size. Data from ground bars, rods, and even tensile specimens are included. A wealth of information is included in this graph as discussed in the text. A key finding is that much of the data, for a variety of silicon nitrides, overlap and fall on a single band at the lower portion of the graph.

Figure 3 is remarkable in that machining crack sizes have been astonishingly consistent. Most of the data shown is for transverse machining damage cracks, which are easier to discern. Other remarkable conclusions are:

- Damage depths in rods and bars are remarkably similar.
- Damage depths are remarkably similar from a variety of studies on variety of silicon nitrides over the course of 30 years.
- Although other factors such as depth of cut, wheel speed, wheel concentration, etc undoubtedly contribute to machining cracks damage, their influence is clearly secondary compared to grit size.
- Westinghouse's old (1970's) calculated estimates for longitudinally-machining crack depths match the experimentally observed outcome much better than the Daimler Benz estimates or Westinghouse's transverse grinding estimates. Other than a single tension test specimen (from Watertown Arsenal but now in the in the author's possession at NIST), there are no corroborating data for machining damage as deep as estimated by Daimler Benz.
- Machining damage data at grit sizes finer than 600 grit are nonexistent. That is because either no one has studied finer grits, or more likely, machining cracks do not control fracture!
- Machining cracks at very coarse grit sizes are rarely if ever deeper than 100 μm.

A comprehensive paper on these findings, which will be copiously illustrated, is in preparation for the Journal Machining Science and Technology. Our goal is to have a first draft completed by the end of April.

The author would welcome any news of other references or data pertinent to Figure 3.
Please contact : **george.quinn@nist.gov**

6. Compare SCF Knoop artificial cracks to machining cracks in Ceradyne SRBSN
In the last quarterly report, we presented data and pictures from a careful fractographic study of artificial Knoop cracks. We compared these to machining cracks. An oral presentation on this subject will be presented at the American Ceramic Society Annual Meeting in April 2002, in the Van Frechette Memorial symposium.

Status of Milestones

We seized on the opportunity to thoroughly characterize the machining damage cracks. This plus, the extra time needed to organize and manage the major revisions to ASTM C 1161 and C 1322, have delayed progress on several tasks such as a new cylindrical rod strength test method and diametral compression work.

412146	Ballot major revisions to ASTM C 1161 flexural strength **Completed , October 2002✓**	Sept. 2001,
412147	Prepare ballot revisions for ASTM C 1322, Fractographic Analysis **Completed, January 2002✓**	April 2002,
412148	Prepare follow on specimen machining revisions to ASTM C 1161 flexural strength if needed **Completed, April 2002✓**	April 2002
412149	Prepare ballot-ready first ASTM draft of cylindrical rod flexure strength test **Delayed**	April 2002
412150	Prepare paper on effect of machining on strength of SRBSN rods. **In progress**	May 2002
412151	Prepare review paper on flexural testing of cylindrical rods.	October 2002

Communications/Visits/Travel
Biljana Mikjelj of Ceradyne, Sam McSpadden of ORNL, Dick Allor of Ford, and Ron Chand of Chand Associates meet with Mr. Quinn at NIST in December to review the ceramic machining results in the Ceramic Machining Consortium.

Data on static fatigue testing, prepared by the author when he was with Watertown Arsenal and while funded by DOE, was complied and sent to Kristin Breder at St. Gobain, Norton. This will help her prepare the new static fatigue ASTM standard test method.

Publications

1. G. D. Quinn and J. A. Salem, "Effect of Lateral Cracks Upon Fracture Toughness Determined by the Surface Crack in Flexure Method," accepted by J. Am. Ceram. Soc. July 2001.
2. S. W. Freiman and G. D. Quinn, "How Property Test Standards Help Bring New Materials to the Market," ASTM Standardization News, Oct. 2001, pp. 26-31.
3. G. D. Quinn, P. Green, and K. Xu, "Cracking and the Indentation Size Effect for Knoop Hardness of Glasses," subm. to J. Amer. Ceram. Soc., Oct. 2001.
4. G. D. Quinn, S. Jahanmir, and L. Ives, "Flexural Strength Testing of Cylindrical Rods and Rectangular Bars," presented at the PAC RIM IV Conference, Maui, Hawaii, Nov. 8, 2001.
5. G. D. Quinn, P. J. Patel, and I. Lloyd, "Effect of Loading rate Upon Conventional Ceramic Microindentation Hardness," accepted by the Journal of Research of NIST, April 2002.